GEOLOGICAL REPORT
ON
RECONNAISSANCE SURVEY (G-4) FOR
REE AND ASSOCIATED MINERALS
IN AND AROUND
LANGMIPI-LACHING THING AREA

DISTRICT - WEST KARBI ANGLONG,
STATE - ASSAM

(Under NMEDT Programme)

TEXT, ANNEXURE AND PLATES

Area
124.68 sq. km

Toposheet
83O/09, 83C/10,
83C/13 & 83C/14

Location
25°43'26.64" N to
25°50'36.56" N
92°44'02.85" E to
92°52'04.06" E

A: Photomicrograph showing an association of quartz, plagioclase and biotite, wherein apatite, zircon and monazite occur as inclusions within biotite, as seen under crossed nicols.
B: Photomicrograph showing fine to very fine grains of pyrite associated with very fine specks of chalcopyrite, as seen under reflected light.
C: A 2-8 cm-thick quartzo-feldspathic vein intruding the migmatite.
D: Quartz vein within an amphibolite band exhibiting folding and shearing.

MECL
MINERAL EXPLORATION & CONSULTANCY LIMITED
(formerly known as Mineral Exploration Corporation Limited)
(A Government of India Enterprise)
Ministry of Mines, Govt. of India
SEPTEMBER 2026

CONTENT

GEOLOGICAL REPORT ON RECONNAISSANCE SURVEY (G-4) FOR REE & ASSOCIATED MINERALS IN AND AROUND LANGMIPI-LACHING THING AREA DISTRICT- WEST KARBI ANGLONG, ASSAM

LIST OF CONTENTS

LIST OF TABLES

GEOLOGICAL REPORT ON RECONNAISSANCE SURVEY (G-4) FOR REE & ASSOCIATED MINERALS IN AND AROUND LANGMIPI-LACHING THING AREA DISTRICT- WEST KARBI ANGLONG, ASSAM

LIST OF TEXT FIGURES

GEOLOGICAL REPORT ON RECONNAISSANCE SURVEY (G-4) FOR REE & ASSOCIATED MINERALS IN AND AROUND LANGMIPI-LACHING THING AREA DISTRICT- WEST KARBI ANGLONG, ASSAM

LIST OF PHOTOGRAPHS

GEOLOGICAL REPORT ON RECONNAISSANCE SURVEY (G-4) FOR REE & ASSOCIATED MINERALS IN AND AROUND LANGMIPI-LACHING THING AREA DISTRICT- WEST KARBI ANGLONG, ASSAM

LIST OF PHOTOMICROGRAPHS

अध्याय–I
कार्यकारी सारांश

1.0.0 कार्यकारी सारांश

1.1.0 पृष्ठभूमि

असम के पश्चिम कार्बी आंगलोंग जिले में स्थित 124.68 वर्ग कि.मी. क्षेत्रफल वाले लांगमिपी–लाचिंग थिंग ब्लॉक में दुर्लभ मृदा तत्वों (REE) एवं सहगामी खनिजों के लिए पूर्वेक्षण सर्वेक्षण (G-4 चरण) का कार्य National Mineral Exploration and Development Trust (NMEDT). के वित्तपोषण के अंतर्गत मिनरल एक्सप्लोरेशन एंड कंसल्टेंसी लिमिटेड (MECL) द्वारा किया गया। यह ब्लॉक भारतीय सर्वेक्षण विभाग के टोपोशीट संख्या 83C/09, 83C/10, 83C/13 एवं 83C/14 के भागों में स्थित है तथा आर्कियन–प्रोटेरोजोइक असम–मेघालय नाइसिक कॉम्प्लेक्स (AMGC) के अंतर्गत शिलांग पठार के पूर्वी सीमांत भाग में अवस्थित है। इस अन्वेषण कार्य की अनुशंसा 26–27 सितम्बर 2024 को आयोजित तकनीकी-सह-लागत समिति-II (TCC-II) की प्रथम बैठक में की गई थी। तत्पश्चात इसे 29 नवम्बर 2024 को आयोजित NMEDT की कार्यकारी समिति (EC) की 38वीं बैठक में अनुमोदित किया गया तथा दिनांक 13 दिसम्बर 2024 के आदेश द्वारा स्वीकृति प्रदान की गई।

1.2.0 अवस्थिति एवं अभिगम्यता

ब्लॉक छह सीमा बिंदुओं (A–F) से सीमांकित है तथा 25°43′26.64″ N से 25°50′36.56″ N अक्षांश और 92°44′02.85″ E से 92°52′04.06″ E देशांतर के मध्य स्थित है। इसके अंतर्गत मोकिंडुर, लांगमिपी, लाचिंग थिंग, रोंगपी एवं थेंगलॉन्ग गाँवों के कुछ भाग आते हैं। अध्ययन क्षेत्र तक खेरोनी–तहपत–जिरिकिंडिंग सड़क के माध्यम से पहुँचा जा सकता है। निकटतम रेलवे स्टेशन लंका, ब्लॉक से लगभग 20 कि.मी. उत्तर-पूर्व में, जबकि निकटतम हवाई अड्डा लोकप्रिया गोपीनाथ बोरदोलोई अंतरराष्ट्रीय हवाई अड्डा, गुवाहाटी, लगभग 250 कि.मी. की दूरी पर स्थित है।

1.3.0 भूविज्ञान एवं खनिजीकरण

ब्लॉक में मुख्यतः असम–मेघालय नाइसिक कॉम्प्लेक्स की माइग्माटाइट, ग्रेनाइट नाइस एवं ऑगेन नाइस शैलें पाई जाती हैं। इनके अतिरिक्त अधीनस्थ रूप से ग्रेनाइट, परिवर्तित कैल्केरियस–सिलिशियस बलुआ पत्थर तथा चतुर्थकल्पीय मृदा/जलोढ़ निक्षेप उपस्थित हैं। इन सभी शैल इकाइयों को पेग्माटाइट, क्वार्ट्ज एवं क्वार्ट्जो-फेल्डस्पैथिक शिराएँ अंतर्वेधित करती हैं। फेल्सिक शैलें मेटाल्यूमिनस, पोटैसिक एवं अत्यधिक विकसित प्रकृति की हैं।

REE खनिजीकरण मुख्यतः फेल्सिक नाइसों तथा पेग्माटाइटिक एवं क्वार्ट्जो-फेल्डस्पैथिक शिराओं में पाया जाता है। इसमें मोनाजाइट प्रमुख REE-वाहक खनिज है, जबकि जिरकॉन, टाइटेनाइट एवं एपेटाइट अन्य सहायक REE-वाहक खनिज हैं। एलनाइट की उपस्थिति अनुमानित है, परंतु पेट्रोग्राफिक अध्ययनों द्वारा इसकी पुष्टि नहीं हुई है। अधीनस्थ सल्फाइड खनिजीकरण, मुख्यतः पाइराइट–चाल्कोपाइराइट, तथा मैग्नेटाइट–इल्मेनाइट खनिजीकरण भी विकसित है। यह खनिजीकरण शैलविज्ञान, अपरूपण/भंजन तथा अंतिम चरण की मैग्माई–हाइड्रोथर्मल प्रक्रियाओं द्वारा नियंत्रित है। सभी शैल इकाइयाँ एवं उनसे व्युत्पन्न नमूना माध्यम HREE की तुलना में LREE की प्रबल समृद्धि तथा सुविकसित ऋणात्मक Eu विसंगति प्रदर्शित करते हैं, जो विकसित फेल्सिक भूपर्पटीय प्रोटोलिथ से उनकी उत्पत्ति को इंगित करता है।

1.4.0 संपादित अन्वेषण कार्य

G-4 चरण के आवीक्षण कार्य के अंतर्गत संपूर्ण 124.68 वर्ग कि.मी. क्षेत्र में 1:12,500 पैमाने पर वृहद्-स्तरीय भूवैज्ञानिक मानचित्रण किया गया। इसके अतिरिक्त 50 बेडरॉक नमूने (BRS), 58 धारा-अवसाद नमूने तथा 65 मृदा (गर्त) नमूने एकत्र किए गए। कुल 173 प्राथमिक नमूनों का 34 तत्वों के लिए ICP-MS तकनीक से विश्लेषण किया गया। साथ ही, 15 बेडरॉक नमूनों का प्रमुख ऑक्साइडों के लिए XRF द्वारा तथा 10 नमूनों का XRD द्वारा विश्लेषण किया गया। इन अध्ययनों के समर्थन में 10 नमूनों का पेट्रोग्राफिक तथा 5 नमूनों का मिनेराग्राफिक अध्ययन भी किया गया। TCC-II की 31वीं बैठक में की गई समीक्षा के अनुसार ब्लॉक में वेधन एवं संसाधन आकलन का कार्य नहीं किया गया।

1.5.0 प्रमुख परिणाम

ICP-MS विश्लेषण से प्राप्त शैल-इकाईवार एवं नमूना-माध्यमवार REE भू-रासायनिक परिणामों का सारांश नीचे दिया गया है। ग्रेनाइट नाइस में औसत कुल REE की सर्वाधिक मात्रा दर्ज की गई है, परंतु इसकी अत्यधिक विस्तृत परास REE की निरंतर समृद्धि के बजाय अनियमित एवं स्थानिक रूप से असतत वितरण को दर्शाती है।

नमूना माध्यम/शैल इकाई	नमूनों की संख्या (N)	ΣREE औसत (ppm)	ΣREE परास (ppm)	ΣREE+Sc+Y औसत (ppm)
ग्रेनाइट नाइस	4	816.73	87.17–1458.80	894.74
पेग्माटाइट शिरा	4	472.20	268.21–579.67	553.30
माइग्माटाइट	20	405.04	68.00–1495.00	464.03
ऑगेन नाइस	11	359.27	27.15–680.80	433.94
क्वार्ट्जो-फेल्डस्पैथिक शिरा	5	334.36	108.80–734.19	409.62
परिवर्तित कैल्केरियस–सिलिशियस बलुआ पत्थर	5	120.23	55.55–185.27	162.60
क्वार्ट्ज शिरा	1	109.12	–	123.37
धारा-अवसाद	58	320.66	51.88–1037.26	355.51
मृदा–B संस्तर	21	383.85	197.64–788.70	443.41
मृदा–B+C संस्तर	44	364.94	139.05–1235.92	428.42

केवल कुछ पृथक नमूनों में ΣREE का मान 1000 ppm से अधिक दर्ज किया गया। इनमें ग्रेनाइट नाइस का एक बेडरॉक नमूना ML BRS-31, जिसमें ΣREE का मान 1458.80 ppm है, तथा एक धारा-अवसाद नमूना सम्मिलित हैं। अधिकांश नमूनों में

REE की मध्यम सांद्रता दर्ज की गई है। उच्च REE मान किसी सतत अथवा मानचित्रण योग्य समृद्ध क्षेत्र के रूप में स्थानिक रूप से समूहित नहीं हैं।

1.6.0 निष्कर्ष

G-4 चरण के आवीक्षण सर्वेक्षण से यह स्थापित हुआ कि लांगमिपी–लाचिंग थिंग ब्लॉक में REE की उपस्थिति असामान्य है, परंतु इसका वितरण छिटपुट एवं स्थानिक रूप से असतत है। REE खनिजीकरण मुख्यतः फेल्सिक नाइसों एवं शिरा प्रणालियों में उपस्थित सहायक खनिज प्रावस्थाओं में निहित है। ब्लॉक में REE समृद्धि का कोई सतत एवं मानचित्रण योग्य क्षेत्र सीमांकित नहीं किया जा सका। इसके अतिरिक्त, खनिजीकरण में वह भूवैज्ञानिक एवं ग्रेड निरंतरता नहीं पाई गई, जो अधःसतही अन्वेषण हेतु उपयुक्त लक्ष्य निर्धारित करने के लिए आवश्यक होती है।

16–17 जून 2026 को आयोजित TCC-II की 31वीं बैठक में समेकित भूवैज्ञानिक मानचित्रण एवं विश्लेषणात्मक परिणामों की समीक्षा के उपरांत यह निर्णय लिया गया कि प्राप्त REE मान महत्वपूर्ण नहीं हैं तथा वेधन सहित किसी अतिरिक्त अन्वेषण कार्य की आवश्यकता नहीं है। फलस्वरूप, अन्वेषण के वर्तमान चरण में किसी खनिज संसाधन का आकलन नहीं किया गया है।

1.7.0 अनुशंसा

लांगमिपी–लाचिंग थिंग ब्लॉक में अन्वेषण कार्य को जाँच के वर्तमान चरण में समाप्त करने की अनुशंसा की जाती है। ब्लॉक में अभिज्ञात REE की उपस्थिति असामान्य होने के बावजूद छिटपुट एवं स्थानिक रूप से असतत है। महत्वपूर्ण REE समृद्धि का कोई सतत एवं मानचित्रण योग्य क्षेत्र सीमांकित नहीं किया गया है। इसके अतिरिक्त, अभिज्ञात खनिजीकरण अधःसतही अन्वेषण के लिए व्यवहार्य लक्ष्य स्थापित करने हेतु आवश्यक भूवैज्ञानिक निरंतरता अथवा ग्रेड स्थायित्व प्रदर्शित नहीं करता है।

उपर्युक्त तथ्यों के आधार पर ब्लॉक को G-3 (प्रारम्भिक) अन्वेषण चरण अथवा वेधन कार्य के लिए आगे बढ़ाने की अनुशंसा नहीं की जाती है। तथापि, ग्रेनाइट नाइस एवं शिरा प्रणालियों से संबद्ध पृथक उच्च-मूल्य REE प्राप्तियों का भविष्य के अन्वेषण कार्यक्रमों में पुनर्मूल्यांकन किया जा सकता है।

CHAPTER - I

EXECUTIVE SUMMARY

1.0.0 EXECUTIVE SUMMARY

1.1.0 Background

The Langmipi–Laching Thing Block, covering an area of 124.68 sq. km in the West Karbi Anglong District of Assam, was taken up by Mineral Exploration and Consultancy Limited (MECL) for a Reconnaissance Survey (G-4 stage) for Rare Earth Elements (REE) and associated minerals under funding of the National Mineral Exploration and Development Trust (NMEDT). The block falls in parts of Survey of India Toposheet Nos. 83C/09, 83C/10, 83C/13 and 83C/14 and lies on the eastern fringe of the Shillong Plateau within the Archaean–Proterozoic Assam–Meghalaya Gneissic Complex (AMGC). The investigation was recommended in the 1st meeting of the Technical-cum-Cost Committee-II (TCC-II) held on 26th–27th September 2024, approved in the 38th meeting of the Executive Committee (EC), NMEDT held on 29th November 2024, and sanctioned vide order dated 13th December 2024.

1.2.0 Location and accessibility

The block is bounded by six cardinal points (A–F) and extends between latitudes 25°43′26.64″ N and 25°50′36.56″ N and longitudes 92°44′02.85″ E and 92°52′04.06″ E. It covers parts of the villages of Mokyndur, Langmipi, Laching Thing, Rongpi and Thenglong. The area is approached by the Kheroni–Tahpat–Jirikinding road; the nearest railhead is Lanka (≈20 km north-east) and the nearest airport is Lokpriya Gopinath Bordoloi International Airport, Guwahati (≈250 km).

1.3.0 Geology and mineralisation

The block is underlain dominantly by migmatite, granite gneiss and augen gneiss of the AMGC, with subordinate granite, altered calcareous siliceous sandstone and Quaternary soil/alluvium, all traversed by pegmatite, quartz and quartzo-feldspathic veins. The felsic lithologies are metaluminous, potassic and highly evolved. REE mineralisation is hosted principally within the felsic gneisses and the pegmatitic and quartzo-feldspathic veins, carried by accessory monazite (the dominant carrier), zircon, titanite and apatite (allanite inferred, not confirmed petrographically). Subordinate sulphide (pyrite–chalcopyrite) and magnetite–ilmenite mineralisation is also developed, controlled by lithology, shearing/fracturing and late-stage magmatic–hydrothermal processes. All lithologies and derived media display strong LREE enrichment over HREE with a well-developed negative Eu anomaly, indicating derivation from evolved felsic crustal protoliths.

1.4.0 Exploration carried out

The G-4 reconnaissance comprised large-scale geological mapping on 1:12,500 scale over the entire 124.68 sq. km, and collection of 50 bedrock samples (BRS), 58 stream sediment samples and 65 soil (pit) samples. A total of 173 primary samples were analysed for 34 elements by ICP-MS, 15 bedrock samples for major oxides by XRF and 10 samples by XRD, supported by 10 petrographic and 5 mineragraphic studies. In accordance with the review of the 31st TCC-II, drilling and resource estimation were not undertaken.

1.5.0 Salient results

The lithology-wise and media-wise REE geochemistry (ICP-MS) is summarised below. Granite gneiss records the highest average total REE, but with a very wide range, reflecting an erratic and spatially discontinuous distribution of REE rather than sustained enrichment.

Sample medium / lithounit	N	ΣREE mean (ppm)	ΣREE range (ppm)	ΣREE+Sc+Y mean (ppm)
Granite gneiss	4	816.73	87.17–1458.80	894.74
Pegmatite vein	4	472.20	268.21–579.67	553.30
Migmatite	20	405.04	68.00–1495.00	464.03
Augen gneiss	11	359.27	27.15–680.80	433.94
Quartzo-feldspathic vein	5	334.36	108.80–734.19	409.62
Altered calcareous siliceous sandstone	5	120.23	55.55–185.27	162.60

Quartz vein	1	109.12	–	123.37
Stream sediment	58	320.66	51.88–1037.26	355.51
Soil – B horizon	21	383.85	197.64–788.70	443.41
Soil – B+C horizon	44	364.94	139.05–1235.92	428.42

Only isolated samples exceed 1000 ppm ΣREE (one granite gneiss bedrock sample, ML BRS-31 at 1458.80 ppm, and one stream sediment sample), while the majority of samples record moderate values. The high values are not spatially clustered into any continuous or mappable zone of enrichment.

1.6.0 Conclusion

The G-4 reconnaissance established that REE occurrences within the Langmipi–Laching Thing Block are anomalous but sporadic and spatially discontinuous, hosted in accessory phases within the felsic gneisses and veins. No zone of sustained, mappable REE enrichment was delineated, and the mineralisation does not exhibit the geological or grade continuity required to define a target for subsurface exploration. On review of the integrated mapping and analytical results in the 31st meeting of TCC-II (16th–17th June 2026), it was decided that the REE values are not significant and that no further exploration, including drilling, is warranted. Consequently, no mineral resource has been estimated at this stage.

1.7.0 Recommendation

Exploration in the Langmipi–Laching Thing Block is recommended to be concluded at the present stage of investigation. The REE occurrences identified within the block are anomalous but sporadic and spatially discontinuous. No sustained, mappable zone of significant REE enrichment has been delineated, and the observed mineralisation does not demonstrate the geological continuity or grade persistence required to establish a viable target for subsurface exploration. In view of the above, the block is not recommended for advancement to G-3 (Preliminary) Stage of Exploration or drilling. However, the isolated high-value REE occurrences associated with granite gneiss and vein systems may be revisited in future investigations.

CHAPTER - II

DETAILS OF THE QUALIFIED PERSON(S) / EXPLORATION AGENCY

2.0.0 DETAILS OF THE QUALIFIED PERSON(S) / EXPLORATION AGENCY

2.1.0 Details of the Exploration Agency

Name of the Exploration Agency: Mineral Exploration and Consultancy Limited (MECL), formerly Mineral Exploration Corporation Limited — A Government of India Enterprise (Miniratna Category-I PSE), Ministry of Mines, Government of India.

Address: Dr. Babasaheb Ambedkar Bhavan, High Land Drive Road, Seminary Hills, Nagpur – 440006, Maharashtra.

E-mail: cmd@mecl.co.in; gm-exploration@mecl.co.in

Telephone: 0712-2510289; 0712-2511829

2.2.0 Details of qualification and experience of persons associated with the exploration

The exploration, data generation, integration and preparation of this Geological Report were carried out by a multidisciplinary team of MECL. The qualified person(s) accepting responsibility for the report, together with the personnel associated with each component of the investigation, are listed below.

Table No 2.1

Details of Personnel Associated with The Exploration Langmipi-Laching Thing Area, Dist.: West Karbi Anglong, Assam

1	**Overall Planning, Co-ordination & Overall supervision**	:	Shri Shrikant Sharma, Dy.GM/HoD (Exploration) Shri Naveen Kumar Pala, Dy.GM (Exploration)
2	**Project management & Field Operation**	:	Shri Vashkar Jit Mahanta, E.T. (Geology)/OIC
3	**Chemical Laboratory, MECL**	:	Shri Rohit Kumar Sharma, Head (Labs)/ Manager (Chemistry)
		:	Dr. (Mrs.) Deepti R. Rahangdale, Manager (Chemistry)
4	**Petrological Laboratory, MECL**	:	Shri Sayantan Pal, Manager (Geology)
5	**Data Processing & Documentation**	:	Shri Vashkar Jit Mahanta, E.T. (Geology)
		:	Mrs. Moumita Ghosh, Assistant Manager (Geology)
		:	Shri Sayandeep Chakraborty, Assistant Manager (Geology)
		:	Shri Uday Ashok Patil, Jr. Superidentent (I.T)
6	**Reprography & Printing**	:	Shri P.S Negi, OIC, Survey
			Shri Durgesh Devarshee, ASMO

CHAPTER - III

3.0.0. TITLE AND OWNERSHIP

3.1.0 GEOLOGICAL REPORT ON RECONNAISSANCE SURVEY (G-4 STAGE) FOR REE & ASSOCIATED MINERALS IN LANGMIPI-LACHING THING AREA DISTRICT- WEST KARBI ANGLONG, ASSAM

Ownership: Government of Assam

Name of Prospector: **MINERAL EXPLORATION AND CONSULTANCY LIMITED (Formerly Mineral Exploration Corporation Limited)**
(A Govt. of India Enterprise; A Miniratna-I PSE)
(Ministry of Mines, Govt. of India)

Address of Prospector: Dr. Babasaheb Ambedkar Bhavan, High Land Drive Road, Seminary Hills, Nagpur, Pin- 440006

E-mail of Prospector: cmd@mecl.co.in; gm-exploration@mecl.co.in

Telephone numbers of Prospector: 0712-2510289; 0712-2511829

3.2.0 Details of period of Prospecting

3.2.1 Reconnaissance Survey (G4) for REE and associated minerals in Langmipi-Laching Thing Block, West Karbi Anglong District, Assam was recommended in the 1st meeting of the Technical-cum-Cost Committee-II (TCC-II) of NMEDT held on 26th–27th September 2024 and was approved in the 38th meeting of the Executive Committee (EC), NMEDT held on 29th November 2024. The same was intimated to MECL vide MoM letter No. F/No./23/532/2024-NMET/591 dated 13th December 2024 (Annexure VIII).

3.2.2 Pursuant to the approval, and after mitigation of the local issues and the monsoon period, MECL commenced the field work on 10th November 2025 and completed the first phase of exploration by March 2026. The first phase comprised detailed geological mapping and collection of surface samples, including bedrock channel samples and petrographic samples, together with pit (soil) samples and stream sediment samples. The results of the first phase were reviewed in the 25th meeting of TCC-II held on 17th–18th March 2026, wherein the Committee opined that the project would be reviewed only after receipt of the complete analytical results. After receipt of the analytical results, the block was reviewed in the 31st meeting of TCC-II held on 16th–17th June 2026, wherein the Committee opined that no further work was required in the block as the REE values are not significant; accordingly, the Committee advised MECL not to take up further exploration, including drilling, and to prepare and submit the Geological Report to NMEDT by 12th September 2026 (Annexure IX).

CHAPTER - IV

4.0.0 DETAILS OF THE AREA UNDER STUDY

4.1.0 Location of the Block

4.1.1 The Langmipi-Laching Thing Block is situated in the West Karbi Anglong District of Assam and falls under the administrative jurisdiction of Karbi Anglong Autonomous Council. The block covers parts of the villages of Mokyndur, Langmipi, Laching Thing, Rongpi and Thenglong, and forms a part of the Survey of India (SOI) Toposheet Nos. 83C/09, 83C/10, 83C/13 and 83C/14. The location map of the block is furnished as Text Fig No-4.1 as well as Plate No-I.

4.1.2 Geographically, the block is demarcated by six cardinal boundary points (A to F), whose coordinates have been established in both the Geographic Coordinate System (Datum WGS-84) and Universal Transverse Mercator (UTM) Zone 46N projection. The block extends between latitudes 25°43′26.64″ N and 25°50′36.56″ N, and longitudes 92°44′02.85″ E and 92°52′04.06″ E. The coordinates of the cardinal points of the block boundary are given below in Table No. 4.1 as well as Annexure IA.

Table No-4.1

Coordinates of cardinal points of Langmipi-Laching Thing Area, District: West Karbi Anglong, Assam

Sl. No.	Point	GCS WGS 1984 (DMS)		UTM Zone: 46N (m)		Area (sq km)
		Latitude	Longitude	Easting	Northing	
1	A	25°48'1.29"N	92°44'2.85"E	473346.98	2853602.01	124.68
2	B	25°49'57.74"N	92°48'9.82"E	480229.55	2857172.08	
3	C	25°50'36.56"N	92°52'4.06"E	486751.69	2858358.07	
4	D	25°48'46.13"N	92°52'4.06"E	486748.27	2854961.09	
5	E	25°43'26.64"N	92°48'37.84"E	480992.29	2845140.19	
6	F	25°43'26.64"N	92°44'2.85"E	473329.94	2845153.41	

4.2.0 Accessibility to the Block

4.2.1 The Langmipi-Laching Thing block is connected through Kheroni-Tahpat-Jirkinding road passes through the eastern part of the block. Lanka is the nearest railhead which is located 20 km north eastern side of the block. The nearest airport is Lokpriya Gopinath Bordoloi International Airport which is located at a distance of 250 km West from the block.

4.3.0 Land Use Pattern

4.3.1 The Langmipi-Laching Thing Block covers a total aerial extent of approximately 124.68 sq. km (12468 ha) and exhibits a mixed land-use pattern comprising forest land, private land, agricultural areas, and water bodies. The dominant land-use category is Reserved Forest, occupying approximately 8104.2 ha, which constitutes about 65% of the total block area. This indicates that the block is predominantly under forest cover and suggests limited anthropogenic disturbance over a major portion of the area.

4.3.2 The remaining 4363.8 ha (35%) consists of privately owned land, representing areas utilized for settlement, cultivation, and other local land-use activities. Within the private land category, approximately 1134.59 ha is under agricultural use, accounting for around 26% of private land and 11% of the total block area. Agricultural activities in the block are mainly dependent on surface water availability, particularly from the stream network flowing through the agricultural fields, indicating a predominantly stream-fed or rain-supported cultivation system.

4.3.3 In addition, approximately 261.83 ha of the total area is occupied by a lake/water body, which contributes to local hydrological conditions and may support agricultural requirements and ecological balance within the block.

4.3.4 Overall, the land-use pattern of Langmipi-Laching Thing Block reflects a forest-dominated landscape with localized agricultural activity concentrated within privately owned areas and supported by natural surface water resources. This distribution indicates relatively low land-use intensity and highlights the importance of forest and water resources in controlling the environmental and socio-economic characteristics of the block.

4.4.0 Mineral(s) under investigation or granted under license or lease

4.4.1 The Langmipi-Laching Thing Block was explored for the occurrences of Rare Earth Elements and associated minerals.

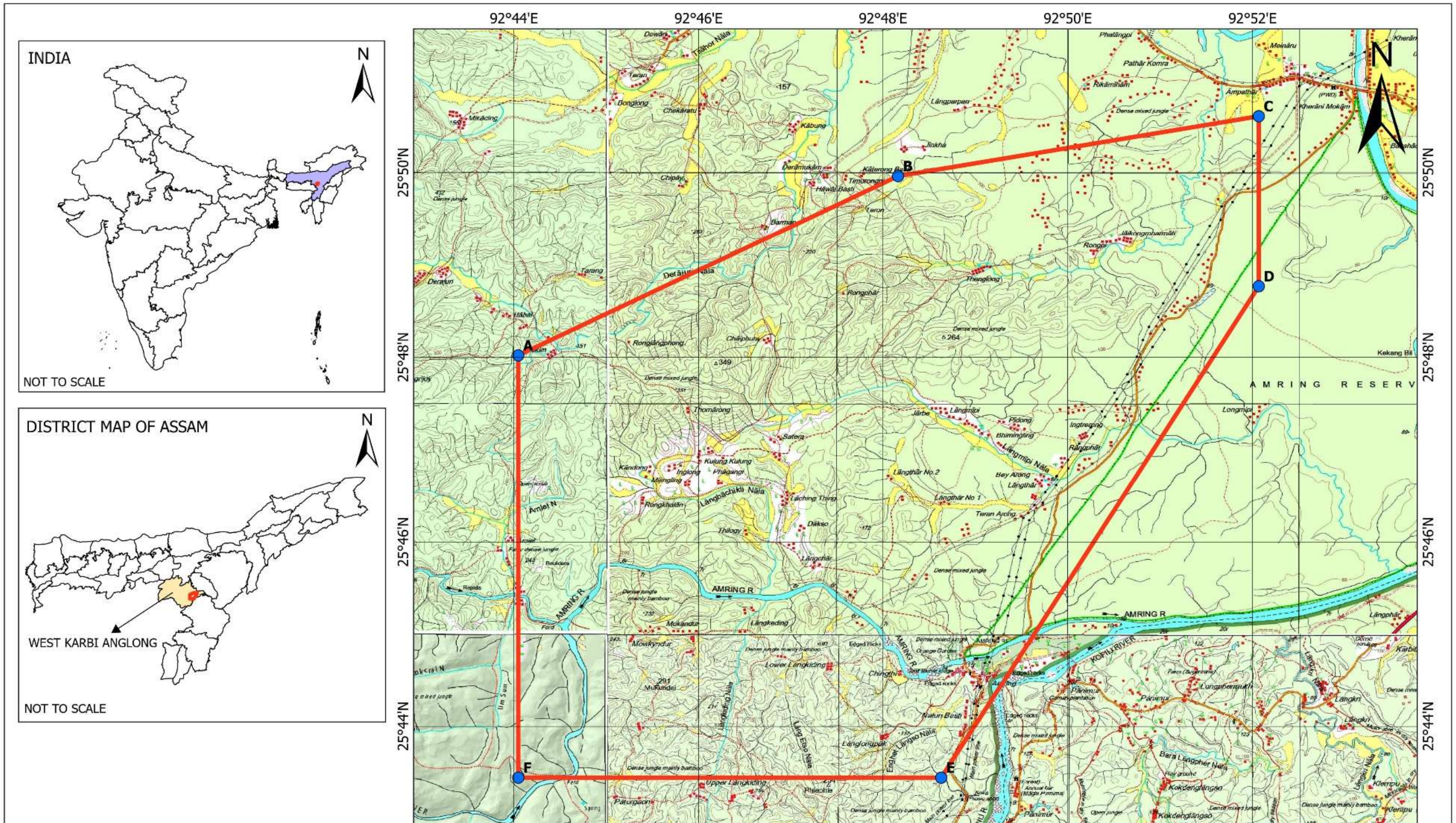

Co-ordinate Points in GCS (DMS)			UTM ZONE 46N (m)	
Points	Latitude	Longitude	Easting	Northing
A	25° 48' 1.27" N	92° 44' 2.32" E	473346.98	2853602.01
B	25° 49' 57.73" N	92° 48' 9.3" E	480229.55	2857172.08
C	25° 50' 36.62" N	92° 52' 3.74" E	486751.69	2858358.07
D	25° 48' 46.54" N	92° 52' 3.74" E	486748.27	2854961.09
E	25° 43' 26.4" N	92° 48' 37.86" E	480992.29	2845140.19
F	25° 43' 26.4" N	92° 44' 2.32" E	473329.94	2845153.41

Text Fig. 4.1: Location map of Langmipi-Laching Thing Block, District West Karbi Anglong, Assam

CHAPTER - V

5.0.0 PHYSIOGRAPHY AND ENVIRONMENT

5.1.0 Topography

5.1.1 The Langmipi–Laching Thing Block is characterized by moderately rugged to rugged topography, with elevations generally ranging from approximately 300 m to 850 m above mean sea level (MSL). The terrain consists of a series of elongated hills, ridges, narrow valleys, and steep to moderately steep slopes, reflecting prolonged fluvial dissection of the Precambrian basement rocks. Hill slopes are commonly covered by dense forest and thick residual soil, while rocky outcrops are exposed along ridge crests, stream channels, road cuts, and locally on steep hill slopes.

5.1.2 The higher elevation zones are represented by hilltops and elevated ridges, whereas the lower elevation areas correspond to valleys, stream channels, and gently sloping terrain. The gradual to moderate slope development facilitates surface runoff from elevated regions towards the lower reaches, contributing to the formation and maintenance of local drainage systems.

5.1.3 The topographic configuration of the block exerts an important control on drainage pattern, weathering processes, soil development, vegetation distribution, and land use activities. Agricultural activities are mainly concentrated in relatively low-lying and gently sloping areas where water availability is supported by stream flow, while the elevated areas remain predominantly under forest cover.

5.1.4 Overall, the Langmipi-Laching Thing Block exhibits a moderate relief landscape with dissected hill slopes and intervening valleys, reflecting active geomorphic processes and topographic control over hydrological and land-use characteristics of the area.

5.2.0 Connectivity

5.2.1 The Langmipi-Laching Thing Block is well connected through road, rail, and air transportation facilities, which provide accessibility for exploration activities and movement of personnel and materials. The block is accessible through the

Kheroni–Tahpat–Jirikinding Road, which passes through the eastern part of the block and provides the principal road connectivity to the area.

5.2.2 Within the study area, accessibility is supported by a network of metalled roads and kutcha (unpaved) roads, most of which originate from the Kheroni–Tahpat–Jirikinding Road and extend into different parts of the block. In addition, foot tracks and local trails are developed within the interior areas, facilitating access to forested and elevated terrains where vehicular movement is limited.

5.2.3 The nearest railway connectivity is provided by Lanka Railway Station (LKA), located approximately 20 km northeast of the block, offering linkage to major regional and national railway networks. The nearest airport facility is available at Lokpriya Gopinath Bordoloi International Airport, Guwahati, which provides air connectivity to the study area and supports logistical requirements.

5.2.4 Overall, the Langmipi-Laching Thing Block possesses moderate to good connectivity, with primary access controlled by the national highway network and secondary access supported by local roads and foot tracks, enabling efficient movement for geological exploration and field operations.

5.3.0 Population

5.3.1 The Langmipi–Laching Thing Block is sparsely populated, with settlements concentrated along the road corridors and narrow valley floors. The principal villages within and around the block are Langmipi and Laching Thing, having populations of 2,587 and 843, respectively, as per the Census of India 2011. Smaller settlements such as Langkiding and a number of scattered hamlets are also present in the vicinity of the block. The total population of the principal villages within the study area is approximately 3,600.

5.3.2 The inhabitants are predominantly members of the Karbi Scheduled Tribe, with smaller populations of Dimasa, Garo, Khasi, and other indigenous communities. Agriculture, shifting cultivation (*jhum*), horticulture, livestock rearing, and collection of forest produce constitute the primary sources of livelihood.

5.3.3 The population density within the block is generally low due to the rugged hilly terrain, dense forest cover, and limited cultivable land. Overall, the Langmipi-Laching Thing Block exhibits a sparsely populated rural settlement pattern, where habitation is largely confined to Langmipi and Laching Thing village and influenced by the physical characteristics and land-use distribution of the area.

5.4.0 Socio Demographic profile

5.4.1 The Langmipi–Laching Thing Block is situated in the West Karbi Anglong District, Assam, and is characterized by a sparse rural population distributed among small, scattered villages. The area is predominantly inhabited by the Karbi Scheduled Tribe, with smaller populations of Dimasa, Khasi, Garo, Bodo, and Assamese communities. Scheduled Tribes constitute more than 95% of the population in the principal villages, reflecting the tribal character of the region.

5.4.2 Educational facilities are available in the form of primary and middle schools in larger villages, whereas higher secondary schools and colleges are located in nearby towns such as Kheroni and Hamren. Basic healthcare services are provided through Primary Health Centres (PHCs) and Sub-Centres, while advanced medical facilities are available at Hamren, Diphu, and Guwahati.

5.4.3 Agriculture forms the backbone of the local economy. The majority of the population depends on rain-fed agriculture, shifting cultivation (jhum), horticulture, livestock rearing, and the collection of minor forest produce for their livelihood. Crops such as paddy, maize, millets, ginger, turmeric, banana, pineapple, and various seasonal vegetables are cultivated. Collection of bamboo, cane, fuelwood, and other non-timber forest products also supplements household income. Wage labour under government development programmes provides seasonal employment.

5.4.4 The Karbi language is the predominant language spoken in the area, while Assamese, Hindi, and English are commonly used for education, administration, and commercial activities. Traditional tribal customs, festivals, and community institutions continue to play an important role in the social and cultural life of the inhabitants.

5.4.5 Overall, the socio-economic condition of the Langmipi–Laching Thing Block reflects a predominantly tribal, agrarian economy, where livelihoods are closely linked to agriculture and forest resources. The rugged terrain, dense forest cover, and relatively limited infrastructure have influenced settlement patterns, accessibility, and the pace of socio-economic development.

5.5.0 Historical / Archaeological Site

5.5.1 Based on field observations and available records, no historical or archaeological sites have been identified within the Langmipi-Laching Thing Block. The study area does not contain any known monuments, heritage structures, archaeological remains, or culturally significant historical features of protected or documented importance.

5.5.2 The absence of such sites indicates that the block is predominantly characterized by natural landscapes, forest cover, agricultural land, and rural habitation, with no recognized historical or archaeological constraints affecting land use or exploration activities within the area.

5.6.0 Forests, sanctuaries, national park and wild life sanctuaries

5.6.1 The Langmipi–Lachingthin Block is situated in the forested hill tract of West Karbi Anglong District, Assam, where tropical forests constitute the dominant land cover. The block is characterized by dense to moderately dense tropical moist deciduous and semi-evergreen forests, interspersed with secondary forests, bamboo brakes, and patches of shifting cultivation (*jhum*). The vegetation is dominated by species such as *Sal (Shorea robusta)*, *Hollong (Dipterocarpus macrocarpus)*, *Nahor (Mesua ferrea)*, *Ajhar (Lagerstroemia speciosa)*, bamboo, cane, and a variety of shrubs and climbers.

5.6.2 The exploration block does not fall within any National Park, Wildlife Sanctuary, Tiger Reserve, Elephant Reserve, Eco-sensitive Zone, or other notified Protected Area.

5.7.0 Flora and Fauna within and nearby

5.7.1 The Langmipi–Lachingthin Block is situated within the forested hill tract of West Karbi Anglong District, Assam, where the natural vegetation is dominated by tropical moist deciduous and semi-evergreen forests. The terrain comprises densely forested hills, bamboo brakes, secondary forests, shrublands, and patches of grasslands interspersed with shifting cultivation (*jhum*) and agricultural fields. Thick undergrowth, consisting of grasses, shrubs, climbers, and ferns, is common throughout the block, particularly along valley slopes and stream courses.

5.7.2 The dominant tree species include Sal (*Shorea robusta*), Hollong (*Dipterocarpus macrocarpus*), Nahor (*Mesua ferrea*), Bonsum (*Phoebe cooperiana*), Ajhar (*Lagerstroemia speciosa*), Gamari (*Gmelina arborea*), Sissoo (*Dalbergia sissoo*), Simul (*Bombax ceiba*), Terminalia spp., Artocarpus spp., Ficus spp., and Albizia spp. Bamboo (*Bambusa* spp. and *Dendrocalamus* spp.), cane (*Calamus* spp.), wild banana (*Musa* spp.), and numerous medicinal and ethnobotanical plant species are abundant in the area. The forest floor is covered by grasses, herbs, orchids, ferns, mosses, and climbers, particularly during the monsoon season.

5.7.3 The forests support a rich diversity of wildlife typical of the Karbi Anglong hill ecosystem. Commonly encountered mammals include the Asian Elephant (*Elephas maximus*), Leopard (*Panthera pardus*), Wild Boar (*Sus scrofa*), Barking Deer (*Muntiacus muntjak*), Hog Deer (*Axis porcinus*), Sambar (*Rusa unicolor*), Indian Gaur (*Bos gaurus*), Capped Langur (*Trachypithecus pileatus*), Rhesus Macaque (*Macaca mulatta*), Assamese Macaque (*Macaca assamensis*), Hoolock Gibbon (*Hoolock hoolock*), Indian Hare (*Lepus nigricollis*), and Small Indian Civet (*Viverricula indica*).

5.7.4 Overall, the Langmipi-Laching Thing Block supports a forest-dominated ecosystem characterized by bamboo-rich vegetation, mixed tree species including teak and simul, and associated wildlife populations, indicating the ecological significance of the forest landscape and its role in sustaining local biodiversity.

5.8.0 Drainage Pattern

5.8.1 The drainage pattern of the Langmipi-Laching Thing Block is controlled primarily by the topography and geomorphological characteristics of the area. The block is characterized by moderately to highly undulating terrain comprising ridges, hills, and intervening valleys, which influence the development and orientation of surface drainage channels.

5.8.2 The drainage density of the block is moderate to high, owing to the rugged topography, high seasonal rainfall, relatively impermeable crystalline rocks, and well-developed fracture systems. The alignment of several stream segments along NW–SE and NE–SW structural trends indicates that regional lineaments, faults, and shear zones have exerted considerable influence on the evolution of the drainage network.

5.8.3 The block falls within the Kopili River Basin, with the Amreng River and Dera River forming the principal drainage systems within the study area. The Amreng River, an important tributary of the Kopili River, drains a major part of the block, while the Dera River and numerous first-, second-, and third-order seasonal streams constitute the secondary drainage network. These streams originate from the rugged hill slopes and ultimately discharge into the Amreng River and subsequently into the Kopili River. The drainage characteristics of the district are controlled by the upper catchment of the Kopili River, including the Amreng drainage system.

5.8.4 The drainage configuration reflects the influence of terrain relief, slope orientation, and structural controls, resulting in efficient surface runoff and stream development. The stream network also plays a significant role in supporting local agricultural activities, sediment transport, and maintaining the hydrological balance of the Langmipi-Laching Thing Block.

5.9.0 Climatic Condition

5.9.1 The Langmipi-Laching Thing Block experiences a humid subtropical climate characterized by warm, humid summers, a pronounced southwest monsoon, and cool, dry winters. Owing to the undulating topography and variation in elevation across the Karbi Anglong hills, local climatic conditions vary within the block.

5.9.2 The block receives abundant rainfall under the influence of the Southwest Monsoon, with approximately 80–85% of the annual precipitation occurring between May and September. The average annual rainfall in the district is about 2,416 mm, although local variations occur due to topographic effects. Relative humidity generally varies between 73% and 85%, reaching its maximum during the monsoon months.

5.9.3 The climate is broadly divided into three distinct seasons: summer (March–May), monsoon (June–September), and winter (November–February), with October representing the transition from the monsoon to the winter season. During summer, the weather remains warm and humid, with maximum temperatures generally ranging from 23°C to 32°C, while winter temperatures vary between 6°C and 12°C. The mean annual air temperature is approximately 23.5°C.

5.9.4 Overall, the climatic conditions of the Langmipi-Laching Thing Block are favourable for the development of dense vegetation, agricultural activities, and stream-fed hydrological systems, while seasonal rainfall and moderate temperature variations play an important role in controlling geomorphic and ecological processes within the area.

5.10.0 Any other factor having potential to affect the viability of the project and assessment of resources and reserves.

5.10.1 The feasibility or pre-feasibility studies were not undertaken during the G-4 stage of exploration, since the preliminary exploration did not establish mineralization to warrant further techno-economic evaluation or resource/reserve estimation.

CHAPTER - VI

6.0.0 INFRASTRUCTURE

6.1.0 Local infrastructure Connectivity and facilities

6.1.1 The Langmipi-Laching Thing Block possesses basic rural infrastructure that supports the day-to-day socio-economic requirements of the local population. The available infrastructure facilities indicate the presence of essential educational, healthcare, recreational, and community services within and around the habitation areas.

6.1.2 Basic civic infrastructure is available in the nearby service centres of Kheroni, Jirikinding, and Hamren. Educational facilities include primary and middle schools in villages such as Langmipi and Lachingthin, whereas secondary schools, higher secondary schools, and colleges are available at Kheroni and Hamren. Healthcare facilities are provided through the Kheroni Model Hospital, Primary Health Centres (PHCs), and Sub-Centres, while specialized medical services are available at Hamren Civil Hospital and larger hospitals in Diphu and Guwahati.

6.1.3 The villages within and around the block have access to electricity, mobile telecommunication, and drinking water through springs, tube wells, and community water supply schemes. Weekly markets, banking facilities, public distribution system (PDS) outlets, and other essential services are available at Kheroni, which serves as the principal commercial centre for the surrounding villages. Mobile network coverage is available in most roadside areas but remains intermittent in the interior forested and hilly terrain.

6.1.4 Overall, the infrastructure within the Langmipi-Laching Thing Block is rural in character and provides basic educational, healthcare, recreational, and social amenities, supporting the livelihood and community development of the local inhabitants while maintaining connectivity with surrounding areas.

CHAPTER - VII

7.0.0. GEOLOGY

7.1.0. Regional Geology

7.1.1 The study area in toposheet No. 83C/09, 83C/10, 83C/13 and 83C/14 lies in the eastern fringe of the Shillong Plateau. The study area is regionally sandwiched between NNW-SSE trending Kopili Fault in the east NE-SW trending Barapani-Tyrsad shear zone in the north west.

7.1.2 The Assam Meghalaya Gneissic Complex is considered as the tectonically detached and uplifted part of the Indian Peninsular Shield separated by the "Garo-Rajmahal Gap" (Evans 1964) from the Chhotanagpur Gneissic Complex. The main structural trend in the Assam Meghalaya Plateau is NE-SW, which is persistent all over the area and variation of this trend is apparent at places near the contact of granite pluton intrusions. The NE extension of the Assam Meghalaya Plateau is known as Mikir Hills. The Mikir Hills are separated from the Meghalaya plateau by the alluvium tract of the Kopili River and the NE-SW Kopili Fault (Nandy, et al., 1986).

7.1.3 The lithounits in and around the region belong to the Archean-Proterozoic Assam-Meghalaya Gneissic Complex (AMGC) which is unconformably overlain by metasedimentary rocks by Paleo-Meso Proterozoic Shillong Group, all intruded by Neo-Proterozoic-early Palaeozoic granite plutons. The AMGC comprises of ortho and para gneisses, schists, migmatites and granulites and the Shillong Group comprises meta-sedimentary rocks of Quartzite, phyllite, quartz sericite schist, conglomerate.

7.1.4 In the present study region around Kheroni-Tahpat-jirkinding, exposures include granite gneiss, migmatite, augen gneiss and limestone of the AMGC (Text figure 7.1 as well as Plate No II). Numerous quartz, pegmatite and aplite veins traverse all lithologies and are interpreted as late-stage magmatic-hydrothermal products of granite emplacement. Locally, some quartz veins carry sparse disseminated base-metal sulphide specks; this sulphide mineralisation is minor and of no established economic significance at the present stage of investigation.

7.1.5 The Shillong Plateau represents one of the most tectonically dynamic intraplate regions of northeastern India and is interpreted as an uplifted horst or pop-up block within the Himalayan foreland basin. Its present-day tectonic configuration is primarily governed by the ongoing convergence between the Indian and Eurasian plates, together with tectonic interactions associated with the Indo-Burman ranges. Geodetic studies indicate that approximately 1.5–3.5 mm/year of north–south shortening is currently being accommodated within the plateau, contributing to its continued uplift and deformation.

7.1.6 The plateau is structurally bounded by several major crustal-scale fault systems, namely the Brahmaputra Fault System to the north, the Dauki Fault to the south, the Kopili Fault to the east, and the Dhubri Fault to the west. These fault zones exert a significant influence on the regional tectonic framework and have played an important role in shaping the present geomorphology and seismic behaviour of the plateau. The basement rocks have experienced repeated episodes of magmatism, metamorphism, deformation and crustal reworking rather than representing a single tectonic event. Geochronological investigations indicate major felsic magmatic episodes at approximately 1.8 Ga, 1.6 Ga, 1.4 Ga and 0.5 Ga, with evidence for recycling of older Neoarchaean crust into the Proterozoic basement (Yin et al., 2017)

7.1.7 The dominant structural fabric of the Shillong Plateau exhibits a pronounced NE–SW orientation and is reflected in the alignment of foliation planes, lithological contacts, fracture networks, and fault systems. The Precambrian to Early Palaeozoic foliation (~500 Ma) represents an ancient tectono-metamorphic fabric developed during the early geological evolution of the basement and is distinct from the much younger Neogene pop-up uplift (ca. 5.2–4.9 Ma). The Neogene uplift mainly resulted in the exhumation and reactivation of pre-existing structures and did not generate the original foliation observed in the basement rocks (Bilham & England, 2001; Govin et al., 2018). The lithological and structural architecture of the AMGC therefore records a poly-orogenic history. Zircon and monazite geochronology has identified Mesoproterozoic age populations around 1.6–1.5 Ga, followed by younger Grenvillian/Neoproterozoic events around 1.1–0.8 Ga, and a pronounced Pan-African/Early Palaeozoic event around 500–470 Ma. In the Sonapahar region, for example, monazite domains of approximately 1571 ± 22 Ma, 1034 ± 91 Ma and 478 ± 7 Ma have been reported, whereas other studies have identified populations around 1472 Ma, 1078 Ma and ~500 Ma. These results indicate that the AMGC has undergone repeated thermal and tectonic reworking, with the youngest Cambrian event substantially overprinting the older basement record.

7.1.8 U–Pb SHRIMP zircon studies have established that several granite plutons cutting the basement and Shillong Group were emplaced during the Cambrian, with reported ages of approximately 529 Ma, 516 Ma, 513 Ma, 507 Ma and 535 Ma. These granitoids are broadly correlated with the Pan-African tectonothermal activity associated with the assembly of East Gondwana, and their emplacement is considered an important expression of crustal reworking during the late stages of Gondwana assembly. The Cambrian magmatism also demonstrates that the basement was not simply passively deformed but underwent substantial crustal melting and granitoid production during the Early Palaeozoic (Choudhary et al., 2017)

7.1.9 The eastern boundary of the plateau is delineated by the Kopili Fault, a NE–SW trending dextral strike-slip to oblique-slip fault that separates the Shillong Plateau from the Mikir Hills and the Kopili Valley. The fault remains seismically active, exhibiting estimated slip rates of about 2–3 mm/year, and constitutes one of the principal sources of seismicity in the region. Repeated episodes of uplift, fault reactivation, granitoid emplacement, and prolonged denudation have collectively resulted in the present-day structural architecture of the Shillong Plateau, characterized by fault-bounded basement highs, lineament-controlled intrusive bodies, and extensive brittle deformation manifested by joints, fractures, and quartz–pegmatite vein systems.

7.1.10 The regional Stratigraphic Succession around the area as established by GSI is furnished below-

Table No 7.1

Regional Stratigraphy of Meghalaya (GSI, Misc. Pub. No.30 Part IV Vol 2(ii) Meghalaya, 2009).

Age	Group Name	Formation	Lithology
HOLOCENE	**Newer Alluvium**	Unclassified	Sand, silt and clay
PLEISTOCENE	**Older Alluvium**	Unclassified	Sand, clay, pebble, gravel and boulder deposit
--------------------Unconformity--------------------			
MIO-PLIOCENE		Dupitila Formation	Mottled clay, feldspathic sandstone and conglomerate
--------------------Unconformity--------------------			
OLIGOMIOCENE	**Garo Group**	Chengapara Formation (700m) Baghmara Formation (530m) Simsang Formation (1150m)	Coarse sandstone, siltstone, clay and marl Coarse feldspathic sandstone pebble, conglomerate, clay, silty clay with fossiliferous limestone horizon at the top Siltstone and fine sandstone and alternations of siltstone-mudstone
EOCENEOLIGO CENE	**Barail Group**	------------------------	Coarse sandstone, shale, carbonaceous shale with streaks and minor lenses of coal
PALAEOCENEE OCENE	**Jaintia Group**	Kopili Formation (50m)	Shale, Sandstone, marl
		Shella Formation (600m)	Upper Sylhet Limestone (Prang Limestone) Upper Sylhet Sandstone (Narpuh Sandstone) Middle Sylhet Limestone (Umlatdoh Limestone) Middle Sylhet Sandstone (Lakadong sandstone) Lower Sylhet Limestone (Lakadong Limestone) Lower Sylhet Sandstone (Therria Sandstone)
		Langpar Formation (100m)	Calcareous shale, sandstone and limestone
UPPER CRETACEOUS	**Khasi Group**	Mahadek Formation(150m) Conglomerate (25m) Jadukata Formation(140m)	Arkosic sandstone (often Glauconitic and Uraniferous) Conglomerate Conglomerate/sandstone
--------------------Unconformity--------------------			
CRETACEOUS	**Alkaline-Ultramafic-Carbonatite Complex of Sung**	------------------------	Pyroxenite-Serpentinite with abundant development of melilite pyroxene rock, ijolite, syenite and carbonatite
--------------------Unconformity--------------------			
CRETACEOUS	**Sylhet Trap (600m)**	------------------------	Basalt, alkali basalt, rhyolite and acid tuff

Age	Group Name	Formation	Lithology
---Unconformity---			
CARBONIFEROUS TO PERMIAN	**Lower Gondwana**	Karharbari Formation	Very coarse to coarse grained sandstone with conglomerate lense, siltstone, shale, carbonaceous shale and coal
		Talchir Formation	Basal tillite with sandstone bands, siltstone and shale
---Unconformity---			
NEO PROTEROZOIC TO EARLY PALAEOZOIC		Granite plutons: Kyrdem Granite Pluton Nongpoh Granite Mylliem Granite South Khasi Granite	Porphyritic coarse granite, pegmatite, aplite/quartz vein traversed by epidiorite, dolerite and basal dykes
---Intrusive contact---			
PROTEROZOIC	**Khasi basic-Ultrabasic intrusive (Khasi greenstone)**	------------------------	Epidiorite, dolerite, amphibolite and pyroxenite dykes and sills.
PALAEO-MESOPROTEROZOIC	**Shillong Group**	------------------------	Quartzite, phyllite, quartz sericite schist, Conglomerate.
---Unconformity---			
ARCHAEAN (?)-PROTEROZOIC	Meghalaya Gneissic Complex		Biotite gneiss, biotite hornblende gneiss, granite gneiss, mica schist, sillimanite quartz schist, biotite-granulite-amphibolite, pyroxene granulite, gabbro and diorite.

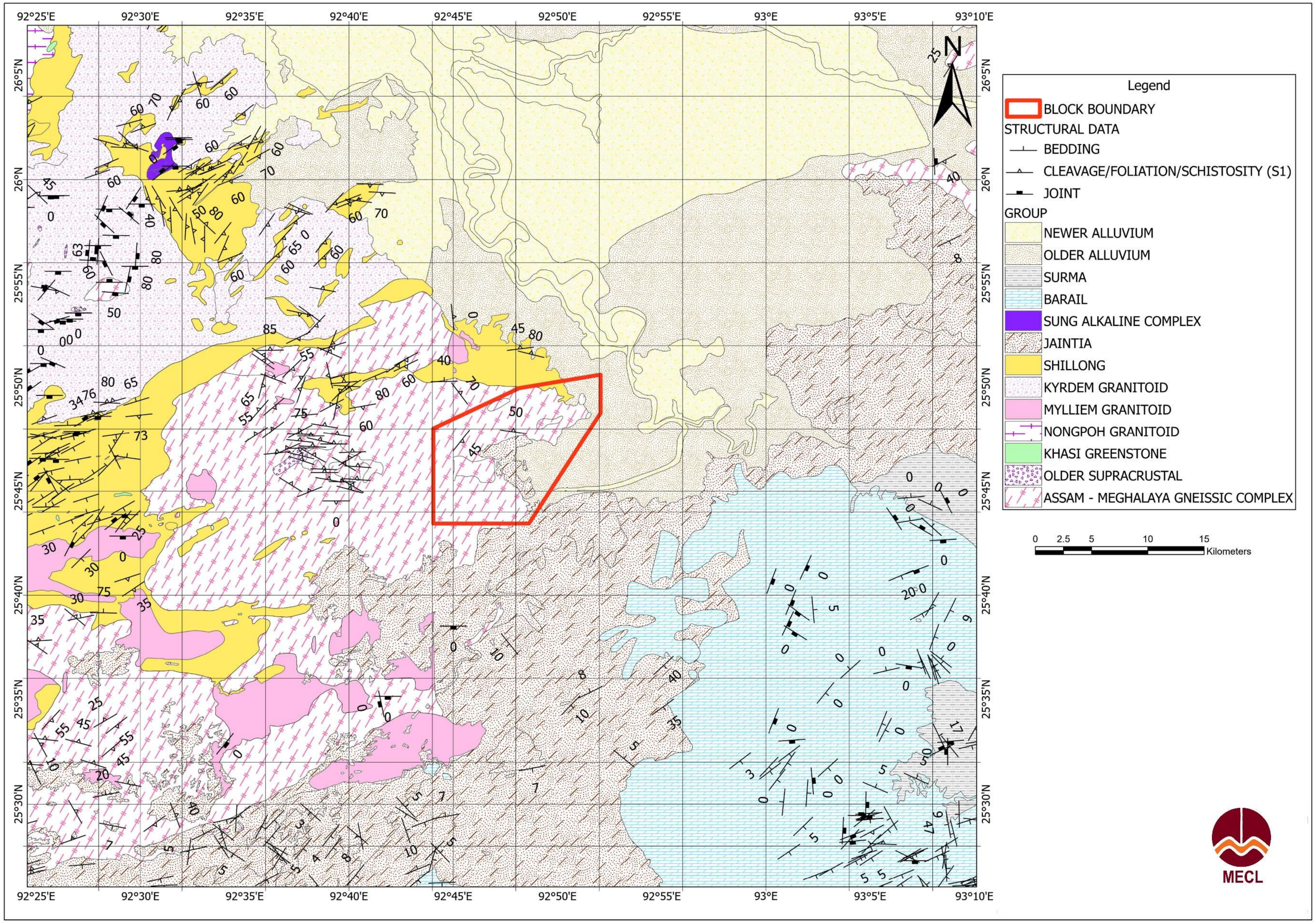

Text Fig 7.1: Regional Geology Map of the study region.

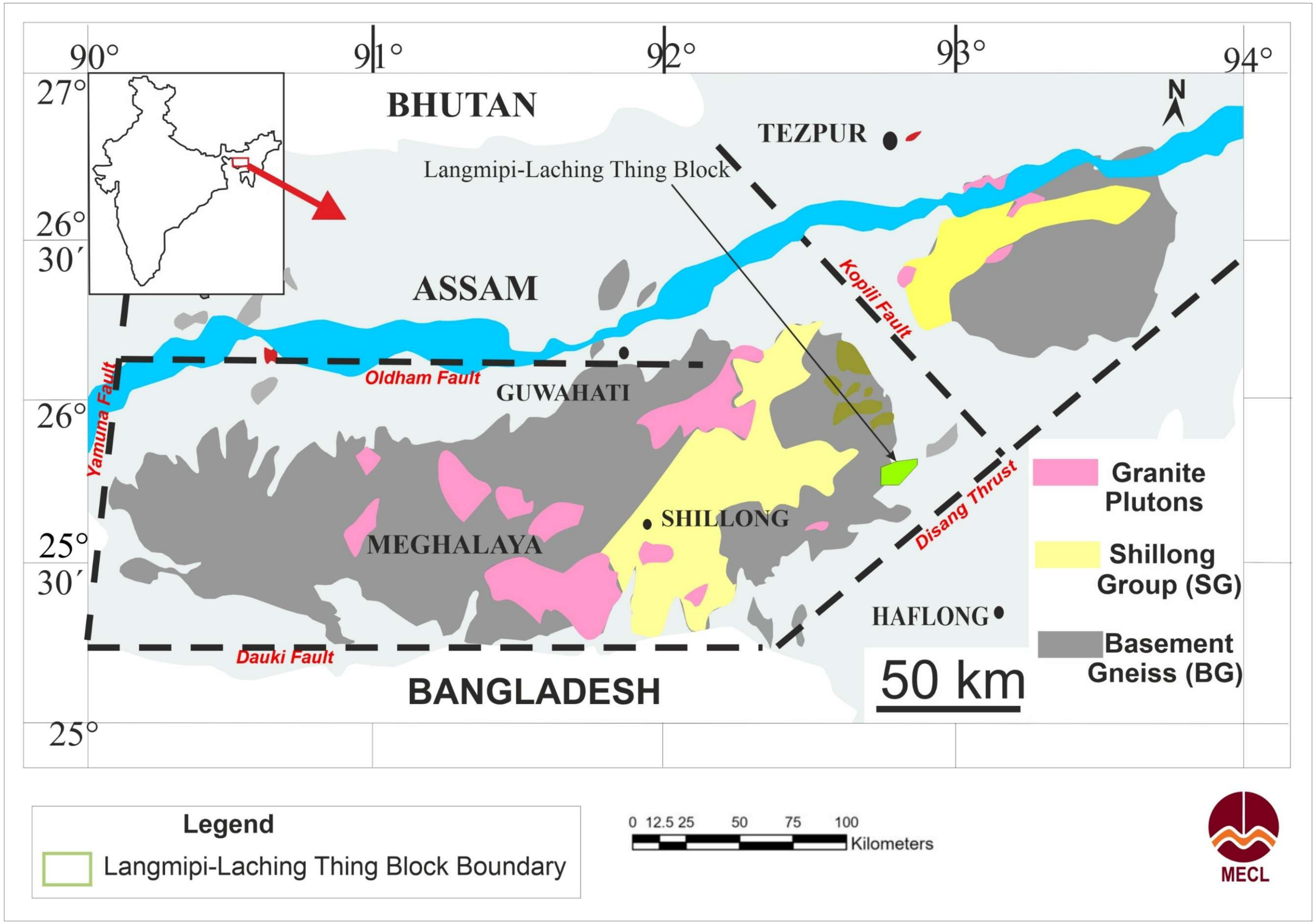

Text Fig 7.2 Tectonic map of Shillong Plateau.

7.2.0 GEOLOGY OF THE BLOCK

7.2.1 The Langmipi-Laching Thing Block mainly composed of Migmatite, Granite Gneiss, Augen Gneiss, with subordinate altered calcareous siliceous sandstone forming a thin cover in the north. Pegmatite veins, Quartzo feldspathic vein and Quartz vein are intruded into the Granite Gneiss and Migmatite. Though the amount of outcrop, the lithology are less but based on total number and area of outcrop the migmatite is the dominant lithology. The topographic and detailed geological map of the block and the locations of bedrock samples are furnished in Text Figures No. 7.3 and Text figure No. 7.4, as well as in Plates III and IV, respectively. The generalized stratigraphy of the block area is given in Table No 7.2

Table- 7.2

The generalized stratigraphic succession in the block.

AGE	Group	LITHO UNITS
Recent	Quaternary Deposits	Weathered soil and Fluvial deposits
Palaeocene–Eocene	Jaintia / Barail Group (cover)	Altered calcareous siliceous sandstone
Neo-Proterozoic to Early Palaeozoic	Intrusive Body	Veins (Pegmatitic Vein, Quartzo Feldspathic vein and Quartz Vein)
		Granite
Archaean to Proterozoic	Assam Meghalaya Gneissic Complex	Augen Gneiss
		Granite Gneiss
		Migmatite

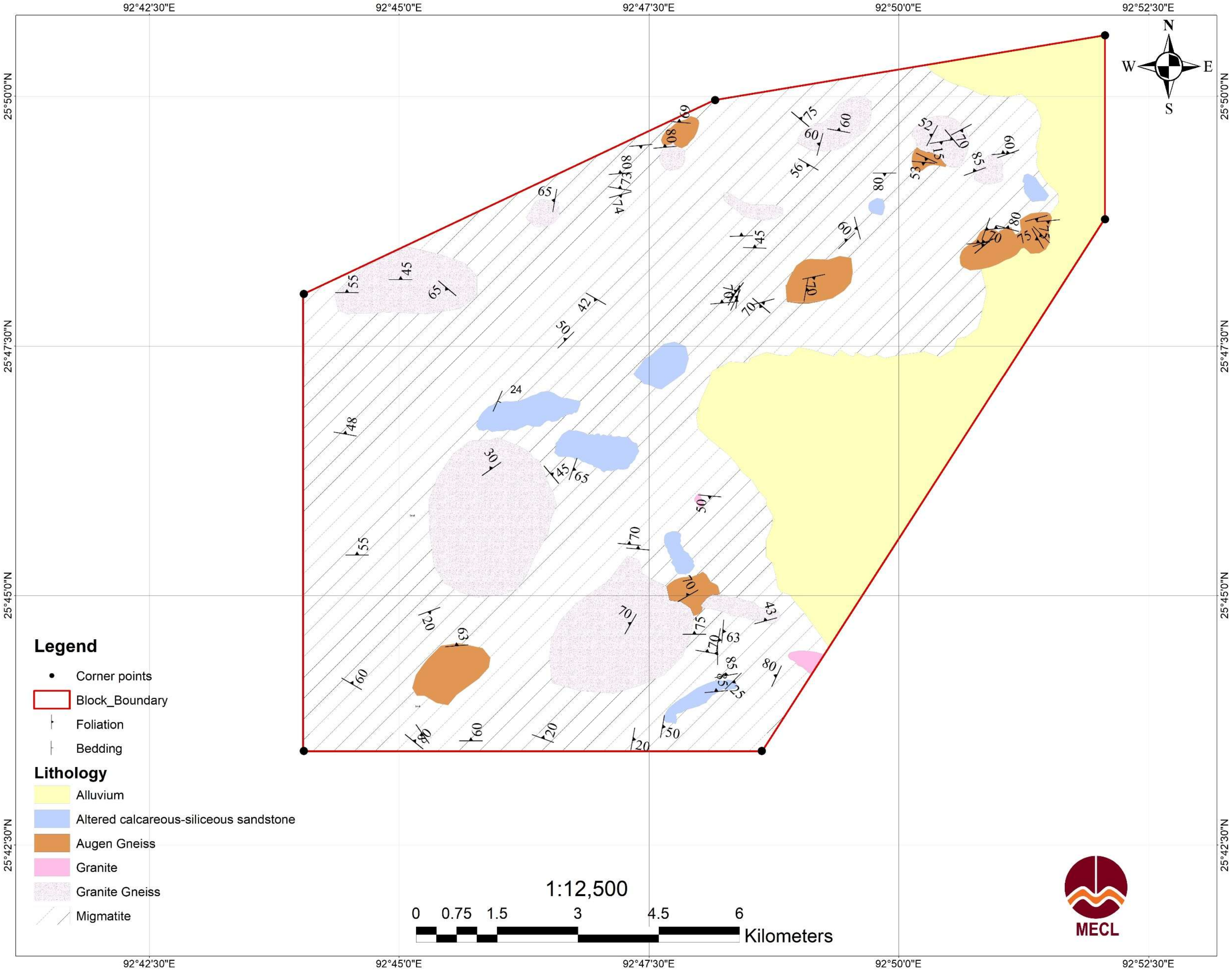

Text Fig. 7.3. Detail Geological map of Langmipi-Laching Thing Block, District West Karbi Anglong, Assam.

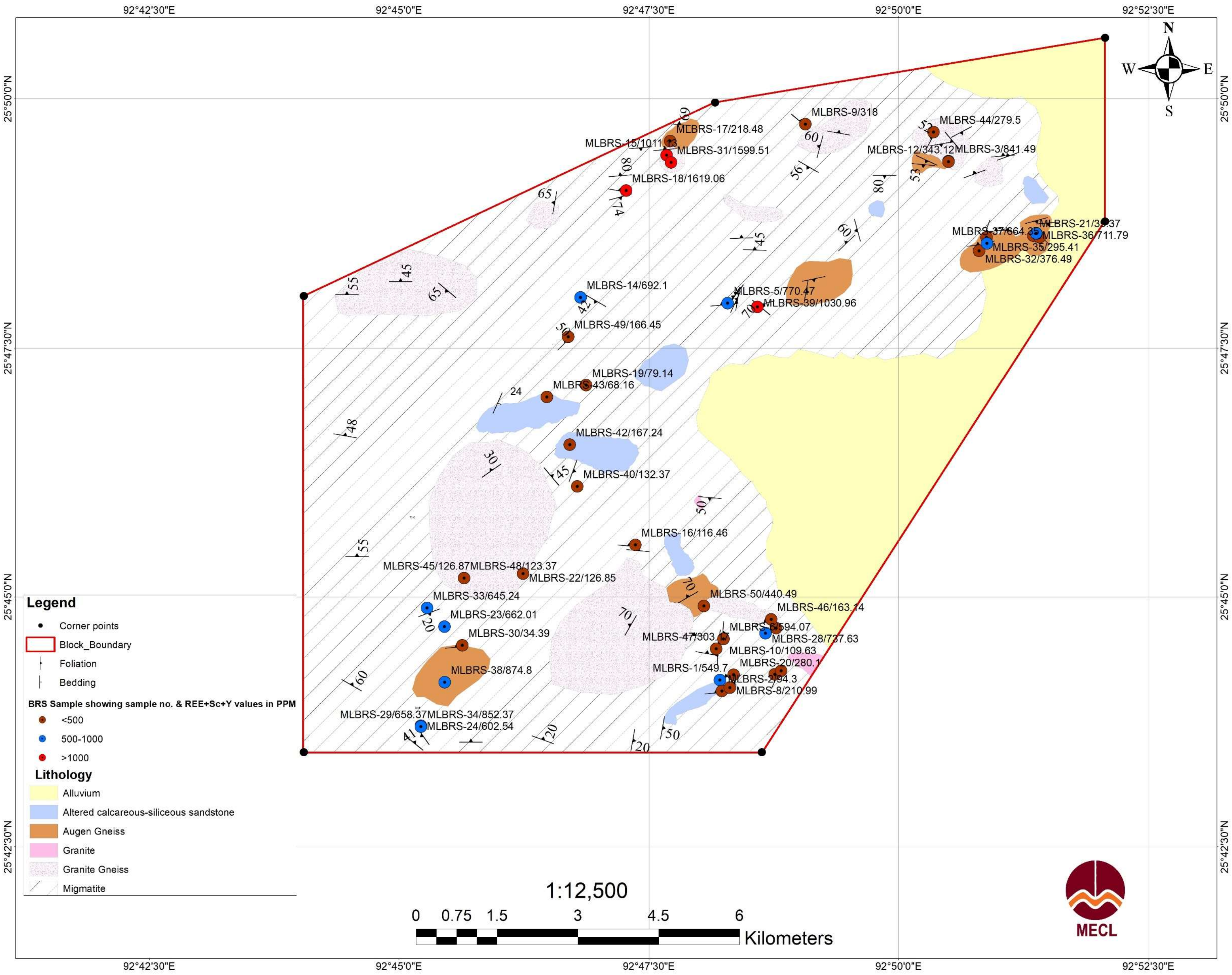

Text Fig No. 7.4: Location of the 50 Bed rock samples along with ∑REE+Sc+Y value in ppm

7.2.2 Description of lithology

7.2.2.1 Migmatite:

Migmatite is one of the dominant lithological units exposed in the Langmipi-Laching Thing Block. These rocks occur as composite gneisses characterized by alternating melanocratic (dark-colored) and leucocratic (light-colored) bands, giving them a distinctive migmatitic texture (Photograph No 7.1). The rock is generally pinkish to greyish-pink in colour due to the abundance of potassium feldspar (K-feldspar) in the leucocratic portions. It is medium- to fine-grained and exhibits faint to well-developed foliation. The migmatite consists of alternating melanosome and leucosome layers in varying proportions. The melanosome is rich in ferromagnesian minerals such as biotite, hornblende, and other mafic constituents, whereas the leucosome is composed predominantly of quartz, K-feldspar, and plagioclase.

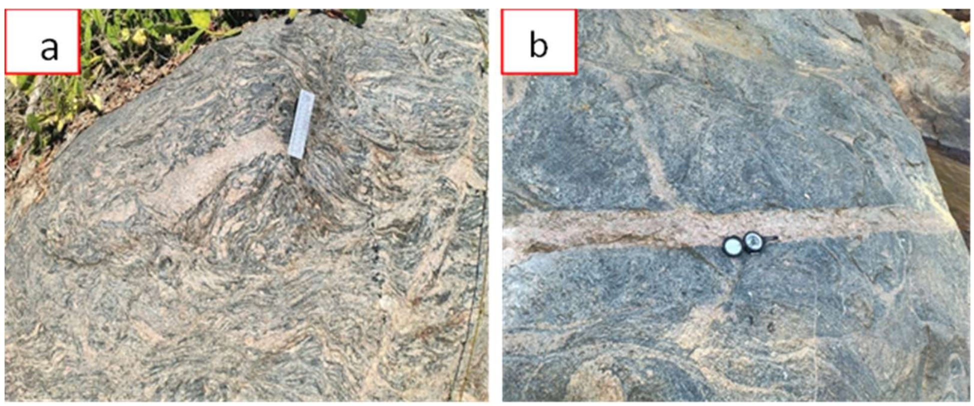

Photograph No 7.1: a) Migmatite rock exposed near the Kheroni area towards the north-eastern part of the block. b) 2-8cm of Quartzo feldspathic vein intruded the migmatite rock.

Thin quartzo-feldspathic veins, varying from 2 cm to 8 cm in thickness, are observed intruding both parallel and transverse to the foliation planes. Weathering has affected many exposures, resulting in subdued and poorly exposed outcrops. Fresh exposures reveal distinct mineral banding and textural relationships, whereas weathered surfaces often display a pale grey to brown appearance. Differential weathering between felsic and mafic layers commonly accentuates the banded nature of the rock. Sulphide mineralization is locally observed within the migmatite and associated quartz veins suggesting the circulation of hydrothermal fluids along structurally weak zones.

Photograph No. 7.2: Chalcopyrite specks and stains seen near Jengkro road.

Under microscope rocks shows medium to coarse grained and predominantly composed of Quartz, plagioclase, microcline/orthoclase and biotite. Orthoclase/ microcline occur as medium to moderately coarse subhedral grains showing perthitic exsolutions and crude alignment. Quartz occurs as medium anhedral grains, patches and lenses. Plagioclase is present as medium to fine subhedral prismatic grains altering to sericite. Biotite occurs as fine to medium flakes and flaky aggregates showing crude alignment. Opaques are present as fine subhedral to anhedral grains, blades and patches, often showing association with biotite.

Accessory minerals apatite, sericite, epidote, monazite and zircon are present. Apatite occurs as very fine to fine hexagonal and subrounded grains in accessories. Epidote, monazite and zircon are noted as very fine grains in association with and being included within biotite.

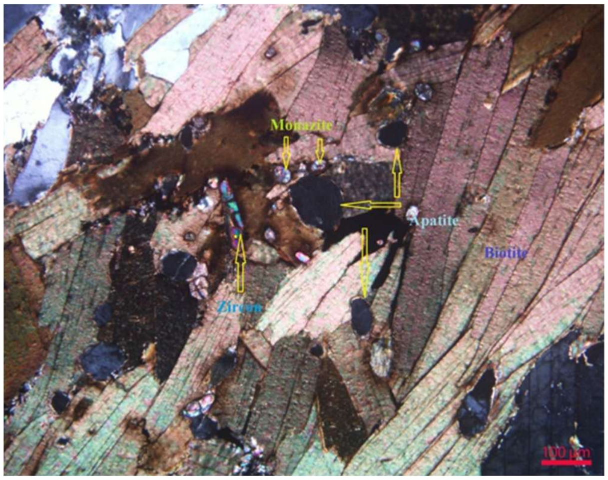

Pmg – 4: Photomicrograph showing inclusions of apatite, zircon and monazite within biotite as seen under crossed nicols.

The unit is retained as migmatite on the basis of its field and megascopic character — notably its composite, banded (melanosome–leucosome) fabric. Petrographically, the leucosome-dominated portions are quartzo-feldspathic and mineralogically comparable to the granite gneiss, consistent with derivation of the neosome from an in-situ felsic (granitic) protolith through high-grade metamorphism and partial melting (anatexis). In accordance with standard practice, the field nomenclature is retained, and petrography and geochemistry are used to characterise the protolith and its evolution rather than to reclassify the unit.

Geochemistry of migmatite

A total of twenty migmatite samples from the Langmipi Laching-Thing Block were analysed for 34 elements through ICP-MS analysis to evaluate the distribution of REE and associated trace elements within the lithounit (Table 7.1 and annexure II). The summarized analytical values are given in table no 7.1 and annexure II.

Table no 7.3. Summarized table of ICP-MS analysis of Migmatite (N=20) for 34 elements.

Elements	Max(ppm)	Min(ppm)	Mean(ppm)
Li	44.00	3.43	20.00
Be	13.80	0.58	4.23
Sc	16.92	1.50	8.30
V	103.42	5.59	31.24

Cu	32.53	11.06	18.80
Zn	148.04	17.42	60.84
Ga	45.69	2.62	21.27
Rb	427.29	5.74	258.86
Sr	500.4	31.71	185.32
Y	108.40	9.64	50.70
Zr	530.73	39.18	241.65
Nb	23.5	1.03	8.20
Sn	2.69	0.10	0.64
Ba	954.77	99.73	538.03
La	384.58	11.50	93.0
Ce	682.82	25.97	178.54
Pr	69.57	2.55	19.04
Nd	244.67	8.72	67.21
Sm	34.60	2.23	11.56
Eu	5.21	0.32	1.80
Gd	25.69	2.28	9.86
Tb	3.62	0.38	1.66
Dy	20.35	1.90	9.52
Ho	4.17	0.37	1.87
Er	10.00	0.84	4.63
Tm	1.32	0.11	0.58
Yb	9.41	0.80	4.22
Lu	1.45	0.13	0.65
Hf	16.38	1.19	8.08
Ta	2.58	0.13	1.15
W	525.34	3.25	207.77
Pb	80.00	5.96	49.68
Th	108.61	7.18	46.94
U	52.53	0.89	10.19
∑REE	1495.00	68.00	405.04
∑REEc+Sc+Y	1619.06	79.14	464.03

The Rare Earth Element (REE) geochemistry of the migmatite samples from the Langmipi–Laching Thing Block indicates a distinct enrichment of Light Rare Earth Elements (LREE) over Heavy Rare Earth Elements (HREE), which is characteristic of evolved felsic crustal rocks. The total REE (ΣREE) concentration ranges from 68.00 ppm to 1495.00 ppm, with an average of 405.04 ppm, while the combined ΣREE+Sc+Y values range from 79.14 ppm to 1619.06 ppm, averaging 464.03 ppm.

The REE chondrite-normalized spider diagram (Boynton, 1984), (Text Fig 7.1) exhibits a steeply declining trend from La to Lu, indicating strong LREE enrichment relative to HREE. The average concentrations of La (93.90 ppm), Ce (178.54 ppm), Nd (67.21 ppm), and Sm (11.56 ppm) are significantly higher than those of the HREEs, such as Dy (9.52 ppm), Er (4.63 ppm), Yb (4.22 ppm), and Lu (0.65 ppm). The nearly parallel nature of the REE patterns among the samples suggests that the migmatites were derived from a common felsic protolith and subsequently experienced similar petrogenetic processes, although variations in the magnitude of enrichment indicate variable concentrations of REE-bearing accessory minerals.

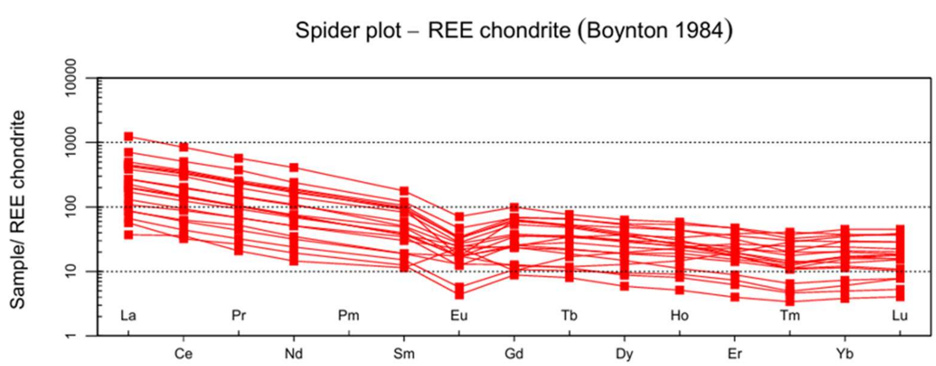

Text Fig 7.5: The chondrite-normalised REE spider diagram of migmatite (N=20)

Eu shows variable behaviour among the samples, with some samples displaying a distinct positive Eu anomaly while others show a negative Eu anomaly**.** The positive Eu anomalies may indicate plagioclase accumulation or involvement of feldspar-rich material, whereas the negative Eu anomalies can be attributed to plagioclase fractionation or retention of Eu^{2+} in feldspar during magmatic evolution. The contrasting Eu behaviour therefore suggests variable feldspar control and/or differences in the degree of magmatic differentiation among the samples. Beyond Eu, the HREE segment of the spider diagram remains comparatively flat, indicating limited fractionation among the HREEs and suggesting that residual garnet did not play a significant role during melt generation.

The migmatite samples are also enriched in several incompatible and high field strength elements (HFSE), including Zr (average 241.65 ppm), Hf (8.08 ppm), Th (46.94 ppm), Y (50.70 ppm), Rb (258.86 ppm), and Ba (892.35 ppm). The elevated concentrations of these elements indicate an evolved felsic composition and reflect the abundance of accessory minerals capable of hosting REEs and HFSEs. The dataset also reports very high tungsten (W) contents; however, these values are anomalously high and uniform across every lithology and sample medium and are attributed to probable tungsten-carbide contamination during sample preparation. Tungsten is therefore excluded from petrogenetic interpretation. The elevated Rb and Ba contents further indicate extensive feldspar fractionation and potassic enrichment during the evolution of the parental magma. Overall, the geochemical characteristics of the migmatites suggest that they represent products of highly evolved crustal magmatism generated through partial melting and subsequent magmatic differentiation of felsic continental crust.

Major oxides, i.e., SiO_2, Al_2O_3, Fe_2O_3, MnO, MgO, CaO, Na_2O, K_2O, TiO_2, P_2O_5, LOI were analysed for 4 nos of selected migmatite samples. The major oxide composition of the migmatite samples indicates a silica-rich, felsic to intermediate-felsic composition, with SiO_2 contents ranging from 55.07 to 70.58 wt.%. The relatively high Al_2O_3 values (14.74–16.15 wt.%) suggest the abundance of aluminosilicate minerals such as feldspars and micas. Fe_2O_3 shows a wide variation (0.98–10.19 wt.%), indicating differences in the proportion of ferromagnesian minerals, with the lower Fe_2O_3 content in the most silica-rich sample reflecting a more evolved felsic composition. The low concentrations of MgO (0.10–2.49 wt.%) and CaO (1.39–4.48 wt.%) further support the felsic nature of the rocks and indicate limited mafic mineral content. Na_2O (2.16–3.07 wt.%) and particularly high K_2O (6.13–8.47 wt.%) values indicate the dominance of alkali feldspars, especially K-feldspar, which is characteristic of granitic and migmatitic rocks. The relatively low TiO_2 (0.05–1.59 wt.%) and P_2O_5 (0.08–0.77 wt.%) contents suggest only minor amounts of Ti-bearing and phosphate minerals such as ilmenite, titanite, and apatite. MnO remains consistently low (0.12–0.14 wt.%), while LOI values (0.68–0.97 wt.%) indicate minimal alteration and low volatile content. Overall, the major oxide geochemistry suggests that the migmatites are predominantly potassic, silica-rich felsic rocks, with mineralogical characteristics controlled by quartz and alkali feldspar, and exhibit compositional variations that likely reflect differing degrees of partial melting, melt segregation, and magmatic differentiation during migmatite formation.

Granite tectonic discrimination-Frost et al. (2001)

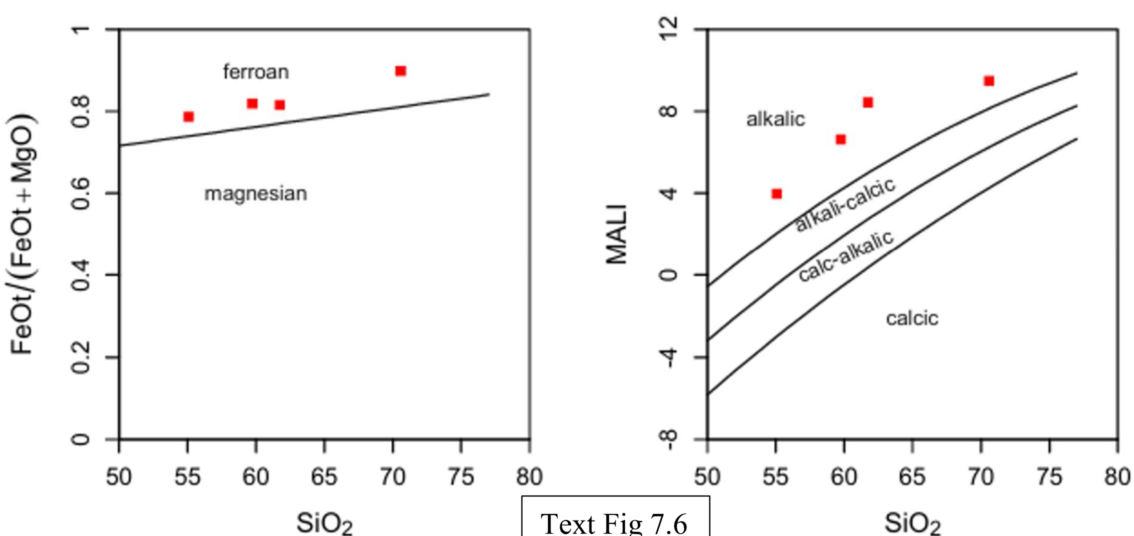

Text Fig 7.6

The Frost et al. (2001) tectonic discrimination diagrams (Text Fig 7.6) indicate that all migmatite samples belong to the ferroan granite series, characterized by high FeOt/(FeOt+MgO) ratios, suggesting an evolved iron-rich felsic composition. In the MALI versus SiO_2 diagram, the samples predominantly plot within the alkalic field, with one sample occurring near the alkali-calcic boundary, indicating enrichment of alkali elements over CaO. The combined geochemical characteristics suggest that the migmatites are highly differentiated felsic rocks derived from evolved crustal melts, consistent with an evolved, ferroan, metaluminous and strongly potassic felsic granitoid protolith produced by extensive differentiation and/or partial melting of continental crust.

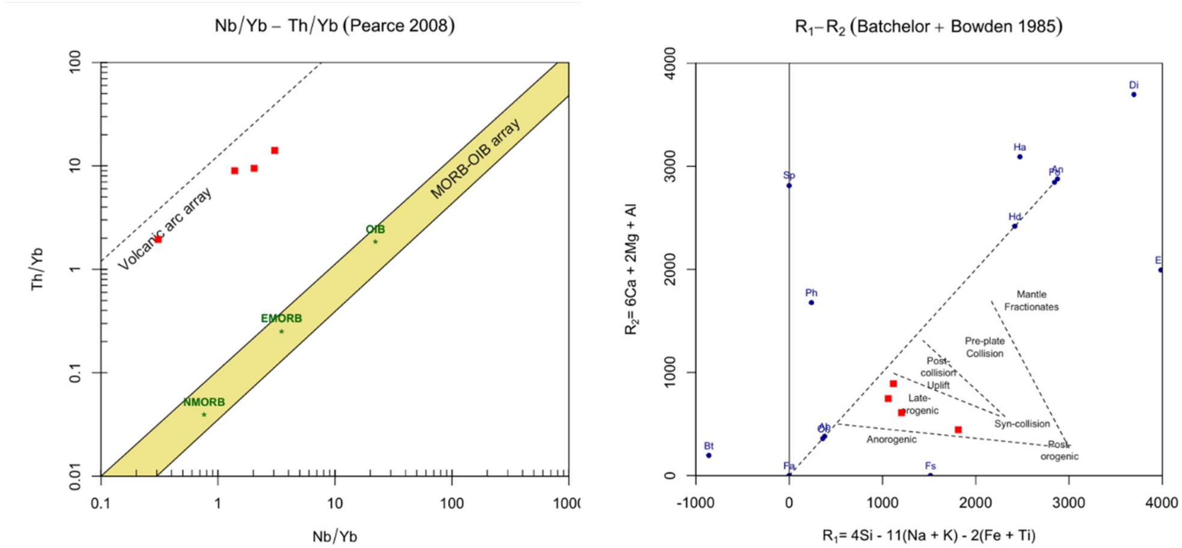

Text Fig 7.7

The Nb/Yb–Th/Yb discrimination diagram (Pearce, 2008) shows that all migmatite samples plot within the volcanic arc array, well above the MORB–OIB array, indicating significant crustal enrichment and a strong subduction-related signature. Their elevated Th/Yb ratios reflect extensive crustal involvement during magma generation through partial melting of continental crust. The R_1–R_2 tectonic discrimination diagram (Batchelor and Bowden, 1985) places the samples predominantly within the Late-orogenic field, with one sample approaching the post-collision uplift field. These results suggest that the migmatites were generated during the late stages of orogenic evolution through crustal anatexis associated with continental collision and subsequent tectonic uplift, consistent with the evolution of granitoids in collisional orogens (Text Fig 7.7)

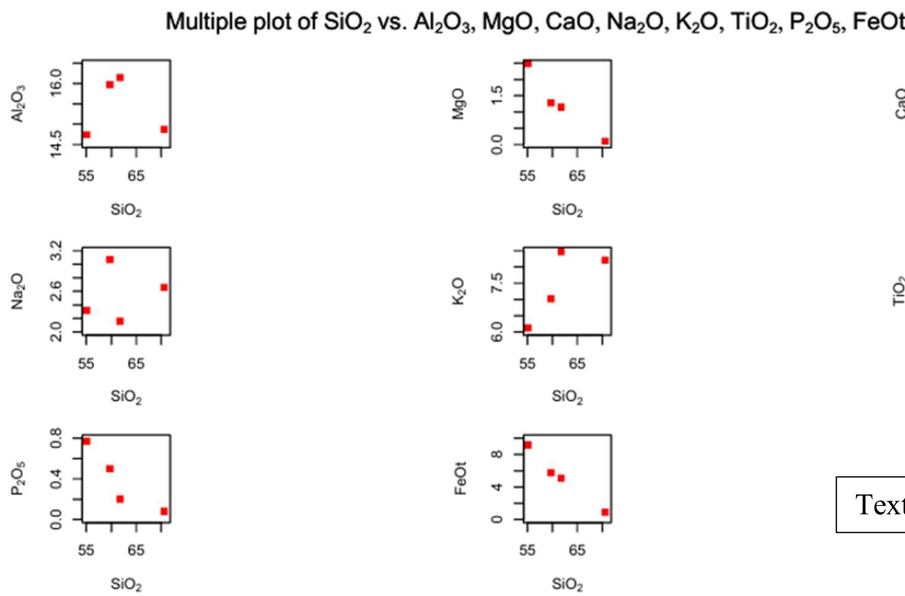

Text Fig 7.8

The Harker variation diagrams (Text Fig 7.8) reveal systematic geochemical trends that reflect magmatic differentiation and metamorphic evolution. With increasing SiO_2, the concentrations of MgO, CaO, TiO_2, P_2O_5, and total FeO (FeOt) generally decrease, indicating the progressive removal of ferromagnesian minerals (biotite, hornblende, pyroxene), calcic plagioclase, Fe–Ti oxides, and apatite during fractional crystallization and partial melting. In contrast, K_2O shows an overall positive correlation with SiO_2, suggesting enrichment of potassium during magmatic evolution through crystallization of K-feldspar and concentration of alkali-rich melts. Al_2O_3 and Na_2O display only minor variations, implying that feldspar remained a dominant constituent throughout the differentiation process. These geochemical trends indicate that the migmatites evolved through felsic differentiation associated with anatexis (partial melting) and crustal reworking, producing silica-rich, potassium-enriched melts while progressively depleting mafic components. Such trends are characteristic of evolved felsic migmatitic rocks derived from continental crustal protoliths.

7.2.2.2 Granite Gneiss:

Granite gneiss constitutes one of the most extensive and significant lithological units within the block. The granite gneiss is predominantly composed of quartz, K-feldspar, plagioclase feldspar, and biotite. The rock is generally coarse- to medium-grained, although grain size varies considerably from outcrop to outcrop. It commonly exhibits a pinkish-grey to grey colour owing to the abundance of K-feldspar. A well-developed gneissic fabric is observed in most exposures, defined by the preferred orientation of biotite flakes and elongated feldspar and quartz grains. However, the intensity of gneissosity varies spatially, with some exposures displaying strong foliation and compositional banding, while others retain remnants of the original granitic texture with weakly developed foliation.

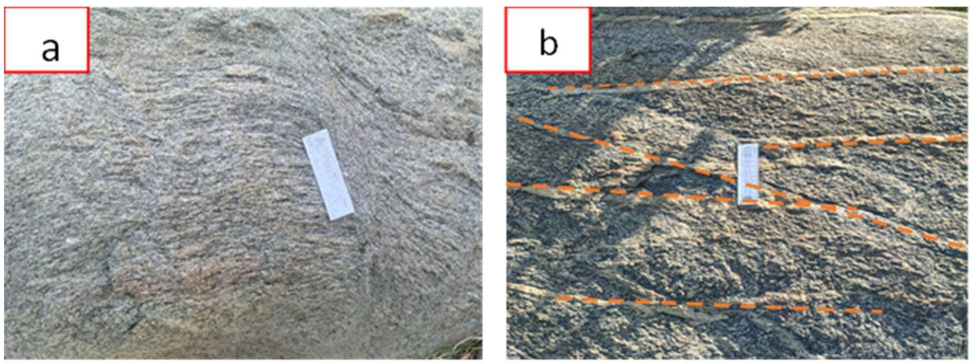

Photograph No 7.3: a) Granite gneiss exposed towards the northern part of the block showing gneissic foliation. b) Granite gneiss is intruded by several cross-cutting quartzo-feldspathic veins, suggesting multiple generations of vein emplacement.

σ-type porphyroclasts are observed within the granite gneiss, characterized by asymmetric tails developed around relatively rigid feldspar porphyroclasts. These structures serve as reliable kinematic indicators, recording the sense of shear during ductile deformation and suggesting that the granite gneiss underwent significant non-coaxial shearing under ductile crustal conditions.

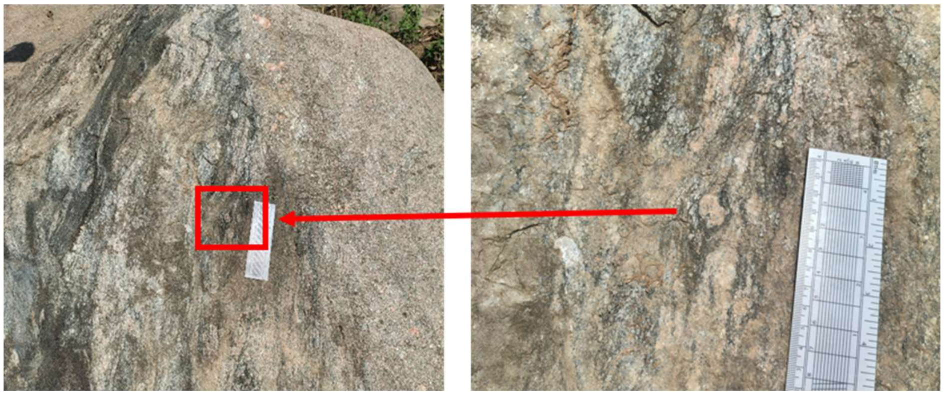

Photograph No 7.4: σ-type porphyroclast observed within the granite gneiss.

Under microscope rocks shows medium to coarse grained and predominantly composed of Quartz, plagioclase, microcline/orthoclase and biotite. Orthoclase/ microcline occur as medium to coarse subhedral to anhedral grains showing perthitic exsolutions and crude alignment. Quartz occurs as medium to fine anhedral grains. Plagioclase is present as medium to fine subhedral prismatic grains showing myrmekitic intergrowths in areas. Biotite occurs as fine disseminated flakes showing parallel alignment.

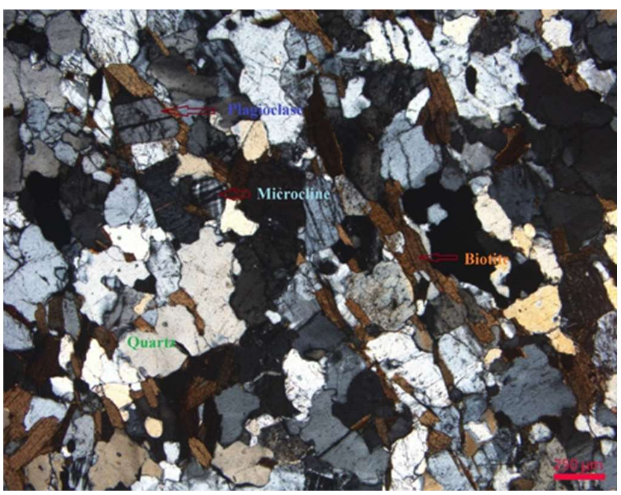

Pmg – 2: Photomicrograph showing association and parallel alignment of microcline, quartz, plagioclase and biotite in granite gneiss as seen under crossed nicols.

Opaques are present as medium anhedral patches and as fine subhedral to anhedral grains aligned along the foliations. Apatite is noted as fine to very fine subrounded and hexagonal grains in accessories. Zircon and monazite are seen present as very fine slender prismatic and subrounded grains and as inclusions within biotite. Sphene is noted as very fine wedges in association with biotite. Petrographically the rock is classified as granite gneiss.

Geochemistry of granite gneiss

A total of four granite gneiss samples from the Langmipi Laching-Thing Block were analysed for 34 elements through ICP-MS analysis to evaluate the distribution of REE and associated trace elements within the lithounit (Table 7.4 and Annexure II). Of these four samples, one sample records more than 1000 ppm total REE (ΣREE) and two samples exceed 1000 ppm ΣREE+Sc+Y, whereas one sample is comparatively depleted (ΣREE 87.17 ppm), reflecting the erratic distribution of REE within this lithounit. The summarized analytical values are given in Table 7.2 and Annexure II.

Table no 7.4. Summarized table of ICP-MS analysis of Granite gneiss (N=4) for 34 elements.

Elements	Max(ppm)	Min(ppm)	Mean(ppm)
Li	39.56	9.00	21.71
Be	5.04	3.87	4.47
Sc	16.39	4.50	8.78
V	112.52	11.88	47.42
Cu	28.55	13.61	20.05
Zn	129.93	49.21	76.63
Ga	44.44	23.95	34.80
Rb	297.36	205.82	253.03
Sr	581.74	182.69	321.62
Y	124.32	36.17	82.01
Zr	612.22	162.56	402.21
Nb	21.83	4.99	11.49
Sn	0.17	0.17	0.17
Ba	2200.00	684.26	1291.56
La	352.93	173.91	257.01
Ce	667.15	326.65	489.16
Pr	73.65	35.62	51.74
Nd	250.44	128.15	176.80

Sm	35.60	21.10	26.57
Eu	5.15	2.13	3.17
Gd	26.49	14.28	19.89
Tb	3.64	1.78	2.89
Dy	19.43	7.75	14.96
Ho	3.90	1.35	2.90
Er	10.02	3.30	7.34
Tm	1.23	0.32	0.82
Yb	7.98	2.42	5.77
Lu	1.20	0.40	0.91
Hf	17.19	5.46	12.79
Ta	1.95	0.60	1.32
W	223.43	42.83	161.75
Pb	87.77	33.96	54.35
Th	317.42	93.11	189.76
U	22.83	6.40	12.18
∑REE	1458.80	750.49	1059.92
∑REEc+Sc+Y	1599.51	841.49	1150.71

The granite gneiss samples from the Langmipi–Lachingthin Block exhibit a highly enriched Rare Earth Element (REE) signature, characterized by strong Light Rare Earth Element (LREE) enrichment and comparatively lower Heavy Rare Earth Element (HREE) concentrations. The total REE (ΣREE) values range from 841.49 ppm to 1458.80 ppm, with an average of 750.49 ppm, while the combined ΣREE+Sc+Y values vary between 841.49 ppm and 1599.51 ppm, averaging 841.49.74 ppm. These values are considerably higher than the average upper continental crust, indicating substantial enrichment of REEs within the granite gneiss.

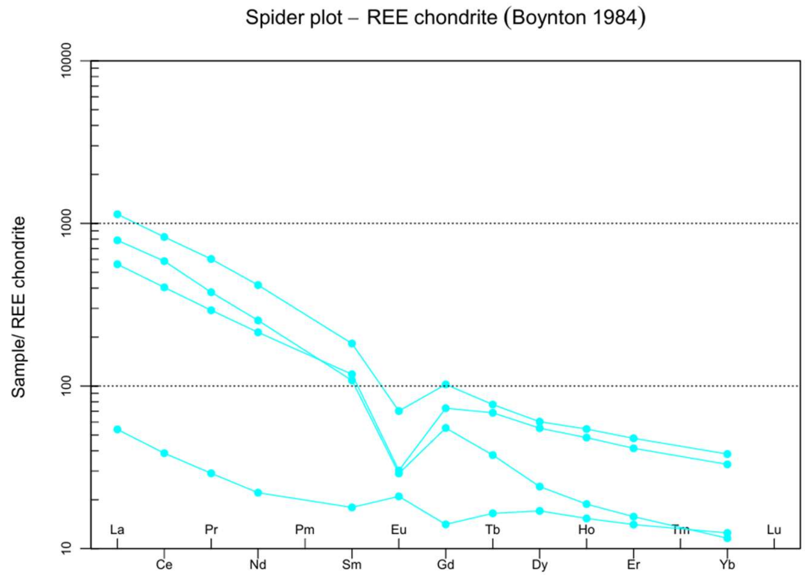

Text Fig 7.9: The chondrite-normalised REE spider diagram of granite gneiss (N=4).

The chondrite-normalized REE spider diagram (Text Fig 7.9) of the granite gneiss exhibits a characteristic geochemical pattern of highly evolved felsic rocks, marked by strong enrichment of Light Rare Earth Elements (LREEs), a pronounced negative europium (Eu) anomaly, and comparatively lower Heavy Rare Earth Element (HREE) abundances. The REE patterns show a steep decline from La to Sm, indicating significant LREE enrichment, followed by a sharp negative Eu anomaly and a relatively flat to gently decreasing HREE segment from Gd to Lu. The high normalized values of La and Ce, together with the gradual decrease towards the HREEs, indicate strong LREE/HREE fractionation resulting from extensive magmatic differentiation.

The REE spider diagram exhibits a conspicuous negative Eu anomaly, indicating significant plagioclase fractionation during the crystallization of the parental felsic magma. This geochemical feature is typical of highly evolved granitic rocks and reflects extensive magmatic differentiation and partial melting of continental crust.

The granite gneiss samples are enriched in incompatible elements such as Rb (mean 253.03 ppm), Ba (1291.56 ppm), Zr (402.21 ppm), Hf (12.79 ppm), Th (189.76 ppm), U (12.18 ppm), and W (161.75 ppm), which are typically concentrated during the late stages of magmatic differentiation. High Rb and Ba concentrations indicate the involvement of K-feldspar-rich granitic melts, whereas elevated Zr and Hf suggest abundant zircon crystallization. The enrichment of Th and U reflects a significant continental crustal contribution to the parental magma, while the elevated tungsten concentration indicates the influence of late-stage magmatic-hydrothermal processes that are commonly associated with evolved granitic systems.

Overall, the geochemical characteristics indicate that the granite gneiss represents a highly evolved felsic crustal lithology generated through partial melting and prolonged magmatic differentiation of continental crust. The strong enrichment of LREEs, pronounced negative Eu anomaly, relatively flat HREE profile, and elevated concentrations of HFSEs and incompatible elements collectively indicate that REE mineralisation is primarily hosted by accessory phases such as monazite (the dominant REE carrier identified petrographically), with subordinate zircon and titanite (allanite and xenotime inferred but not confirmed in thin section). With an average ΣREE content of 1059.92 ppm — the highest among the mapped lithounits — together with elevated Th, Y and W concentrations, the granite gneiss represents the most REE-enriched lithological unit within the Langmipi–Laching Thing Block. However, the wide range in ΣREE (750.49–1458.80 ppm) indicates that this enrichment is highly erratic and spatially discontinuous rather than uniform.

Major oxides, i.e., SiO2, Al2O3, Fe2O3, MnO, MgO, CaO, Na2O, K2O, TiO2, P2O5, LOI were analysed for 3 nos of selected granite gneiss samples. The major oxide composition of the granite gneiss samples indicates a silica-rich, felsic composition, with SiO_2 contents ranging from 65.06 to 68.25 wt.%, characteristic of granitic rocks. The consistently high Al_2O_3 values (15.56–16.59 wt.%) reflect the abundance of aluminosilicate minerals, primarily feldspars and micas. Low Fe_2O_3 (2.01–2.86 wt.%), MgO (0.31–0.45 wt.%), and MnO (0.03–0.06 wt.%) contents indicate a limited proportion of ferromagnesian minerals, consistent with the felsic nature of the granite gneiss. CaO values (0.87–2.96 wt.%) are relatively low, suggesting minor amounts of calcic plagioclase, whereas Na_2O (2.03–3.53 wt.%) and particularly elevated K_2O (5.16–11.50 wt.%) indicate the dominance of alkali feldspar, especially K-feldspar, a characteristic feature of granitic gneisses. The low concentrations of TiO_2 (0.18–0.38 wt.%) and P_2O_5 (0.17–0.20 wt.%) suggest only minor contributions from accessory Ti-bearing and phosphate minerals such as ilmenite, titanite, and apatite. Overall, the major oxide geochemistry indicates that the granite gneiss is a potassic, highly evolved felsic rock dominated by quartz and alkali feldspar, with compositional characteristics typical of granitic protoliths that have undergone gneissic metamorphism.

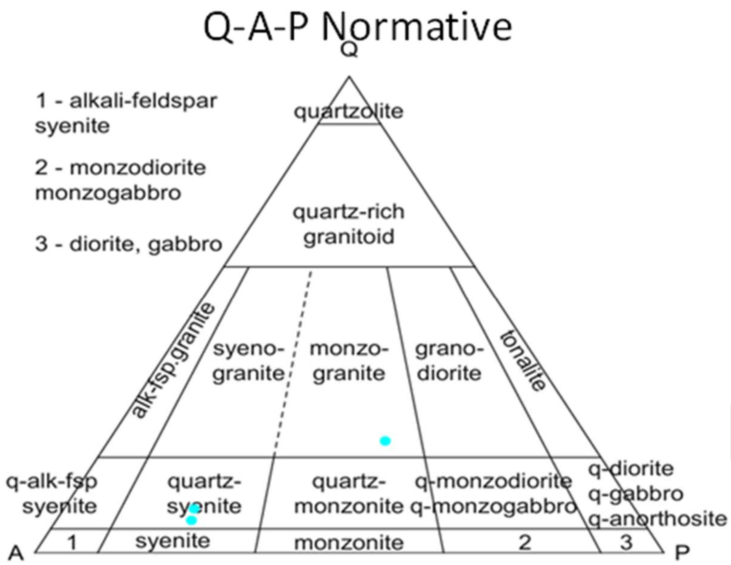

Text Fig 7.10

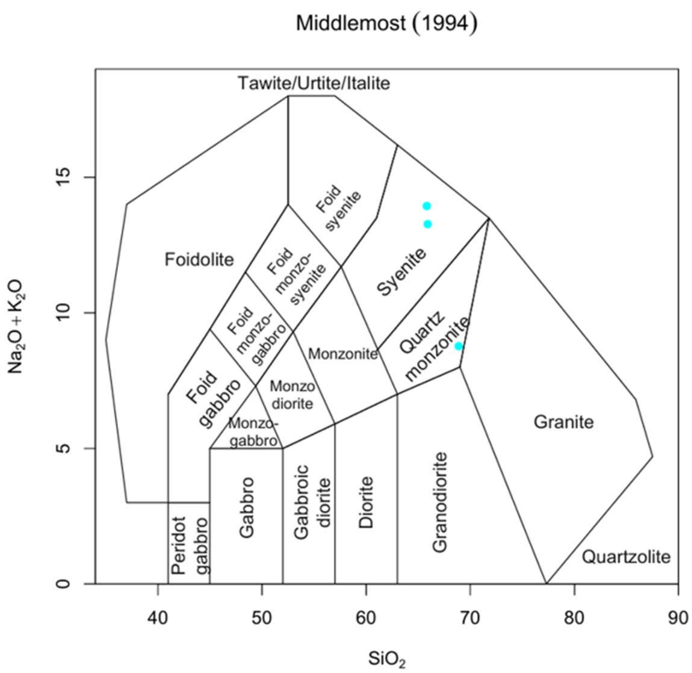

Text Fig 7.11

The Q–A–P normative classification diagram (Text Fig 7.10) shows that the granite gneiss samples plot predominantly within the quartz syenite and quartz monzonite fields. The Middlemost (1994) SiO_2– (Na_2O + K_2O) classification diagram (Text Fig 7.12) classifies the samples mainly within the syenite and quartz monzonite fields. The relatively high SiO_2 (≈65–70 wt.%) and elevated total alkali contents ($Na_2O + K_2O$ ≈9–14 wt.%) indicate that the granite gneisses are highly evolved, alkali-rich felsic rocks.

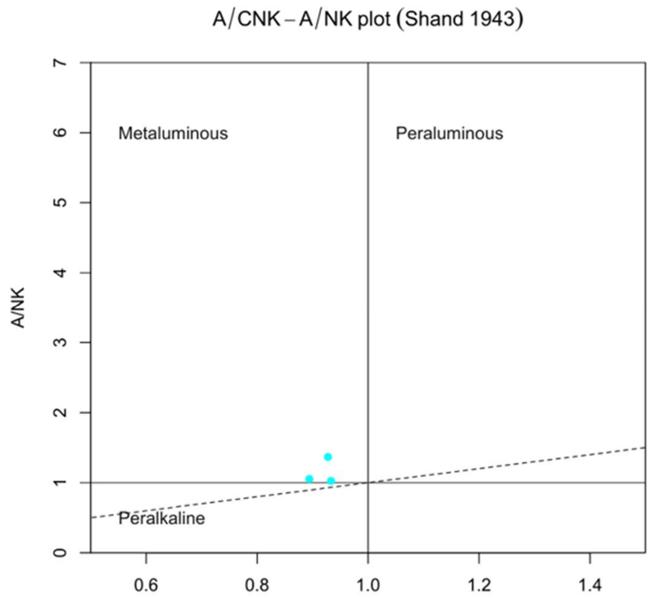

Text Fig 7.12

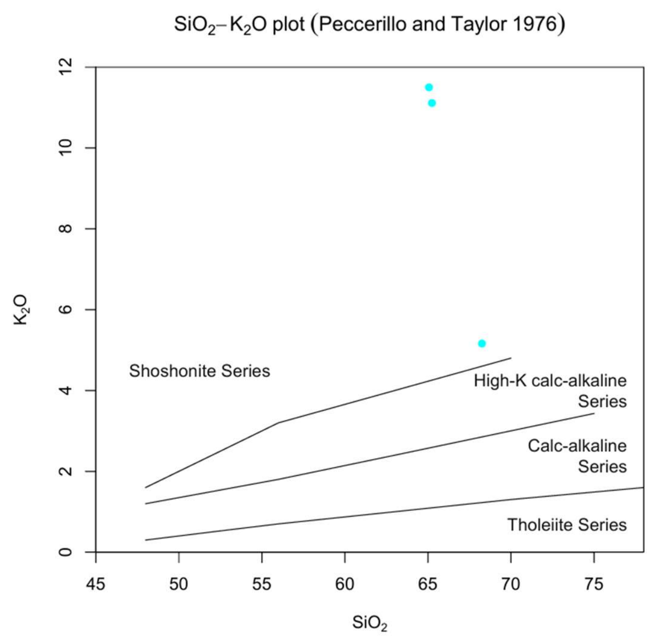

Text Fig 7.13

The A/CNK–A/NK plot (Text Fig 7.12) shows that all the granite gneiss samples plot within the metaluminous field (A/CNK < 1.0), with A/NK values slightly greater than 1. This indicates that the rocks are metaluminous in character, suggesting that aluminium is balanced by alkalis and calcium, and that the mineral assemblage is dominated by feldspars with minor aluminous minerals. Such compositions are consistent with an evolved, metaluminous granitoid protolith that has subsequently undergone high-grade metamorphism to form the granite gneiss.

The SiO_2–K_2O diagram (Text Fig 7.13) shows that most of the granite gneiss samples plot within the shoshonitic series, while one sample falls within the high-K calc-alkaline field. The very high K_2O contents (≈5–11 wt.%) indicate strong potassium enrichment, reflecting abundant K-feldspar and biotite in the granitoid protoliths.

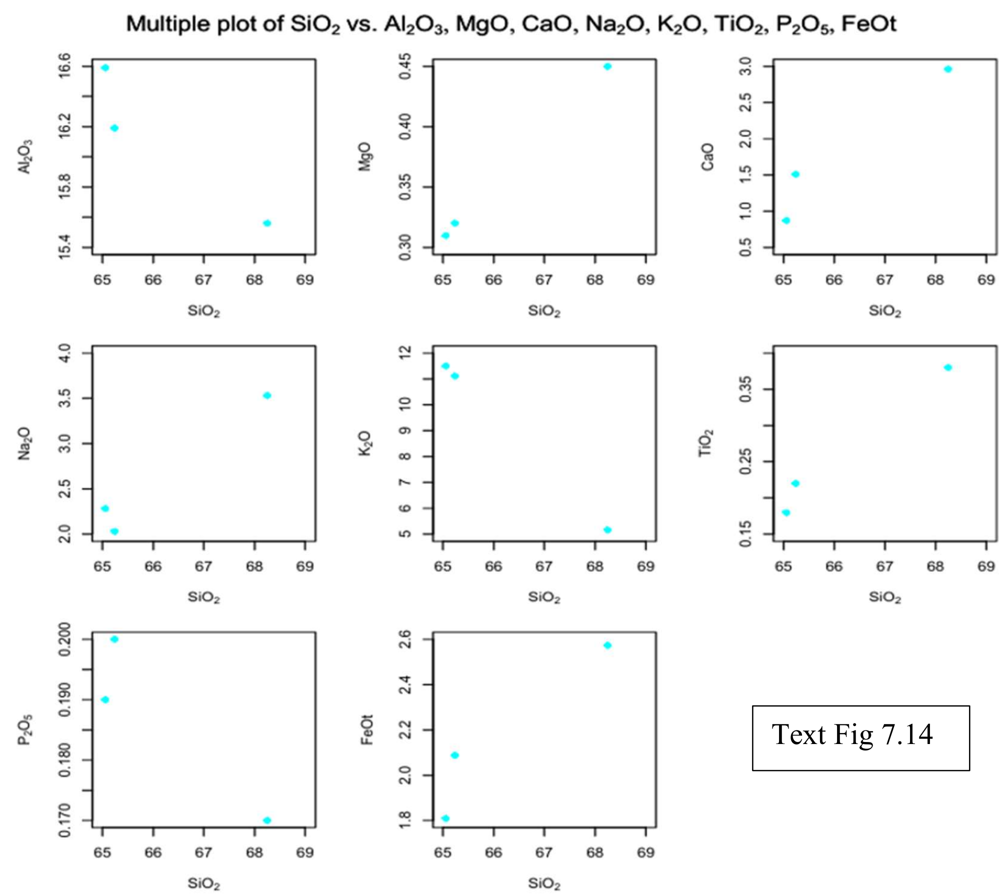

Text Fig 7.14

The Harker variation diagrams (Text Fig 7.14) for the granite gneiss samples illustrate the geochemical evolution of the rocks during magmatic differentiation and subsequent metamorphism. The samples are characterized by relatively high SiO_2 contents (≈65–68 wt.%), confirming their felsic nature. With increasing SiO_2, Al_2O_3, K_2O, and P_2O_5 exhibit a slight negative correlation, suggesting fractionation of K-feldspar, plagioclase, and apatite during magma evolution. Na_2O shows a positive correlation with SiO_2, reflecting enrichment in sodic feldspar (albite) in the more evolved compositions. MgO, CaO, TiO_2, and FeOt remain consistently low with only minor variations, indicating significant depletion of mafic minerals and Fe–Ti oxides due to advanced fractional crystallization and crustal differentiation. Overall, the Harker trends suggest that the granite gneisses represent highly evolved felsic granitoids, derived through extensive magmatic differentiation and later modified by high-grade metamorphism, while largely preserving the geochemical characteristics of their granitic protoliths.

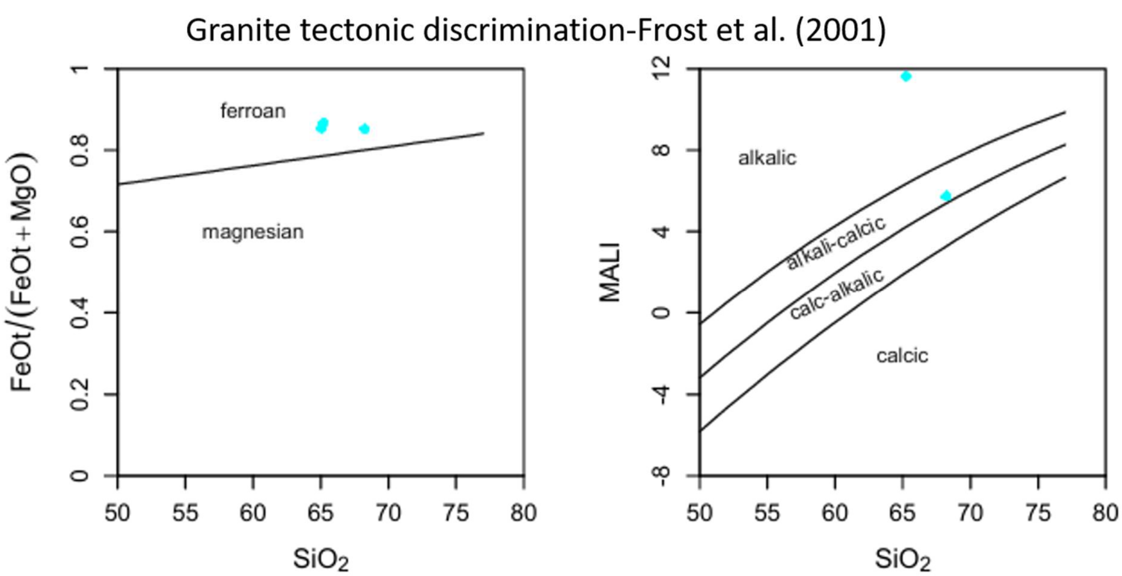

Text Fig 7.15

The Frost et al. (2001) granite classification diagrams (Text Fig 7.15) indicate that the granite gneiss samples belong to the ferroan granite series, characterized by high FeOt/(FeOt + MgO) ratios, reflecting iron enrichment relative to magnesium. In the MALI versus SiO_2 diagram, the samples plot within the alkalic to alkali-calcic fields, indicating enrichment in alkali elements over CaO. These geochemical characteristics suggest that the granite gneiss represents an evolved felsic granitoid formed through significant magmatic differentiation and/or partial melting of continental crust.

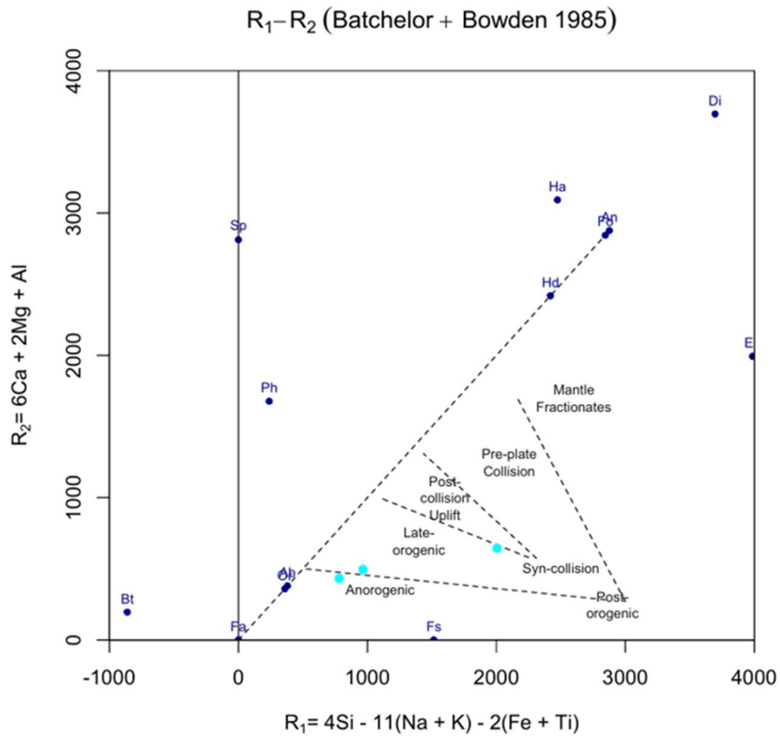

Text Fig 7.16

The R_1–R_2 tectonic discrimination diagram (Batchelor and Bowden, 1985), (Text Fig 7.16) indicates that the granite gneiss samples are distributed mainly within the anorogenic, late-orogenic, and syn-collisional granite fields. Two samples plot in the anorogenic field, suggesting emplacement in an extensional intracontinental setting following the cessation of major orogenic activity. One sample fall within the late-orogenic field, indicating magmatism associated with the waning stages of mountain-building, whereas other plots close to the syn-collisional field, reflecting a contribution from crustal melting during continental collision. The spread of samples across these tectonic fields suggests that the granite gneisses record a complex magmatic evolution, involving both collisional and post-collisional tectonic processes.

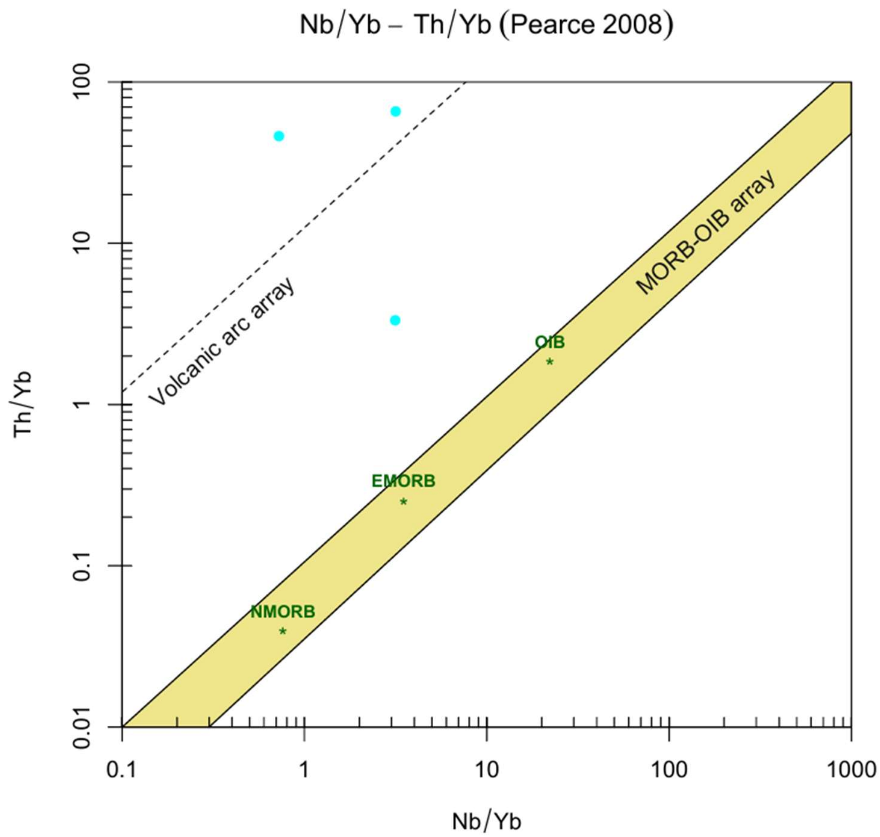

Text Fig 7.17

The Nb/Yb–Th/Yb discrimination diagram (Pearce, 2008) (Text Fig 7.17) shows that all granite gneiss samples plot well above the MORB–OIB array within the volcanic arc array. Their elevated Th/Yb ratios indicate significant enrichment in thorium relative to niobium, reflecting substantial crustal involvement during magma generation. The displacement from the mantle array suggests that the granite gneiss was derived through partial melting of continental crust, with geochemical characteristics inherited from a subduction-modified source. The variation in Th/Yb values among the samples further indicates differences in the degree of crustal contamination and magmatic evolution. Overall, the diagram suggests that the granite gneiss was generated in a convergent continental margin (volcanic arc) setting, where crustal anatexis and subduction-related processes played a dominant role in magma genesis.

7.2.2.3 Augen Gneiss:

Augen Gneiss is coarse-grained and is readily distinguished by its characteristic augen texture, which is defined by the presence of large, eye-shaped feldspar porphyroclasts embedded within a comparatively finer-grained quartzofeldspathic matrix. This augens is predominantly composed of potassium feldspar and impart a conspicuous pinkish colour to the rock, making the lithology easily recognizable in the field.

Photograph No. 7.5: Augen gneiss is characterized by the presence of prominent eye-shaped porphyroclasts embedded within a comparatively fine-grained quartzo-feldspathic matrix.

The rock exhibits a well-developed gneissic fabric characterized by alternating felsic and mafic bands. The felsic bands are mainly composed of quartz and feldspar, whereas the mafic bands consist predominantly of biotite, amphibole, and other ferromagnesian minerals. This compositional segregation results in prominent mineral banding, which is one of the defining features of the augen gneiss exposed within the block. Field observations indicate that the augen gneiss has undergone intense ductile deformation and shearing. The large feldspar augens are commonly stretched, rotated, and asymmetrically deformed within the finer-grained matrix, reflecting the effects of progressive strain during regional metamorphism and tectonic deformation. In highly strained zones, the augens exhibit sigma- and delta-type geometries, and the surrounding matrix displays a strong planar fabric defined by the preferred orientation of mica and elongate quartz grains.

Under microscope rocks shows medium to coarse grained and predominantly composed of Quartz, plagioclase, microcline/orthoclase and biotite. Orthoclase/ microcline occur as coarse to medium subhedral grains showing perthitic exsolutions. Plagioclase occurs as medium to fine subhedral prismatic grains showing myrmekitic intergrowths in areas. Quartz is present as anhedral grains and patches. Biotite is seen present as fine disseminated flakes showing parallel alignment. Opaques occur as anhedral grains, blades and patches, mostly in association with biotite. Apatite occurs as fine subrounded and prismatic grains in accessories. Sericite is seen developing as very fine flakes after plagioclase alterations. Zircon is noted as very fine inclusions within biotite, around which pleochroic halos are observed.

The unit is retained as augen gneiss on the basis of its diagnostic field and megascopic character — large, eye-shaped K-feldspar porphyroclasts set in a finer-grained quartzo-feldspathic matrix. Petrographically its mineral assemblage is that of a quartzo-feldspathic orthogneiss comparable to the granite gneiss, indicating a common evolved granitoid protolith subsequently modified by intense ductile shearing that generated the augen (porphyroclastic) texture. The field nomenclature is therefore retained (see §7.5).

Geochemistry of augen gneiss

A total of eleven augen gneiss samples from the Langmipi Laching-Thing Block were analysed for 34 elements through ICP-MS analysis to evaluate the distribution of REE and associated trace elements within the lithounit (Table 7.5 and annexure II).

Table no 7.5. Summarized table of ICP-MS analysis of Augen gneiss (N=11) for 34 elements.

Elements	Max(ppm)	Min(ppm)	Mean(ppm)
Li	66.07	6.82	23.52
Be	5.52	0.79	3.39
Sc	21.05	0.87	9.18
V	93.72	3.32	33.25
Cu	28.00	13.21	19.18
Zn	115.86	23.64	57.99
Ga	31.31	4.90	20.61
Rb	402.35	2.79	244.27
Sr	409.45	37.18	221.72

Y	176.14	4.67	65.49
Zr	450.55	58.02	236.22
Nb	15.74	0.77	6.80
Sn	0.25	0.10	0.15
Ba	2200.00	100.36	536.27
La	157.93	6.55	80.22
Ce	280.48	10.37	152.75
Pr	29.29	1.20	16.74
Nd	103.82	4.22	59.53
Sm	19.06	0.83	10.91
Eu	3.60	0.13	2.06
Gd	18.59	0.73	9.75
Tb	3.82	0.10	1.70
Dy	26.33	0.72	10.72
Ho	5.96	0.16	2.22
Er	15.57	0.38	5.75
Tm	2.02	0.33	0.91
Yb	15.48	0.43	5.34
Lu	2.42	0.39	1.02
Hf	12.18	1.97	7.39
Ta	1.37	0.23	0.71
W	634.38	179.20	287.99
Pb	99.86	4.84	52.53
Th	76.08	2.72	35.52
U	22.89	0.43	7.56
∑REE	680.80	27.15	359.27
∑REEc+Sc+Y	874.80	34.39	433.94

The augen gneiss samples from the Langmipi–Laching Thing Block exhibit a characteristic REE distribution marked by pronounced enrichment of Light Rare Earth Elements (LREE) relative to Heavy Rare Earth Elements (HREE), indicating an evolved felsic crustal affinity. The total REE (ΣREE) content ranges from 27.15 ppm to 680.80 ppm, with an average of 359.27 ppm, while the combined ΣREE+Sc+Y values vary from 34.39 ppm to 433.94 ppm.

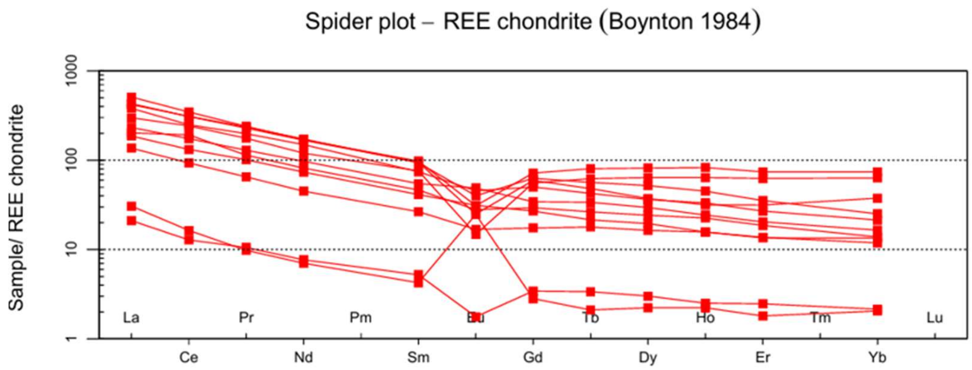

Text Fig 7.18: The chondrite-normalised REE spider diagram of augen gneiss (N=11).

The chondrite-normalized REE spider diagram (Boynton, 1984) (Text Fig 7.19) displays a steeply fractionated pattern with marked enrichment of LREEs (La–Sm) over HREEs (Gd–Lu), indicating strong LREE/HREE fractionation. The average concentrations of La (80.22 ppm), Ce (152.75 ppm), Nd (59.53 ppm) and Sm (10.91 ppm) are substantially higher than those of Er (5.75 ppm), Yb (5.34 ppm) and Lu (1.02 ppm), confirming that the REE budget is dominated by LREEs. The combined ΣREE+Sc+Y values range up to 874.80 ppm, averaging 433.94 ppm.

Most augen gneiss samples display a negative Eu anomaly (Eu depleted relative to Sm and Gd), indicating plagioclase fractionation in the felsic protolith. However, a subset of samples shows positive Eu anomalies (Eu/Eu* > 1), including one strongly positive value, which record local feldspar accumulation. The augen gneiss is further characterized by enrichment in several incompatible and high field strength elements (HFSE), including Zr (average 236.22 ppm), Hf (7.39 ppm), Y (65.49 ppm), Rb (244.27 ppm), and Th (35.52 ppm), reflecting the evolved felsic nature of the rock. Elevated concentrations of zirconium and hafnium suggest the presence of abundant zircon, whereas thorium enrichment indicates the occurrence of REE-bearing accessory phases such as monazite and allanite.

Overall, the geochemical characteristics indicate that the augen gneiss represents a highly evolved felsic lithology formed through partial melting and progressive differentiation of continental crust. The strong enrichment of LREEs, distinct negative Eu anomaly, elevated concentrations of HFSEs collectively suggest that REE mineralisation is primarily hosted by accessory minerals such as monazite, with subordinate zircon and titanite (allanite inferred, not petrographically confirmed).

Major oxides, i.e., SiO2, Al2O3, Fe2O3, MnO, MgO, CaO, Na2O, K2O, TiO2, P2O5, LOI were analysed for 3 nos of selected augen gneiss samples.

The major oxide composition of the augen gneiss samples indicates a felsic to intermediate-felsic composition, with SiO_2 contents ranging from 62.07 to 69.60 wt.%, reflecting the dominance of quartz and feldspar. The Al_2O_3 content (15.06–15.43 wt.%) remains relatively uniform, indicating a significant abundance of aluminosilicate minerals, particularly feldspars and micas. Fe_2O_3 exhibits considerable variation (0.59–6.35 wt.%), suggesting differences in the proportion of ferromagnesian minerals among the samples, while MgO (0.11–1.39 wt.%) and MnO (0.02–0.13 wt.%) remain consistently low, supporting the overall felsic character of the rocks. CaO values (0.99–3.18 wt.%) and Na_2O contents (2.01–2.85 wt.%) indicate the presence of plagioclase feldspar, whereas K_2O ranges from 4.71 to 10.25 wt.%, reflecting a strong enrichment in alkali feldspar, particularly K-feldspar, which is characteristic of augen gneiss containing large feldspar porphyroclasts. The low TiO_2 (0.07–0.92 wt.%) and P_2O_5 (0.02–0.25 wt.%) contents indicate only minor amounts of accessory Ti-bearing and phosphate minerals such as ilmenite, titanite, and apatite. The LOI values (0.67–0.84 wt.%) are low, suggesting limited alteration and a low volatile content.

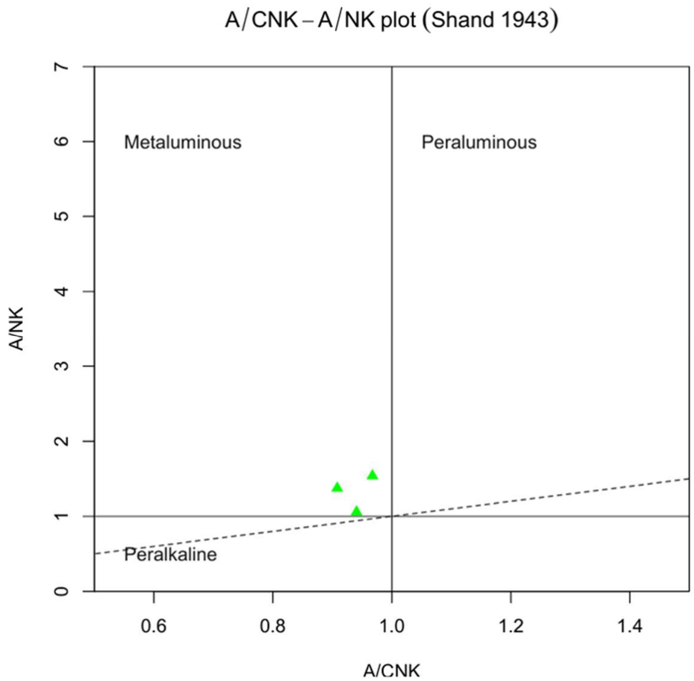

Text Fig 7.19

The A/CNK–A/NK diagram (Shand, 1943) (Text Fig 7.19) shows that all the augen gneiss samples plot within the metaluminous field (A/CNK < 1.0), with A/NK values greater than unity.

The Harker variation diagrams (Text Fig 7.23) exhibit relatively high SiO_2 contents (approximately 62–70 wt.%), confirming their felsic nature. With increasing SiO_2, MgO, TiO_2, P_2O_5, and total FeO (FeOt) show a distinct decrease, indicating progressive fractionation of ferromagnesian minerals (biotite and hornblende), Fe–Ti oxides, and apatite during magma evolution. Al_2O_3 exhibits only minor variation with a slight decreasing trend, suggesting that feldspar remained a major constituent throughout differentiation. CaO and Na_2O display variable concentrations, reflecting differences in plagioclase abundance among the samples. In contrast, K_2O shows an overall enrichment in the more evolved samples, indicating crystallization and accumulation of K-feldspar, which is consistent with the characteristic feldspar augen developed during metamorphism.

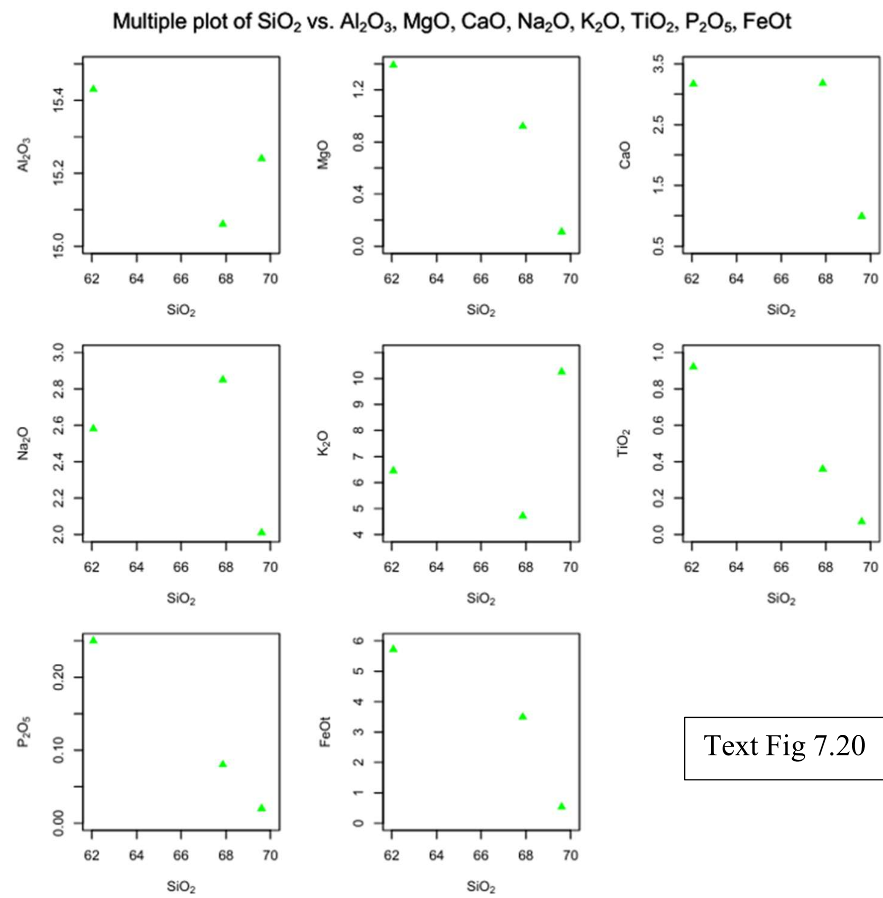

Text Fig 7.20

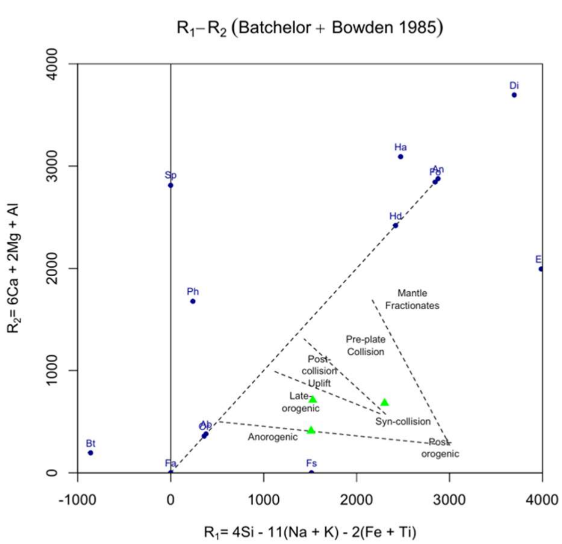

Text Fig 7.21

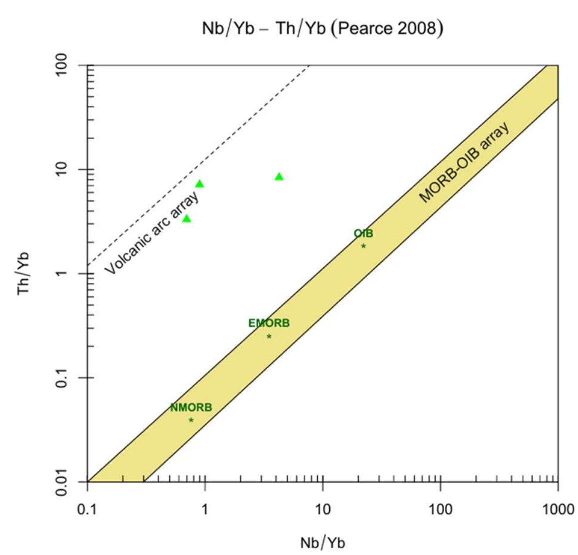

Text Fig 7.22

The R_1–R_2 tectonic discrimination diagram (Text Fig 7.21) indicates that the augen gneiss samples are distributed mainly within the anorogenic, late-orogenic, and syn-collisional granite fields. One sample plot within the anorogenic field, suggesting emplacement of its granitoid protolith in an intracontinental extensional setting. Another sample falls within the late-orogenic field, indicating magmatism associated with the final stages of orogenic activity. The third sample plots within the syn-collisional field, reflecting magma generation during continental collision through partial melting of the continental crust. The distribution of the samples across these tectonic fields suggests that the augen gneisses were derived from granitoid magmas generated during different stages of a prolonged tectono-magmatic evolution. The Nb/Yb–Th/Yb discrimination diagram (Pearce, 2008) (Text Fig 7.22) shows that all augen gneiss samples plot above the MORB–OIB array within the volcanic arc array, indicating a strong subduction-related geochemical signature. The elevated Th/Yb ratios relative to Nb/Yb reflect significant enrichment of thorium due to extensive crustal involvement during magma generation.

7.2.2.4 Granite:

The granites exposed in a few parts occur as isolated bodies and are generally massive, compact, and devoid of significant deformation features. Unlike the surrounding migmatites and granite gneisses, these granites do not exhibit well-developed tectonic foliations, shearing, or mineral stretching.

Photograph No. 7.6: The granite is medium- to coarse-grained and is predominantly composed of quartz and feldspar.

The granites are predominantly composed of quartz and feldspar, which constitute the felsic framework of the rock. Quartz occurs as anhedral to subhedral, glassy grey grains, whereas feldspar, mainly potassium feldspar with subordinate plagioclase, imparts a pinkish to whitish appearance to the rock. Mafic minerals are generally sparse and may include minor biotite and amphibole in some exposures. The coarse- to medium-grained texture and interlocking arrangement of mineral grains indicate slow crystallization from a granitic magma at considerable crustal depths. Although the granites are mostly massive and isotropic, magmatic foliation is locally observed at a few outcrops. Under microscope rocks shows medium to coarse grained and predominantly composed of Quartz, plagioclase, microcline/orthoclase and biotite. Orthoclase/ microcline and plagioclase occur as medium to moderately coarse subhedral grains, where alkali feldspar is showing perthitic exsolutions and plagioclase is showing myrmekitic intergrowths. Quartz occurs as fine to moderately coarse anhedral grains, patches and lenses. Biotite and muscovite are present as fine disseminated flakes. Sericite occurs as very fine flakes developing after plagioclase alterations. Opaques are present as fine subhedral to anhedral grains and as streaky fillings along cleavage traces of biotite. Chlorite occurs as fine flakes, often being interleaved with biotite and seen replacing it. Zircon is noted as very fine inclusions within biotite around which pleochroic halos are observed.

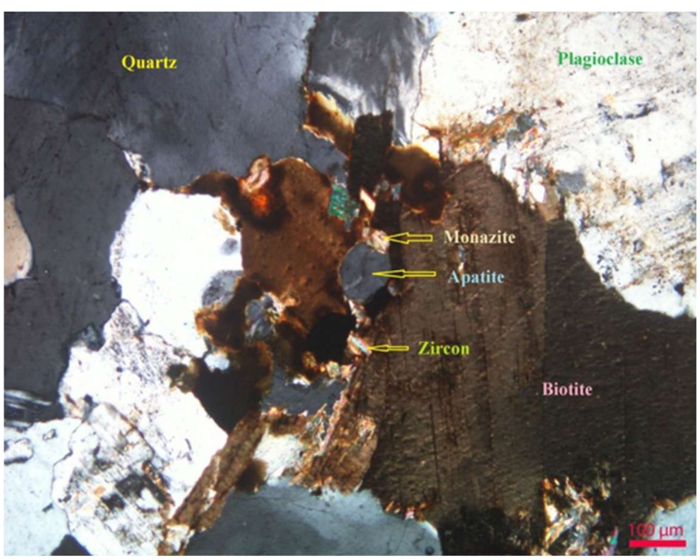

Pmg – 1: Photomicrograph showing association of quartz, plagioclase and biotite, where apatite, zircon and monazite are included within biotite as seen under crossed nicols.

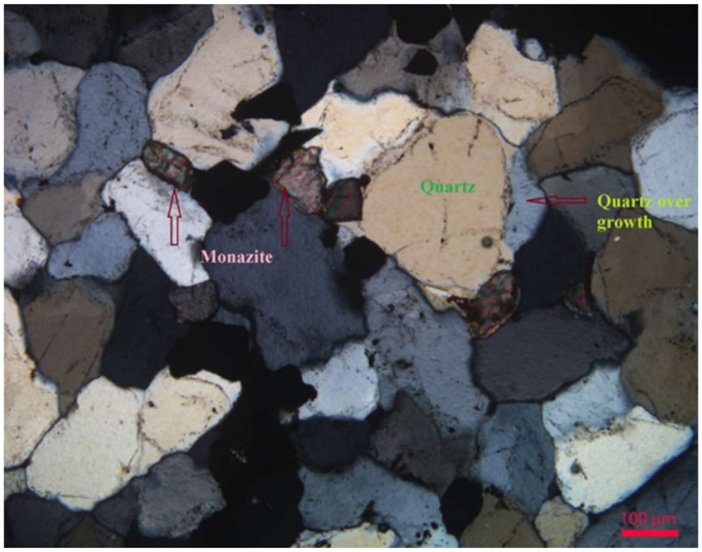

Pmg – 3: Photomicrograph showing quartz over growth and monazite grains in quartz arenite as seen under crossed nicols.

7.2.2.5 Altered Calcareous Silicious Sandstone:

The altered calcareous silicious sandstone exposed in the Langmipi–Laching Thing Block is whitish to light grey in colour and occurs as a massive to thickly bedded, hard and compact carbonate rock. The exposure is traversed by several steeply dipping joints and fractures, some of which appear to be filled with secondary calcite veinlets, indicating post-depositional fluid circulation and recrystallization. At some locations, the rock has undergone moderate to intense weathering, producing a reddish-brown weathering profile and disintegrating into angular carbonate fragments.

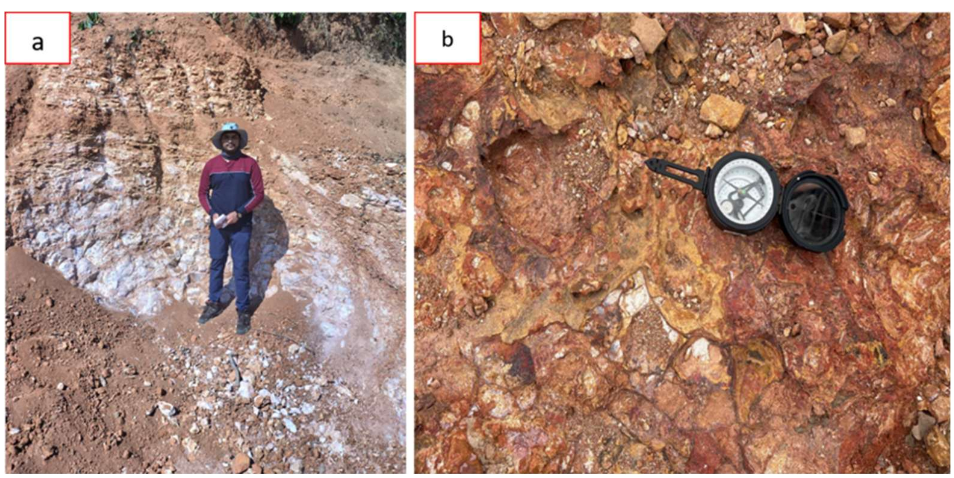

Photograph No. 7.7: a) The exposure near the Amreng river, b) exposure showing evidences of hydrothermal activity.

The lithounit undergone intense hydrothermal alteration and weathering, resulting in a highly ferruginized, reddish-brown appearance. The original carbonate rock is extensively altered, with only remnant patches of whitish carbonate rock is preserved within the weathered matrix. The outcrop exhibits a network of fractures and brecciated zones that have served as pathways for hydrothermal fluids, leading to silicification and iron oxide staining. Small specks and disseminations of copper-bearing minerals are observed along fractures and within the altered rock, indicating hydrothermal mineralization.

Photograph No. 7.8: Small specks of copper-bearing minerals are observed on altered calcareous-siliceous sandstone.

Geochemistry of the altered calcareous siliceous sandstone

A total of five altered calcareous silicious sandstone samples from the Langmipi Laching-Thing Block were analysed for 34 elements through ICP-MS analysis to evaluate the distribution of REE and associated trace elements within the lithounit (Table 7.4 and annexure II).

Table no 7.6. Summarized table of ICP-MS analysis of Altered Calcareous Siliceous Sandstone (N=5) for 34 elements

Elements	Max(ppm)	Min(ppm)	Mean(ppm)
Li	66.57	5.94	26.17
Be	2.53	0.66	1.55
Sc	86.73	0.94	21.01
V	812.02	1.98	178.13
Cu	132.68	11.57	37.48
Zn	230.32	17.99	66.85

Ga	42.20	2.43	19.05
Rb	267.70	9.67	71.76
Sr	163.02	18.71	69.06
Y	54.04	9.41	21.35
Zr	647.13	44.94	255.68
Nb	20.29	2.08	8.31
Sn	0.29	0.11	0.18
Ba	1000.00	24.17	265.47
La	43.03	13.14	25.63
Ce	95.07	21.75	53.88
Pr	7.32	2.52	4.80
Nd	23.40	9.20	16.70
Sm	4.57	1.88	3.43
Eu	1.29	0.24	0.82
Gd	4.71	1.99	3.38
Tb	1.26	0.32	0.66
Dy	9.44	1.93	4.21
Ho	2.40	0.38	0.92
Er	6.92	0.92	2.40
Tm	0.91	0.12	0.30
Yb	8.01	0.99	2.64
Lu	1.37	0.16	0.45
Hf	22.95	1.89	9.15
Ta	3.56	0.14	1.57
W	373.35	15.85	177.86
Pb	53.32	5.77	27.95
Th	142.72	4.69	37.71
U	9.75	0.80	6.23
∑REE	185.27	55.55	120.23
∑REEc+Sc+Y	272.30	68.16	162.60

The samples exhibit comparatively lower Rare Earth Element (REE) concentrations than the associated felsic lithologies, namely granite gneiss, augen gneiss and migmatite, but retain a distinct REE distribution pattern indicative of crustal influence. The total REE (ΣREE) values range from 55.55 ppm to 185.27 ppm, with an average of 120.23 ppm, while the combined ΣREE+Sc+Y values vary from 68.16 ppm to 272.30 ppm, averaging 162.60 ppm. The relatively low REE abundance reflects the carbonate nature of the rock, where REE-hosting accessory minerals are comparatively sparse. Nevertheless, the limestone displays systematic enrichment of Light Rare Earth Elements (LREE) over Heavy Rare Earth Elements (HREE), suggesting that the REE budget was influenced by detrital input and interaction with surrounding felsic rocks during deposition or subsequent metamorphism.

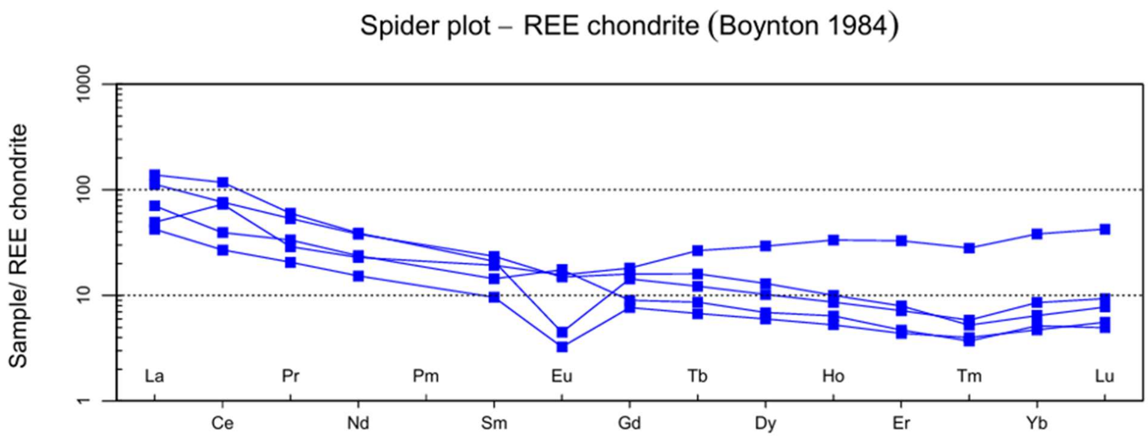

Text Fig 7.23: The chondrite-normalised REE spider diagram (N=5).

The chondrite-normalized REE spider diagram (Boynton, 1984) shows a moderately fractionated pattern characterized by enrichment of La, Ce, Nd and Sm relative to the HREEs. The lithounit also contains moderate concentrations of incompatible and high field strength elements (HFSE), including Zr (average 255.68 ppm), Hf (9.15 ppm), Th (37.71 ppm), Y (21.35 ppm) and Nb (8.31 ppm), indicating the presence of detrital zircon and other resistant accessory minerals within the carbonate sequence. The relatively high scandium (average 21.01 ppm) and vanadium (average 178.13 ppm) contents further indicate local enrichment by mafic minerals or hydrothermal alteration.

The REE spider diagram reveals generally sub-parallel patterns among most samples, indicating a broadly similar provenance and geochemical evolution.

However, a few samples display comparatively flatter HREE segments and slight HREE enrichment, suggesting localized variations in accessory mineral assemblages or secondary hydrothermal modification.

Overall, the geochemical characteristics suggest that the altered calcareous-siliceous sandstone represents a chemically mature, LREE-enriched sedimentary rock that has undergone significant hydrothermal alteration, resulting in enrichment incompatible elements while largely preserving the characteristic REE signature of its sedimentary protolith.

A total of three altered calcareous siliceous sandstone samples were subjected to major oxide analysis by X-ray Fluorescence (XRF).

The major oxide geochemistry of samples exhibits considerable compositional variability, reflecting differences in the degree of silicification, ferruginization, and chemical alteration. The analyzed samples are characterized by high SiO_2 contents (13.31–73.07 wt.%), indicating that silica is a major constituent in most of the samples. Al_2O_3 values (12.19–15.78 wt.%) are consistently high, implying the presence of aluminosilicate minerals such as clay minerals and feldspars. The samples also show a wide variation in Fe_2O_3 (0.52–57.71 wt.%), indicating localized iron enrichment, probably due to weathering, hydrothermal activity, or secondary iron oxide mineralization. The generally low CaO (0.02–3.29 wt.%) and MgO (0.04–0.31 wt.%) contents suggest that carbonate minerals constitute only a minor proportion of the analyzed material, whereas the elevated Na_2O (0.03–4.27 wt.%) and K_2O (0.08–8.28 wt.%) reflect the presence of alkali feldspars and other silicate phases. Minor concentrations of TiO_2 (0.04–1.86 wt.%) and P_2O_5 (0.02–0.62 wt.%) indicate the occurrence of accessory Fe–Ti oxides and phosphate minerals.

Overall, the major oxide geochemistry indicates that the altered calcareous-siliceous sandstone has undergone significant post-depositional hydrothermal alteration, resulting in silica enrichment, localized iron mineralization, and alkali redistribution while preserving the siliceous nature of the original sedimentary protolith.

7.2.2.6 Pegmatite, quartz veins and quartzo-feldspathic veins:

Three major types of veins intrude the principal lithological units of the study area. These veins have been classified based on their mineralogical composition.

a) Pegmatite veins: Pegmatite veins intrude all the major lithological units of the study area and represent the youngest intrusive phase. They are predominantly off-white to pale pink in colour, with the pinkish hue imparted by K-feldspar. The veins are medium- to coarse-grained and are mainly composed of quartz and feldspar, with minor accessory minerals. Their thickness is highly variable, ranging from approximately 1 cm to 15–20 cm.


Photograph No. 7.9: Pegmatite vein intruding the migmatite.

Most pegmatite veins are emplaced parallel to the foliation of the host rocks, indicating structural control during emplacement. However, at several locations, pegmatite veins exhibit cross-cutting relationships with the host lithologies, suggesting multiple episodes of magmatic intrusion and deformation. Tourmaline mineralization is observed within some of the pegmatite veins, indicating the involvement of boron-rich residual magmatic fluids during the late stages of crystallization.

Photograph No. 7.10: Photograph showing a pegmatite vein intruding the migmatite, with tourmaline mineralization occurring within the pegmatite.

Geochemistry of pegmatites

A total of four pegmatite samples from the Langmipi Laching-Thing Block were analysed for 34 elements through ICP-MS analysis to evaluate the distribution of REE and associated trace elements within the lithounit (Table 7.6 and annexure II).

Table no 7.7. Summarized table of ICP-MS analysis of Pegmatite veins (N=4) for 34 elements

Elements	Max(ppm)	Min(ppm)	Mean(ppm)
Li	26.66	15.86	22.27
Be	6.49	2.72	3.84
Sc	19.11	9.67	14.76
V	67.00	25.60	48.53
Cu	25.85	16.68	22.12
Zn	110.19	54.19	86.62
Ga	27.89	18.73	24.33
Rb	350.84	156.54	275.62
Sr	323.46	213.55	274.22
Y	70.12	55.80	66.34
Zr	450.72	119.86	301.69
Nb	9.99	5.71	7.57
Sn	0.19	0.11	0.16
Ba	1600.00	738.64	885.58
La	139.30	55.31	103.96
Ce	256.32	113.02	212.54
Pr	27.94	12.26	21.84
Nd	103.71	44.75	78.96
Sm	18.35	8.49	13.58

Eu	2.39	2.04	2.25
Gd	15.64	8.14	11.79
Tb	2.32	1.53	1.92
Dy	13.62	9.63	11.56
Ho	2.76	2.07	2.34
Er	6.90	5.15	5.89
Tm	0.77	0.57	0.66
Yb	5.24	3.02	4.27
Lu	0.77	0.41	0.65
Hf	12.70	3.77	8.94
Ta	0.89	0.48	0.72
W	249.18	199.29	229.85
Pb	60.39	25.29	43.00
Th	69.59	21.44	51.31
U	5.23	1.07	3.32
∑REE	579.67	268.21	472.20
∑REEc+Sc+Y	662.01	343.12	553.30

The pegmatite vein samples from the Langmipi–Laching Thing Block are characterized by significant enrichment in Rare Earth Elements (REEs), reflecting their derivation from highly evolved felsic magmatic melts. The total REE (ΣREE) content ranges from 268.21 ppm to 579.67 ppm, with an average of 472.20 ppm, while the combined ΣREE+Sc+Y values range from 343.12 ppm to 662.01 ppm, averaging 553.30 ppm. These values are substantially higher than those of the augen gneiss, and are comparable to the migmatite, indicating that the pegmatite veins constitute an important repository of REEs within the study area.

The chondrite-normalized REE spider diagram (Boynton, 1984) exhibits a strongly fractionated pattern with marked enrichment of Light Rare Earth Elements (LREEs) over Heavy Rare Earth Elements (HREEs), which is characteristic of evolved granitic pegmatites. The average concentrations of La (103.96 ppm), Ce (212.54 ppm), Nd (78.96 ppm) and Sm (13.58 ppm) are considerably higher than those of Er (5.89 ppm), Yb (4.27 ppm) and Lu (0.65 ppm), indicating pronounced LREE enrichment and efficient fractionation during the late stages of magmatic evolution.

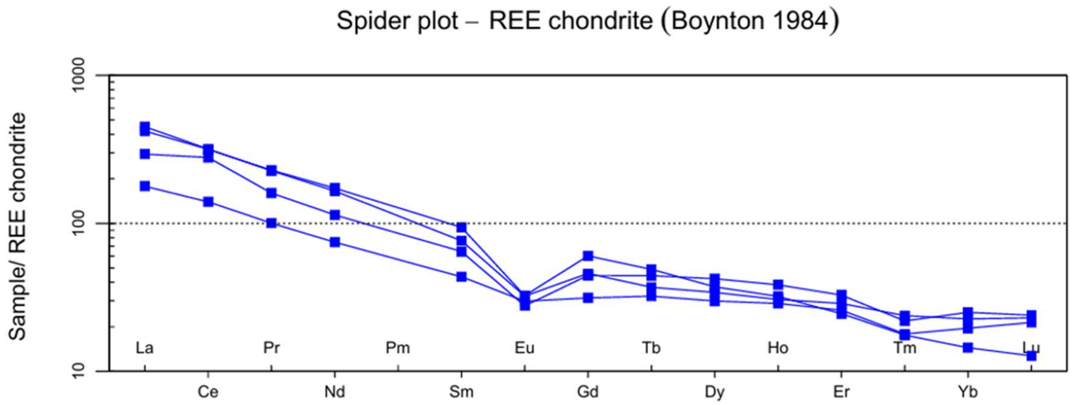

Text Fig 7.24: The chondrite-normalised REE spider diagram of Pegmatite veins (N=4).

The chondrite-normalized REE pattern displays a distinct negative europium (Eu) anomaly, evident from the depletion of Eu relative to the adjacent Sm and Gd. This anomaly indicates extensive plagioclase fractionation prior to pegmatite emplacement, resulting in the preferential removal of Eu from the residual melt. The pegmatite veins are also enriched in several incompatible and high field strength elements (HFSEs), including Zr (average 301.69 ppm), Hf (8.94 ppm), Y (66.34 ppm), Th (51.31 ppm), Rb (275.62 ppm) and Ba (885.58 ppm). The elevated Rb and Ba concentrations reflect a potassium-rich felsic composition and extensive feldspar crystallization during the late stages of magmatic differentiation. High zirconium and hafnium contents indicate abundant zircon, whereas the elevated thorium concentrations suggest the presence of monazite and allanite as the principal REE-bearing accessory minerals.

Overall, the geochemical characteristics indicate that the pegmatite veins represent the most evolved products of felsic magmatism within the Langmipi–Lachingthin Block. Their strong LREE enrichment, well-developed negative Eu anomaly, elevated concentrations of incompatible elements and HFSEs, and significant tungsten enrichment collectively indicate that these veins crystallized from highly fractionated residual melts enriched in incompatible elements. The REE mineralization is likely hosted by accessory minerals such as monazite (the dominant REE carrier identified petrographically), with subordinate zircon and titanite which preferentially concentrate LREEs during pegmatite formation.

A total of two pegmatite samples collected from the Langmipi–Laching Thing Block were subjected to major oxide analysis using X-ray Fluorescence (XRF). The major oxide composition of the pegmatite samples indicates a silica-rich, felsic composition, with SiO_2 contents ranging from 58.84 to 63.46 wt.%. The relatively high Al_2O_3 values (15.86–16.15 wt.%) reflect the abundance of aluminosilicate minerals, chiefly feldspars and micas, which are characteristic constituents of pegmatites. Fe_2O_3 contents vary from 5.08 to 8.18 wt.%, indicating a moderate proportion of ferromagnesian and Fe-bearing accessory minerals, while MgO (1.14–1.80 wt.%) and MnO (0.10–0.16 wt.%) remain low, consistent with the overall felsic nature of the rocks. CaO values (2.22–3.24 wt.%) and Na_2O contents (2.23–2.24 wt.%) suggest the presence of plagioclase feldspar, whereas the relatively high K_2O contents (6.60–7.90 wt.%) indicate a significant enrichment in K-feldspar, a diagnostic feature of granitic pegmatites. The TiO_2 (0.74–1.08 wt.%) and P_2O_5 (0.20–0.28 wt.%) contents are comparatively higher than those of the associated granite gneiss and augen gneiss, suggesting a greater abundance of accessory Ti-bearing and phosphate minerals such as ilmenite, titanite, and apatite. The LOI values (0.49–0.98 wt.%) are low, indicating limited alteration and a low volatile content. Overall, the major oxide geochemistry suggests that the pegmatites are potassic, felsic rocks dominated by quartz and K-feldspar, with moderate enrichment in Fe-bearing accessory minerals

The R_1–R_2 tectonic discrimination diagram (Batchelor and Bowden, 1985), (Text Fig 7.25) indicates that the analysed pegmatite samples predominantly plot within the post-collision uplift field, with some samples lying close to the late-orogenic and syn-collisional boundaries. This distribution suggests that the pegmatites were emplaced during the late stages of orogenic evolution, following continental collision and crustal thickening. Their position reflects derivation from evolved granitic magmas generated mainly through partial melting of the continental crust, accompanied by fractional crystallization during post-collisional tectonic relaxation.

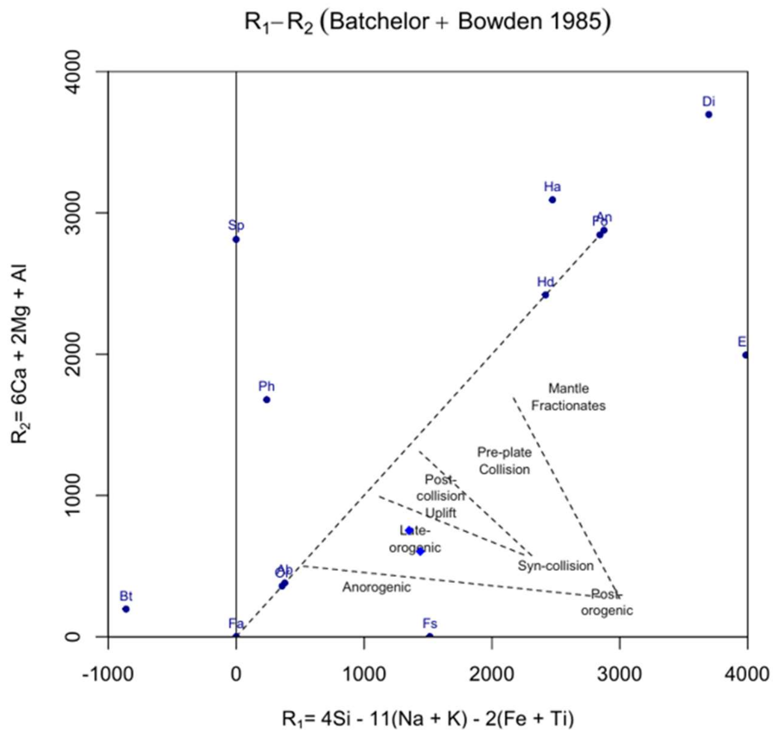

Text Fig 7.25

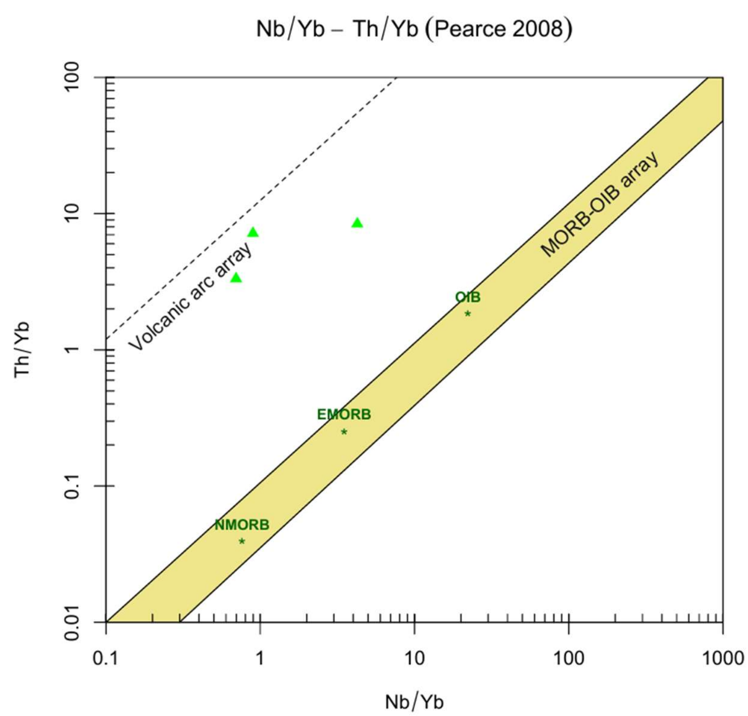

Text Fig 7.26

The Nb/Yb–Th/Yb discrimination diagram (Pearce, 2008) (Text Fig 7.26) shows that all pegmatite samples plot well above the MORB–OIB array within the volcanic arc array, indicating a strong crustal and subduction-related geochemical signature. Their elevated Th/Yb ratios relative to Nb/Yb reflect significant enrichment of thorium due to extensive crustal involvement during magma generation. The displacement from the mantle array suggests that the pegmatites were derived from partial melting of subduction-modified continental crust rather than directly from mantle-derived magmas.

b). Quartz vein: Quartz veins are widely developed throughout the study area, intruding all the major lithological units, including migmatite, granite gneiss and augen gneiss. They are predominantly off-white to slightly pinkish in colour and exhibit a medium- to moderately coarse-grained texture. The veins are mainly composed of quartz, with minor feldspar occurring locally. Their thickness varies from a few centimetres to approximately 20 cm. Most quartz veins are emplaced parallel to the foliation of the host rocks, indicating structural control during their emplacement. However, at several locations, quartz veins display cross-cutting relationships with the foliation and earlier lithological contacts, suggesting multiple episodes of fracturing and subsequent silica-rich fluid intrusion.

Photograph No. 7.11: quartz veins thickness ranging from 10-15 cm intruded the migmatite rock.

The cross-cutting veins are generally younger than the host rock fabric and record late-stage tectonic deformation and hydrothermal activity. In some exposures, quartz veins occur as discontinuous lenses or pinch-and-swell structures, reflecting emplacement within active shear zones. A quartz vein emplaced within the amphibolite band is folded and sheared, indicating that the vein was emplaced prior to or during the deformation event and subsequently deformed under ductile shear.

Photograph No. 7.12: Quartz vein within the amphibolite band exhibiting folding and shearing.

Under microscope rocks mainly composed of quartz with ferruginous matter present in minor amount and tourmaline, sericite and monazite present as accessory minerals. Quartz occurs as fine to medium subrounded to subangular grains showing moderate sorting and tight packing. Quartz overgrowth is noted in the specimen. Yellowish limonitic/ reddish ferruginous patches and fillings are seen present in the specimen. Opaques occur as fine disseminated grains. Tourmaline and monazite are present as very fine prismatic/ subrounded grains in accessories. Sericite is noted as very fine flakes. Accordingly, it is petrographically classified as quartz arenite.

Geochemistry of Quartz veins

A single quartz vein samples from the Langmipi Laching-Thing Block were analysed for 34 elements through ICP-MS analysis to evaluate the distribution of REE and associated trace elements within the lithounits. The quartz vein contains a total REE (ΣREE) concentration of 109.12 ppm, while the combined ΣREE+Sc+Y value is 123.37 ppm, indicating comparatively low REE enrichment relative to the associated granite gneiss, migmatite, augen gneiss and pegmatite veins. The REE distribution is dominated by Light Rare Earth Elements (LREEs), with concentrations of La (25.16 ppm), Ce (47.02 ppm), Nd (16.85 ppm) and Sm (3.22 ppm) exceeding those of the Heavy Rare Earth Elements (HREEs), including Dy (2.57 ppm), Er (1.56 ppm), Yb (1.95 ppm) and Lu (0.31 ppm). This LREE-enriched pattern suggests that the quartz vein was emplaced from a felsic magmatic or hydrothermal fluid that inherited its REE signature from the surrounding granitoid host rocks.

c) Quartzo-feldspathic vein: Quartzo-feldspathic veins are the most prominent and abundant vein type developed within the study area, intruding all the major lithological units. They are typically light pink to pinkish-white in colour owing to the abundance of K-feldspar, and exhibit a medium- to coarse-grained texture. The veins are predominantly composed of quartz and feldspar, with minor biotite and accessory minerals occurring locally. Their thickness varies from a few centimetres to approximately 25–30 cm, while their lateral continuity extends for several metres at some locations.

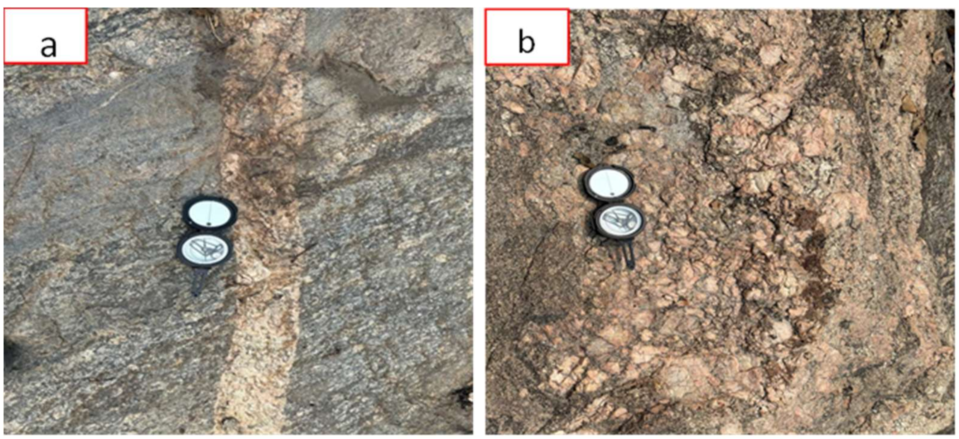

Photograph No. 7.13.: a) quartzo-feldspathic veins intruded across the foliation of migmatite rocks. b) quartzo-feldspathic veins consist of large pinkish K-feldspar grains present within migmatites.

Most quartzo-feldspathic veins are emplaced parallel to the foliation of the host rocks, indicating structural control during emplacement, although cross-cutting veins are also common, suggesting multiple episodes of magmatic intrusion. In several exposures, the quartzo-feldspathic veins are sheared and displaced, exhibiting dextral (right-lateral) shear sense, indicating that they were affected by subsequent tectonic deformation. Local folding, pinch-and-swell structures, and boudinage further evidence to the progressive deformation of the veins within active shear zones.

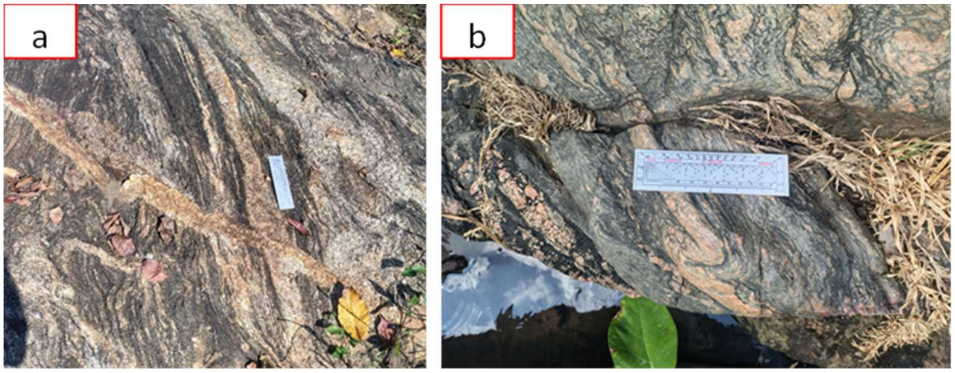

Photograph No. 7.41.: a) cross-cutting of two quartzo-feldspathic veins, b) the quartzo-feldpathic vein got sheared giving dextral shear senses.

Geochemistry of quartzo-feldspathic veins

A total of five quartzo-feldspathic samples from the Langmipi Laching-Thing Block were analysed for 34 elements through ICP-MS analysis to evaluate the distribution of REE and associated trace elements within the lithounit (Table 7.6 and annexure II).

Table no 7.8. Summarized table of ICP-MS analysis of Quartzo-feldspathic veins (N=5) for 34 elements

Elements	**Max(ppm)**	**Min(ppm)**	**Mean(ppm)**
Li	28.58	6.89	17.71
Be	8.59	3.65	5.83
Sc	12.32	1.19	6.13
V	80.07	6.76	28.64
Cu	28.99	10.10	15.81
Zn	99.19	23.00	46.96
Ga	30.91	19.52	23.69
Rb	403.39	196.88	332.78
Sr	310.55	40.46	183.17
Y	105.86	12.48	69.13
Zr	346.36	75.81	183.07
Nb	16.25	4.00	11.33

Sn	2.16	0.14	1.14
Ba	1400.00	110.72	885.58
La	172.56	15.00	71.48
Ce	323.96	28.25	138.57
Pr	35.31	3.65	15.48
Nd	125.12	14.04	54.12
Sm	19.50	3.51	9.55
Eu	2.85	0.48	1.61
Gd	15.39	2.87	8.28
Tb	2.40	0.49	1.67
Dy	17.63	2.56	11.93
Ho	3.56	0.42	2.47
Er	11.49	1.28	7.80
Tm	1.87	0.19	1.26
Yb	12.93	1.42	8.68
Lu	2.20	0.22	1.44
Hf	11.43	2.89	6.56
Ta	2.63	0.81	1.77
W	244.57	8.47	130.05
Pb	99.48	42.22	67.56
Th	62.27	15.50	40.83
U	26.43	9.16	16.11
∑REE	734.19	108.80	334.36
∑REEc+Sc+Y	852.37	126.87	409.62

The quartzo-feldspathic vein samples from the Langmipi–Laching Thing Block exhibit moderate to high Rare Earth Element (REE) concentrations, reflecting their derivation from evolved felsic magmatic melts and subsequent hydrothermal modification. The total REE (ΣREE) content ranges from 108.80 ppm to 734.19 ppm, with an average of 334.36 ppm, whereas the combined ΣREE+Sc+Y values vary from 126.87 ppm to 852.37 ppm, averaging 409.62 ppm. These values indicate that the quartzo-feldspathic veins are moderately enriched in REEs and represent an important lithological unit hosting incompatible elements within the study area.

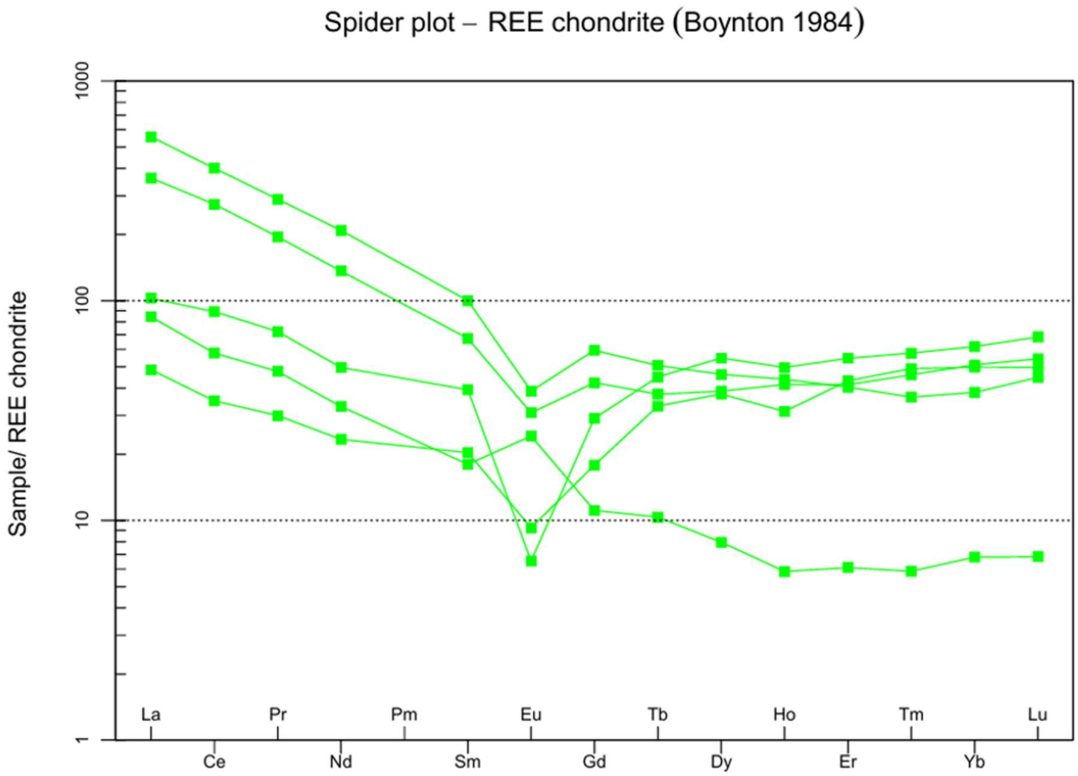

Text Fig 7.27: The chondrite-normalised REE spider diagram of Quartzo-feldspathic veins (N=5).

The chondrite-normalized REE patterns (Boynton, 1984) of the quartzo-feldspathic veins from the Langmipi–Lachingthin Block exhibit a characteristic signature of strongly fractionated felsic magmatic rocks. The patterns are marked by pronounced enrichment of Light Rare Earth Elements (LREE) relative to Heavy Rare Earth Elements (HREE), with steeply declining trends from La to Sm and comparatively flat HREE segments from Gd to Lu. A prominent feature of all the REE patterns is the well-developed negative Eu anomaly, where Eu plots significantly below the smooth trend defined by Sm and Gd. This anomaly indicates extensive plagioclase feldspar fractionation during magmatic differentiation, as Eu^{2+} is preferentially incorporated into plagioclase during crystallization.

The analytical data also demonstrate significant enrichment of REE within the veins, with ΣREE values ranging from 108.80 to 734.19 ppm and an average of 334.36 ppm. The average concentrations of La (71.48 ppm), Ce (138.57 ppm), Nd (54.12 ppm), and Sm (9.55 ppm) are substantially higher than those of the HREE, confirming the dominance of LREE over HREE. In addition to REE enrichment, the veins are characterized by elevated concentrations of incompatible elements such as Rb (332.78 ppm), Ba (885.58 ppm), Y (69.13 ppm), Zr (183.07 ppm), Hf (6.56 ppm), Th (40.83 ppm), U (16.11 ppm), and W (130.05 ppm). Such enrichment is typical of highly evolved granitic melts and late-stage pegmatitic or hydrothermal fluids, where incompatible elements become progressively concentrated during fractional crystallization.

Overall, the REE geochemistry indicates that the quartzo-feldspathic veins represent late-stage differentiates of evolved felsic magmatism. Their strong LREE enrichment, pronounced negative Eu anomaly, elevated incompatible element concentrations collectively suggest crystallization from highly fractionated granitic melts followed by hydrothermal activity.

7.2.2.6 **Soil/Alluvium:** Soil and alluvium constitute the unconsolidated surficial cover over a substantial part of the Langmipi–Laching Thing Block and represent the youngest geological deposits in the area. These deposits are predominantly composed of residual soils formed by the in-situ weathering of the underlying gneissic rocks, together with Quaternary alluvial sediments deposited along drainage channels and low-lying areas.

Based on colour, texture, and parent lithology, the soils of the Langmipi–Laching Thing Block can be broadly classified into two categories: dark brown soil and reddish-brown soil. The dark brown soil is predominantly developed over migmatite and is medium-grained in nature. It contains abundant biotite flakes and quartz grains, reflecting the mineralogical composition of the parent rock. In contrast, the reddish-brown soil is chiefly derived from the weathering of granite gneiss and varies from fine- to medium-grained. It is composed mainly of feldspar and quartz, with minor amounts of biotite. The reddish-brown colour is attributed to the oxidation of iron-bearing minerals during weathering.

Quaternary alluvium is mainly confined to the southern and northeastern parts of the block, where it has been deposited by west-flowing streams draining the area. These alluvial deposits comprise unconsolidated sand, silt, clay, and locally gravel, representing recent fluvial sedimentation. The thickness of the alluvium varies depending on the local topography and proximity to stream channels, with relatively thicker accumulations occurring along valley floors and floodplains.

Photograph No. 7.15: a) Pit near Jengkro Village, b) Pit near Kheroni area.

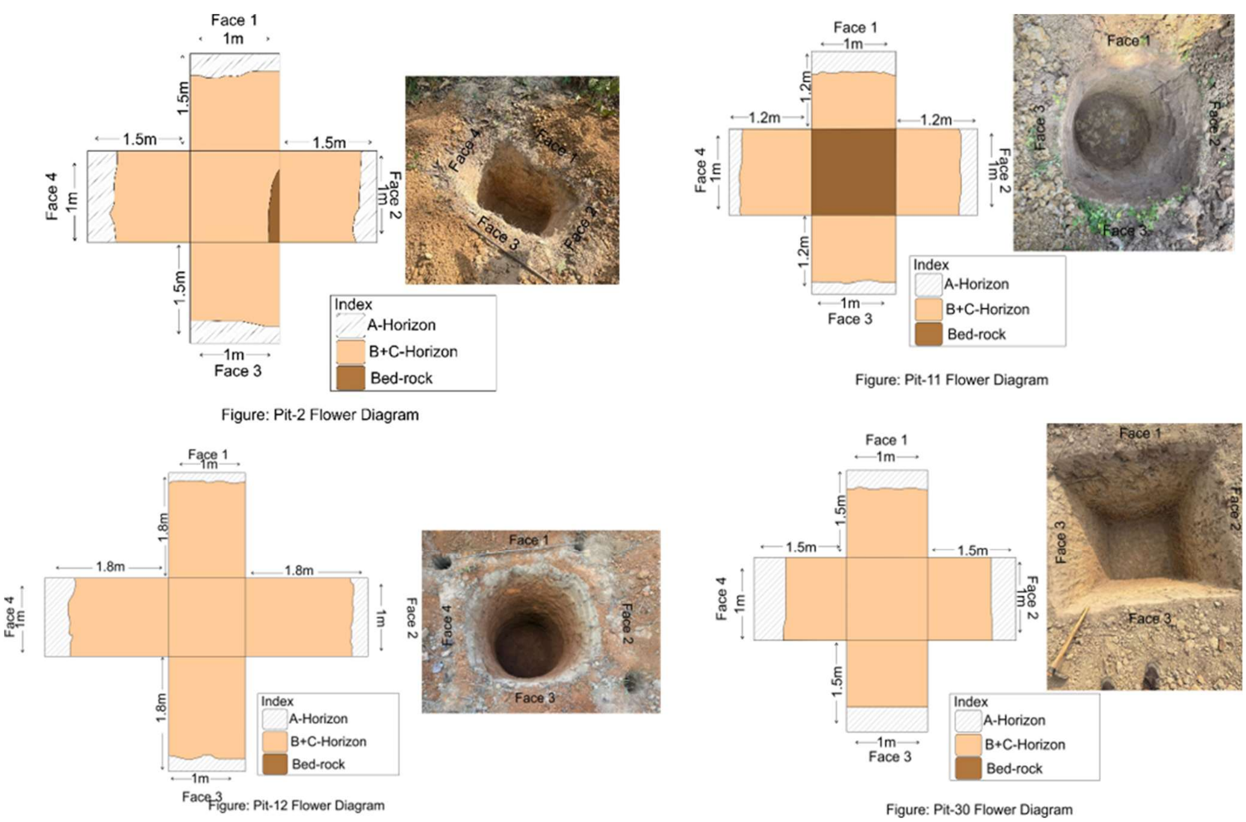

Photograph No. 7.16: Pit flower diagram

A total of 65 soil (pit) samples were collected from the Langmipi Laching-thing Block. The samples were collected from different soil profiles, predominantly from the B-horizon and the combined B + C horizon, to evaluate the geochemical characteristics of the subsurface soil and assess the distribution of rare earth elements (REE) and associated mineralization.

A total of 21 B-horizon soil samples were collected from the Langmipi Laching-thing Block. The B-horizon soils are predominantly clayey in nature, characterized by finer particle size, higher moisture retention, and relatively lower permeability compared to the overlying A-horizon. A clear distinction between the B-horizon and the overlying A-horizon can be observed in terms of texture, colour, and structure, with the B-horizon appearing denser and more compact due to the accumulation of translocated materials. This horizon represents the zone of illuviation, where materials such as clay minerals, iron and aluminium oxides, and organic compounds are translocated and accumulated from the upper layers.

A total of 44 B + C horizon soil samples were collected from the Langmipi Laching-thing Block. In the field, a clear distinction between the B-horizon and the underlying C-horizon was often difficult due to the gradational nature of the soil profile. Consequently, samples collected from this transitional zone were classified as B + C horizon soil samples.

The C-horizon is predominantly sandy and gravelly to rocky in nature, consisting of partially weathered parent material with abundant rock fragments and bedrock clasts. It is characterized by minimal pedogenic development, low organic matter content, and comparatively weaker chemical weathering than the overlying horizons. The presence of weathered bedrock fragments within the C-horizon makes it an important sampling medium for assessing the geochemical signature of the underlying parent rock.

The average thickness of the A-horizon is approximately 30 cm, while the B-horizon averages around 40 cm in thickness. In several pits, fresh to moderately weathered bedrock was encountered at relatively shallow depths; however, on average, the bedrock was intersected at a depth of approximately 1.5 m.

Geochemistry of soil samples

A total of 21 B-horizon was analysed for 34 elements through ICP-MS analysis to evaluate the distribution of REE and associated trace elements. Analytical results indicate that the B-horizon samples record a maximum ΣREE+Sc+Y of 916.65 ppm and an average ΣREE+Sc+Y of 443.41 ppm (ΣREE: maximum 788.70 ppm, average 383.85 ppm), suggesting significant rare earth element enrichment within the sampled horizon.

Table no 7.9. Summarized table of ICP-MS analysis of B-horizon soil samples (N=21) for 34 elements.

Elements	Max(ppm)	Min(ppm)	Mean(ppm)
Li	54.24	15.85	35.76
Be	4.37	0.80	2.35
Sc	23.61	4.45	14.65
V	146.64	42.34	96.84
Cu	49.50	15.81	34.67
Zn	320.55	25.15	84.32
Ga	37.20	7.34	22.97
Rb	287.50	89.13	181.64
Sr	142.42	24.11	51.98
Y	107.98	23.81	44.91
Zr	382.53	121.05	233.98
Nb	14.01	4.79	9.34
Sn	9.14	0.14	3.00
Ba	1200.00	224.06	479.93
La	130.68	42.43	82.70
Ce	425.49	87.81	173.98
Pr	32.39	8.88	18.66
Nd	112.13	32.16	64.01
Sm	18.89	5.96	11.29
Eu	2.41	0.97	1.66
Gd	17.20	5.29	9.57

Tb	3.00	0.91	1.62
Dy	18.24	4.98	9.30
Ho	3.64	0.90	1.71
Er	11.72	2.27	4.52
Tm	1.51	0.29	0.59
Yb	10.08	1.84	3.72
Lu	1.32	0.23	0.53
Hf	11.79	3.80	7.57
Ta	3.65	0.78	1.82
W	142.42	3.59	28.35
Pb	62.29	23.56	42.62
Th	75.77	19.88	41.90
U	11.48	2.81	6.93
∑REE	788.70	197.64	383.85
∑REEc+Sc+Y	916.65	241.58	443.41

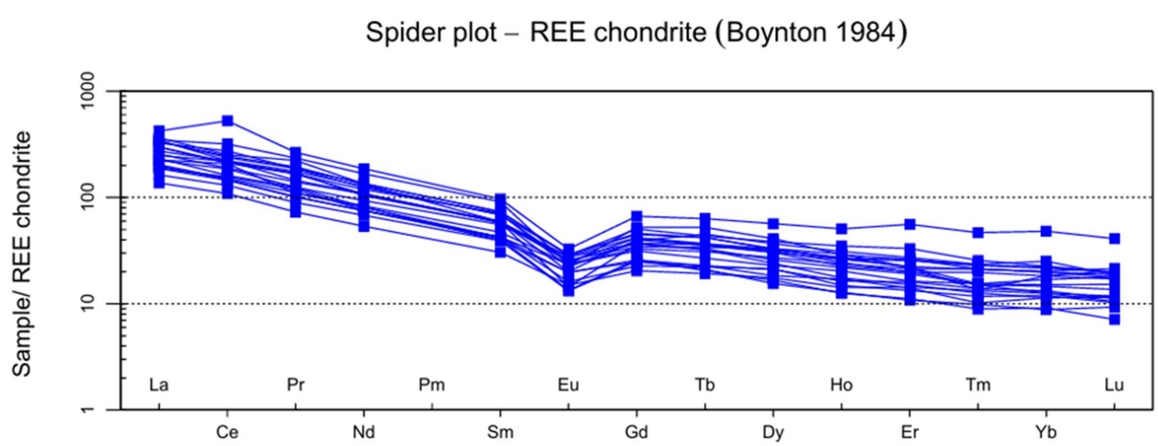

Fig 7.28: The chondrite-normalised REE spider diagram of Soil B-horizon samples(N=21).

The chondrite-normalized REE patterns (Boynton, 1984) of the B-horizon soil samples from the Langmipi–Laching Thing Block exhibit a pronounced enrichment of Light Rare Earth Elements (LREE) relative to Heavy Rare Earth Elements (HREE), reflecting the geochemical signature of the underlying felsic source rocks. The REE patterns are characterized by steeply fractionated trends from La to Sm, followed by relatively flat to gently declining HREE segments from Gd to Lu. A prominent feature of the REE patterns is the well-developed negative Eu anomaly, where Eu plots distinctly below the smooth trend defined by Sm and Gd. This negative Eu anomaly is characteristic of felsic igneous rocks that have undergone extensive plagioclase fractionation, as Eu^{2+} is preferentially incorporated into plagioclase during crystallization. The preservation of this anomaly in the B-horizon soils indicates that chemical weathering has not significantly altered the primary REE distribution inherited from the parent rocks.

The B-horizon soils exhibit moderate to high REE concentrations, with ΣREE values ranging from 197.64 to 788.70 ppm and an average of 383.85 ppm, which is higher than the average REE content of the stream sediments from the same area. The average concentrations of La (82.70 ppm), Ce (173.98 ppm), Nd (64.01 ppm), and Sm (11.29 ppm) are considerably higher than those of the HREE, confirming the dominance of LREE over HREE. The average ΣREE + Sc + Y value of 443.41 ppm further indicates significant enrichment of rare earth and associated incompatible elements within the soil profile. The B-horizon soils are also enriched in several incompatible and high-field-strength elements, including Rb (181.64 ppm), Ba (479.93 ppm), Zr (233.98 ppm), Hf (7.57 ppm), Th (41.90 ppm), U (6.93 ppm), Y (44.91 ppm), and Nb (9.34 ppm). The elevated concentrations of Zr and Hf indicate the accumulation of resistant heavy minerals such as zircon during weathering, whereas the enrichment of Th suggests the presence of accessory REE-bearing minerals such as monazite and allanite. The soils also contain appreciable tungsten concentrations (average 28.35 ppm; maximum 142.42 ppm), indicating that tungsten-bearing minerals are associated with the REE-enriched source rocks within the study area.

Overall, the REE geochemical characteristics of the B-horizon soils indicate that they are derived primarily from the in-situ weathering of REE-bearing granitic gneisses, migmatites, pegmatites, and quartzo-feldspathic veins exposed in the Langmipi–Laching Thing Block. The pronounced LREE enrichment, persistent negative Eu anomaly, enrichment of incompatible trace elements, and relatively high ΣREE values demonstrate that the B-horizon soil samples effectively preserve the geochemical signature of the parent rocks.

A total of 44 B+C-horizon was analysed for 34 elements through ICP-MS analysis to evaluate the distribution of REE and associated trace elements. Geochemical analysis of the B + C horizon samples recorded a maximum ΣREE+Sc+Y of 1,384.95 ppm and an average ΣREE+Sc+Y of 428.42 ppm (ΣREE: maximum 1,235.92 ppm, average 364.94 ppm), indicating significant enrichment of rare earth elements within the B + C horizon and reflecting the influence of the underlying weathered parent material on REE distribution.

Table no 7.10. Summarized table of ICP-MS analysis of B+C-horizon soil samples (N=44) for 34 elements

Elements	Max(ppm)	Min(ppm)	Mean(ppm)
Li	64.62	4.69	41.04
Be	4.96	0.60	2.21
Sc	41.58	2.55	17.05
V	171.53	12.43	111.85
Cu	67.19	11.95	38.02
Zn	251.61	18.91	82.58
Ga	38.07	9.77	25.83
Rb	309.69	56.59	192.25
Sr	125.81	5.74	51.22
Y	130.58	14.30	46.43
Zr	398.00	100.79	220.28
Nb	19.51	3.47	9.78
Sn	6.35	0.14	3.56
Ba	2000.00	225.86	471.87
La	303.56	27.95	77.54
Ce	577.23	62.40	166.91
Pr	62.50	5.45	16.86
Nd	231.51	19.21	60.11
Sm	35.11	3.33	10.55

Eu	5.14	0.66	1.72
Gd	24.48	3.28	9.18
Tb	3.91	0.52	1.54
Dy	22.01	2.99	8.95
Ho	4.14	0.61	1.71
Er	12.26	1.43	4.74
Tm	1.88	0.17	0.65
Yb	10.06	1.30	3.93
Lu	1.53	0.22	0.54
Hf	11.99	3.40	6.69
Ta	4.55	0.36	1.93
W	392.28	2.27	32.72
Pb	81.29	17.39	42.37
Th	80.72	16.01	38.18
U	16.56	2.07	6.59
∑REE	1235.92	139.05	364.94
∑REEc+Sc+Y	1384.95	160.92	428.42

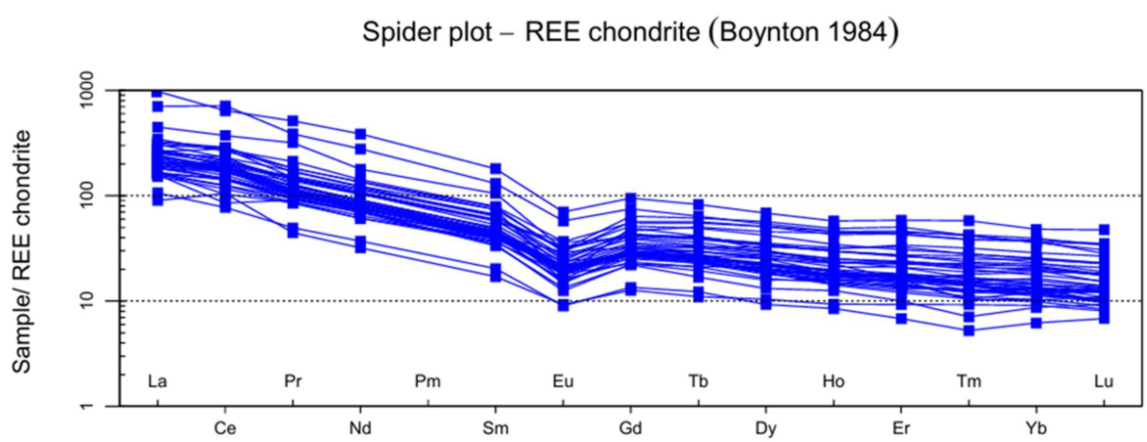

Fig 7.29: The chondrite-normalised REE spider diagram of Soil B+C-horizon samples (N=44).

The chondrite-normalized REE patterns (Boynton, 1984) of the B+C horizon soil samples from the Langmipi–Lachingthin Block display a distinct enrichment of Light Rare Earth Elements (LREE) over Heavy Rare Earth Elements (HREE), reflecting the geochemical characteristics of the underlying felsic basement rocks. The REE patterns exhibit steep negative slopes from La to Sm, followed by comparatively flatter HREE segments extending from Gd to Lu. A prominent characteristic of the REE patterns is the well-developed negative Eu anomaly, where Eu plots significantly below the smooth trend defined by Sm and Gd. The negative Eu anomaly is indicative of extensive plagioclase feldspar fractionation during the evolution of the parental felsic magma, as Eu^{2+} is preferentially incorporated into plagioclase during crystallization. The persistence of this anomaly in the B+C horizon soils suggests that the soils have retained the primary geochemical signature of the source rocks despite prolonged weathering.

The B+C horizon soils exhibit considerable REE enrichment, with ΣREE values ranging from 139.05 to 1235.92 ppm and an average of 364.94 ppm, demonstrating a broad variation in REE concentrations across the study area. The average concentrations of La (77.54 ppm), Ce (166.91 ppm), Nd (60.11 ppm), and Sm (10.55 ppm) are substantially higher than those of the HREE, confirming the predominance of LREE within the soil profile. One sample records ΣREE exceeding 1200 ppm, indicating the presence of localized zones of significant REE enrichment. The average ΣREE + Sc + Y value of 428.42 ppm further reflects the enrichment of rare earth and associated incompatible elements within the B+C horizon soils. Compared with the stream sediments, these soils more closely preserve the geochemical characteristics of the underlying bedrock because they have undergone limited mechanical transport. The B+C horizon soils are also enriched in several incompatible and high-field-strength elements, including Rb (192.25 ppm), Ba (471.87 ppm), Zr (220.28 ppm), Hf (6.69 ppm), Th (38.18 ppm), Y (46.43 ppm), Nb (9.78 ppm), and Ta (1.93 ppm). The elevated Zr and Hf concentrations indicate the concentration of resistant zircon during weathering, while the relatively high Th values suggest the presence of accessory REE-bearing minerals such as monazite and allanite within the source rocks. Tungsten concentrations range from 2.27 to

392.28 ppm, with an average of 32.72 ppm, indicating that W-bearing minerals are associated with the evolved granitic system and are locally concentrated within the weathering profile.

Overall, the REE geochemistry of the B+C horizon soils indicates that they are derived predominantly from the in-situ weathering of REE-bearing granitic gneisses, migmatites, pegmatites, and quartzo-feldspathic veins exposed within the Langmipi–Lachingthin Block. The pronounced LREE enrichment, persistent negative Eu anomaly, enrichment of incompatible trace elements, and relatively high ΣREE values demonstrate that the B+C horizon soils effectively preserve the geochemical signature of the parent lithologies. The occurrence of samples with exceptionally high REE concentrations further suggests the presence of localized REE-enriched zones within the block.

7.3.0 Structure of the block

7.3.1 The Langmipi-Laching Thing Block exhibits well-developed structural features expressed in the form of foliation, and joints.

A. Foliation: The foliation measurements collected from the granite gneiss and migmatite of the Langmipi Laching-Thing Block indicate a well-developed metamorphic fabric throughout the block.

The foliation within both the granite gneiss and migmatite generally E-W to with local variations towards NNE–SSW and ENE–WSW, with moderate to steep dips ranging from 15° to 87° with dominant dip directions towards north. In several locations, the foliation also dips towards northwest and southwest directions, suggesting local structural disturbances and folding.

The variation in foliation orientation across the Langmipi Laching-thing Block indicates that the area has undergone multiple phases of deformation, resulting in the folding, warping, and local reorientation of the foliation planes. The wide range of foliation reflects the complex structural evolution of the terrain under successive tectonic events. Steeply dipping foliations observed at several locations are interpreted to represent zones of intense tectonic deformation and ductile shearing. Overall, the foliation pattern reflects a strongly deformed metamorphic terrain developed under regional tectono-metamorphic conditions.

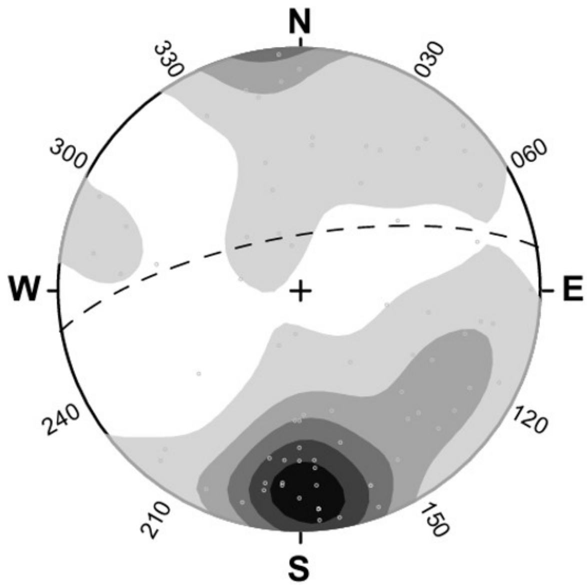

Mean Principal Orientation = 260/72N

Mean Resultant dir'n = 30-330

Mean Resultant length = 0.52

(Variance = 0.48)

Calculated. girdle: 6/50E

Calculated beta axis: 40-276

Text Fig No. 7.30: Stereographic plot of all foliation planes orientation of Langmipi-Laching Thing Block.

B. Folding and shearing: Folding and shearing constitute the most prominent structural features within the Langmipi Laching-Thing Block, indicating that the area has undergone multiple phases of ductile deformation. Folding is manifested by the widespread occurrence of warped pre-existing gneissic fabrics, microfolds, and folded quartzofeldspathic veins. The warping and refolding of earlier foliations suggest superposition of successive deformation events, resulting in the complex structural architecture observed across the block. Fold geometries vary from gentle warps to tight and isoclinal folds at the outcrop scale, reflecting heterogeneous strain distribution during progressive deformation.

Shearing is equally pervasive and is evidenced by the presence of asymmetric σ-type feldspar porphyroclasts within the granite gneiss, offset and boudinaged quartzofeldspathic veins, and the well-developed S–C fabric observed in several outcrops. The σ-type porphyroclasts exhibit characteristic asymmetric tails formed during non-coaxial ductile deformation, while the displacement of quartzofeldspathic veins records significant shear strain. The development of S–C fabrics further indicates progressive simple shear under ductile conditions and provides reliable kinematic indicators for determining the sense of shear. Collectively, these structural features demonstrate that the Langmipi–Lachingthin Block experienced intense ductile shearing accompanied by progressive deformation.

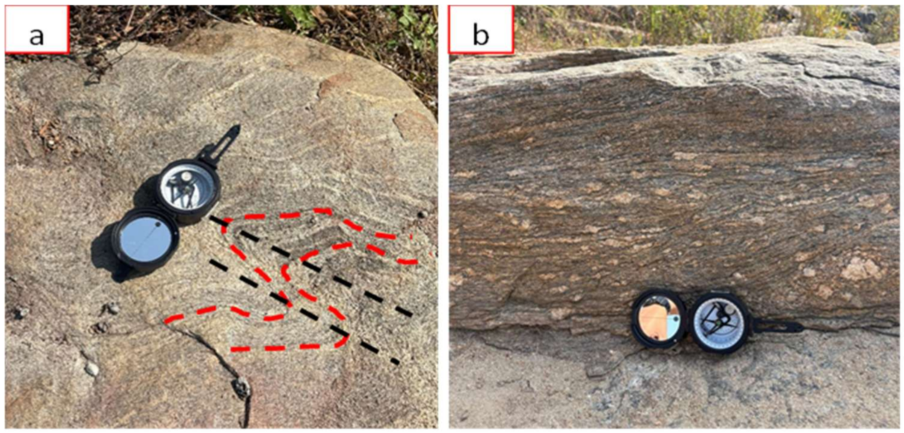

Photograph No. 7.17.: a) warping of the pre-existing fabrics within granite gneiss b) presence of σ-type-porphyroclast present within granite gneiss.

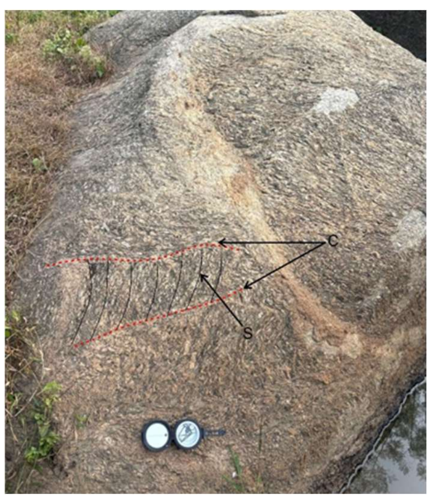

Photograph No. 7.18.: Presence of S-C fabric within granite gneiss.

7.4.0 Mineralisation

7.4.1 The Langmipi–Lachingthin Block exhibits multiple styles of mineralisation associated with granitoid magmatism, pegmatitic emplacement, hydrothermal activity, and structurally controlled sulphide deposition. Mineralisation within the block is predominantly represented by REE-bearing accessory minerals, sulphide phases, and magnetite–ilmenite associations. Petrographic, mineragraphic, and geochemical investigations indicate that the distribution and concentration of mineralisation are primarily controlled by lithology, structural features such as shearing and fracturing, and late-stage magmatic–hydrothermal processes. The emplacement of pegmatitic and quartzofeldspathic veins, together with subsequent hydrothermal alteration and deformation, has played a significant role in the localisation and remobilisation of mineralising fluids, resulting in the observed mineral assemblages and geochemical enrichment within the study area.

7.4.2 REE Mineralisation

REE mineralisation within the Langmipi Laching-Thing Block is primarily associated with granite gneiss, migmatites, pegmatitic veins, and quartzo-feldspathic veins. Notably, total REE concentrations exceeding 1000 ppm have been recorded within the granite gneiss, indicating its significant potential as a host for REE enrichment. Petrographic investigations reveal the presence of several REE-bearing accessory minerals, including monazite, zircon, sphene (titanite), and apatite, hosted predominantly within the felsic lithologies. The occurrence and textural relationships of these accessory minerals indicate their magmatic origin, with subsequent modification during metamorphic and hydrothermal events. XRD mineral-phase analysis identified trace amounts of xenotime, indicating that xenotime is also a REE-bearing mineral in the samples.

Monazite, the principal REE-bearing mineral, occurs as very fine subrounded to irregular grains, commonly associated with or enclosed within biotite. Zircon is present as very fine slender prismatic to subrounded crystals, occurring both as discrete accessory grains and as inclusions within biotite. Well-developed pleochroic halos surrounding zircon inclusions indicate its radioactive nature and prolonged residence within the biotite host. Sphene (titanite) occurs as very fine wedge-shaped grains, commonly associated with biotite, while apatite is present as fine- to very fine-grained subrounded to hexagonal crystals dispersed throughout the felsic matrix. Tourmaline occurs as very fine prismatic grains within the accessory mineral assemblage, particularly in pegmatitic and quartzo-feldspathic veins. Epidote is also locally observed as very fine grains associated with biotite, together with monazite and zircon.

The close spatial association of monazite, zircon, sphene, apatite, and tourmaline with felsic lithologies, particularly pegmatitic and quartzo-feldspathic veins, suggests that REE mineralisation is closely linked to late-stage magmatic differentiation and fluid-assisted hydrothermal processes. The REE mineralisation appears to be controlled primarily by accessory phases, principally monazite, together with zircon and sphene (titanite. Structural features such as fractures, joints, foliation planes, and shear zones acted as favourable pathways for the emplacement of pegmatitic and quartzo-feldspathic veins and for subsequent hydrothermal remobilisation of REE-bearing fluids. Structural controls, including shearing and fracturing, have further influenced the redistribution and localisation of these REE-bearing accessory minerals within the granitoid host rocks.

However, spatial distribution reveals high-value bedrock samples occur in the north-central to north-eastern sector of the block but are separated from one another, and from the block margins, by samples with markedly lower ΣREE (commonly 100–400 ppm), and they do not coincide with any single mappable lithological contact or structural feature. The soil and stream-sediment media reinforce this picture: only one of 58 stream-sediment samples, and only isolated soil samples, exceed 1000 ppm ΣREE. The REE enrichment is therefore erratic and sample-specific — governed by the local modal abundance of REE-bearing accessory minerals — and does not define a continuous, coherent or mappable REE zone at the sampling density employed. This spatial character, rather than the absolute grades alone, provides the principal geological basis for concluding that the block does not warrant advancement to subsurface exploration

7.4.3 Sulphide Mineralisation

Sulphide mineralisation within the Langmipi Laching-Thing Block is primarily associated with migmatite, granite gneiss, quartzo-feldspathic veins, pegmatitic veins, and structurally controlled fracture and shear zones. Field investigations indicate that the sulphide assemblage is dominated by pyrite and chalcopyrite, which occur as disseminated grains, fracture fillings, thin veinlets, and irregular patches within the host rocks. Sulphide mineralisation is particularly concentrated along lithological contacts, silicified zones, quartzofeldspathic and pegmatitic veins, and zones affected by intense fracturing and shearing.

Mineragraphic studies indicate that pyrite and chalcopyrite constitute the major sulphide phases identified within the block (Pmg 5, Pmg 6 as well as annexure VI and IX). Pyrite occurs as very fine specks, irregular patches, and fracture-filling phases, with disseminated grains present in trace amounts within the granitoid host rocks. Chalcopyrite is observed as very fine accessory specks, commonly occurring in association with pyrite and along microfractures, suggesting its precipitation during the later stages of hydrothermal mineralisation. The sulphide mineralisation is interpreted to be related to late-stage hydrothermal activity associated with felsic intrusive emplacement, with subsequent tectonic activity along fractures, joints, foliation planes, and shear zones facilitating the circulation of mineralising fluids and the localisation of sulphide deposition.

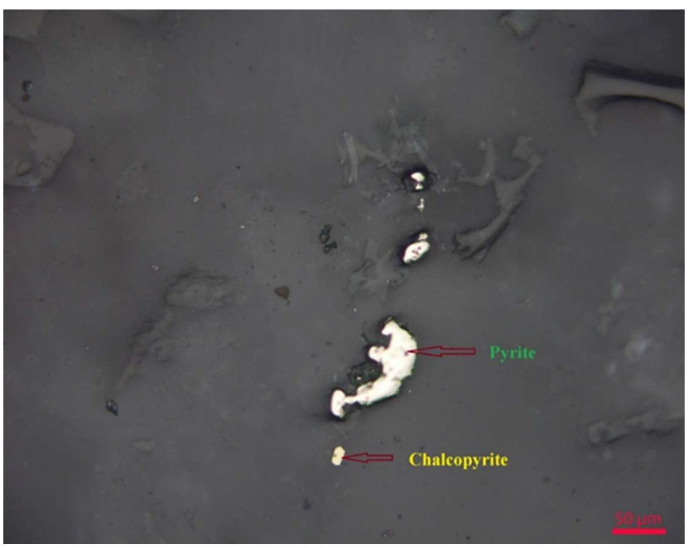

Pmg – 6: Photomicrograph showing fine to very fine grains of pyrite associating very fine specks of chalcopyrite as seen under reflected light.

7.4.4 Magnetite–Ilmenite

Magnetite–ilmenite mineralisation is widely developed within the migmatite, granite gneiss, and quartzo-feldspathic veins of the Langmipi Laching-Thing Block, where these minerals occur as disseminated opaque phases. Magnetite is commonly present as fine- to medium-grained subhedral to anhedral crystals, occurring as disseminated grains, irregular patches, and local concentrations within the host rocks. Ilmenite occurs predominantly as fine bladed grains and as lamellar exsolution textures within magnetite.

Petrographic and mineragraphic studies reveal that magnetite occurs as fine to very fine subhedral to anhedral and locally bladed grains, disseminated throughout the host rocks. It commonly forms disseminations, irregular patches, and fracture-filling phases, and is frequently associated with ilmenite. In several sections, magnetite exhibits martitisation, with partial replacement by hematite, indicating post-magmatic oxidation.

Ilmenite occurs as fine to very fine subhedral to bladed grains, both as discrete crystals and in close association with magnetite. In some sections, magnetite–ilmenite aggregates occur as fracture-fillings and as fine bladed fillings along the cleavage traces of mica minerals, suggesting remobilisation by late-stage hydrothermal fluids.

Hematite occurs as very fine specks, anhedral patches, dendritic aggregates, and fracture-fillings. It is commonly developed as an alteration product of magnetite through martitisation, although it also occurs independently within the oxide assemblage. Goethite is present as patchy and dendritic fillings, locally exhibiting compositional zoning, and represents a secondary oxidation product formed during supergene alteration.

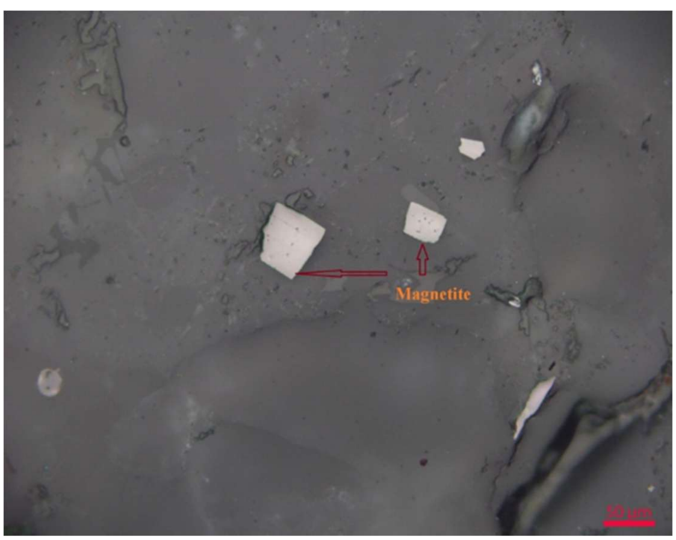

Pmg – 5: Photomicrograph showing fine to very fine subhedral grains of magnetite as seen under reflected light.

CHAPTER - VIII

8.0.0. PREVIOUS EXPLORATION

8.1.0. General

8.1.1 The Langmipi-Laching Thing Block and adjoining areas form part of the Assam–Meghalaya Gneissic Complex (AMGC), which has been investigated by various agencies through geological mapping, geochemical surveys, geophysical investigations and reconnaissance exploration for REE and associated mineralisation. The salient details of earlier work carried out in and around the present block are summarised below.

8.1.2 La Touche was perhaps the first geologist who visited the area during 1883 while taking traverses through Jaintia, Khasi and Dima Hasao. The area was subsequently mapped by Sondhi (1949) and Mukherjee (1944 and 1953). Later, Rao and Chakraborti (1963-64), Dayal and Raj (1964-65), Gangopadhayay (1965-66) etc. studied parts of the area in connection with selection of dam sites for hydel projects over Kopili River. Gopalakrishnan (1962) carried out detailed studies in this area in connection with investigation for cement grade limestones and clay

8.1.3 **Regional Geological Mapping and Mineralisation Studies:**

The earliest geological investigations in the area were carried out by P. Kapali (Senior Geologist), D.P. Das (Junior Geologist), and H.S. Srivastava (Junior Geologist) of the Geological Survey of India during the field season 1984–85. They undertook systematic geological mapping in the Hamren Sub-Division of Karbi Anglong District, Assam, covering an area of approximately 575 km² in parts of Survey of India Toposheet Nos. 83C/9 and 83C/13. The study established the regional geological framework and documented lithological units belonging to the Archaean Gneissic Complex, comprising biotite gneiss, augen gneiss, migmatite, and amphibolite. In addition, the investigation delineated the Precambrian metasedimentary rocks of the Shillong Group, represented by massive and micaceous phyllitic quartzite, porphyritic/porphyroblastic granites and other granitoids, and the Tertiary quartzitic sandstone of the Therria Stage.

Subsequently, C.G. Hemantha Kumar (Senior Geologist), R.T. Bhuyan (Assistant Geologist), B.N. Gohain (Assistant Geologist), and B. Boruah (Assistant

Geologist) carried out Quaternary geological and geomorphological mapping in parts of Dhubri, Nagaon, and Karbi Anglong districts of Assam. The investigation covered a total area of approximately 1,750 km² on 1:50,000 scale, encompassing parts of Toposheet Nos. 78O/13, 78O/15, 83B/16, 83C/13, and 83F/4. Of this, nearly 1,150 km² falls within the Nagaon and Karbi Anglong districts, including parts of Toposheet Nos. 83B/16, 83C/13, and 83F/4. The study focused on the Quaternary geological succession, geomorphological characteristics, and surficial deposits, providing valuable information on the evolution of the landscape and depositional environments of the region.

National Geochemical Mapping program of GSI has in the area reveals anomalous value of ΣREE. A total 30 Nos of stream sediment samples are falling within the proposed block and the ΣREE+Sc+Y value varies form 242.03 ppm to 1618.07. There are 19 samples which shows ΣREE+Sc+Y value more than 500 ppm and 7samples having more than 1000 ppm value.

8.1.4 Systematic thematic mapping

During the 1991–92 field season, J.C. Dutta, S. Chowdhury, D.P. Das, S.N. Sharma, A. Bora, and G.C. Sarmah of the Geological Survey of India (GSI) carried out systematic geological mapping over an area of approximately 905 km² covering parts of Karbi Anglong, North Cachar Hills, and Nagaon districts of Assam. The mapping was undertaken in two separate blocks, one covering parts of Survey of India Toposheet No. 83F/4 and the other encompassing parts of Toposheet Nos. 83G/1, 83G/2, and 83C/13.

The investigation established the regional geological framework of the area and revealed that the block covering Toposheet Nos. 83G/1, 83G/2, and 83C/13 is predominantly underlain by a thick succession of arenaceous and argillaceous sedimentary rocks belonging to the Barail, Surma, and Tipam Groups. The study provided valuable insights into the lithostratigraphy and spatial distribution of these Tertiary sedimentary formations, thereby contributing significantly to the understanding of the regional geology of Karbi Anglong and adjoining areas. As part of the National Geochemical Mapping (NGCM) Programme during Field Season 2017–18, the Geological Survey of India (GSI) carried out systematic thematic mapping of Toposheet No. 83C/09 on a 1:50,000 scale. The programme involved the preparation of geological, drainage, basin, geomorphological, land use/land cover (LULC), slope, aspect and hillshade maps using field observations integrated with remote sensing and GIS techniques. These thematic maps provided a comprehensive understanding of the regional geological setting, geomorphology, drainage characteristics, terrain morphology and land use pattern of the area.

. The study area has undergone polyphase deformation and high-grade metamorphism, as evidenced by the presence of multiple generations of structural and metamorphic features. Migmatitic banding developed within the gneisses represents magmatic segregation associated with partial melting during high-grade metamorphism. The drainage pattern is predominantly sub-dendritic to sub-trellis, reflecting the influence of lithology and structural controls on an undulating terrain. The study also documented a variety of minor structural features, including ptygmatic folds, box folds, kink-band folds, and other small-scale fold structures, indicating multiple phases of deformation. The widespread occurrence of granite gneiss, biotite gneiss, augen gneiss, and migmatite, particularly in the southern part of the mapped area, suggests that the region experienced high-grade regional metamorphism, followed by repeated tectonic reworking. Sulphides occur as specks and are locally disseminated.

8.1.5 Regional Geochemical Exploration

As part of the National Geochemical Mapping (NGCM) Programme, the Geological Survey of India (GSI) carried out regional geochemical exploration over Toposheet No. 83C/09 during Field Season 2017–18, covering an area of approximately 700 km². Systematic geochemical mapping was carried out by collecting 182 composite stream sediment/slope wash samples on a 2 km × 2 km grid, together with nine regolith samples, nine C-horizon soil samples, nine water samples, nine heavy mineral samples and representative petrographic rock samples. The samples were analysed for major oxides and 47 elements, including rare earth elements (REEs), and the analytical data were processed using descriptive statistics, histograms, box-and-whisker plots, correlation matrices, Voronoi diagrams and contour maps. Elemental distribution maps for major oxides, trace elements and REEs provided a robust regional geochemical framework for identifying anomalous zones and prioritising areas for detailed exploration.

Subsequently, geochemical mapping was extended to the adjoining Toposheets 83C/13 and 83C/14 during the same field season. In Toposheet No. 83C/14, an area of 698 km² was covered by collecting 182 stream sediment/slope wash samples on a 2 km × 2 km grid. The analytical results revealed significant enrichment of Rare Earth Elements (ΣREE) in stream sediments derived from granitic gneiss around Charchim, Gilangso and Phanglangso villages in the northwestern part of the toposheet. The stream sediment samples recorded ΣREE (REE+Sc+Y) values ranging from 57.80 to 1468.48 ppm, with ΣLREE values between 43.93 and 1263.52 ppm (average 204.65 ppm) and ΣHREE values between 13.87 and 240.15 ppm, indicating favourable conditions for REE mineralisation. Similarly, in Toposheet No. 83C/13, geochemical mapping covering 698 km² involved the collection of 182 stream sediment/slope wash samples on the same sampling grid. The analytical results showed that Total Rare Earth Elements (TREE) ranged from 140.77 to 1818.89 ppm. Seventeen anomalous stream sediment samples collected from Rikangmiham, Deory Tinali, Langparpam and Thenglong villages in the southwestern part of the toposheet recorded TREE values ranging from 618.38 to 1920.88 ppm, with an average of 1024.50 ppm. These samples also exhibited LREE concentrations between 401.16 and 1608.78 ppm (average 753.50 ppm) and HREE concentrations between 207.82 and 380.21 ppm. In Toposheet No. 83C/10, anomalous TREE values reaching 3621 ppm were recorded in stream sediment samples collected from the Mawriyap and Sarucha areas over migmatitic terrain, and GSI recommended the area for G–4 stage REE investigation. Similarly, Toposheet No. 83C/14 recorded ΣREE (REE+Sc+Y) values ranging from 57.80 ppm to 1468.48 ppm, with significant enrichment around Charchim, Gilangso and Phanglangso villages where granitic gneisses constitute the dominant lithology.

8.1.6 REE Prospecting in Adjacent Areas

The adjoining Toposheet No. 83C/13, located immediately east of the present block, was investigated by GSI under the National Geochemical Mapping Programme during Field Season 2017–18. Geochemical mapping covering about 698 km² resulted in the collection of 182 stream sediment samples, along with regolith, C-horizon soil, water and heavy mineral samples. Analytical results identified seventeen stream sediment samples containing anomalous Total Rare Earth Element (TREE) values ranging from 618.38 ppm to 1920.88 ppm, with an average TREE value of 1024.50 ppm. The anomalous zones occur around Rikangmiham, Deori Tinali, Langparpam and Thenglong villages in the south-western part of Toposheet 83C/13.

8.1.7 Geophysical Exploration

Ground geophysical investigations were carried out by GSI during Field Season 1997–98 to evaluate the Total Intensity Aeromagnetic Anomaly Zone (MZ–13) covering parts of Karbi Anglong and Nagaon districts, including portions of Toposheet No. 83C/09. The investigations confirmed that the area comprises highly dissected terrain underlain by Precambrian crystalline rocks with thick weathered profiles in several sectors. The aeromagnetic anomaly evaluation contributed to understanding the regional subsurface geological framework and identified structural features that could influence mineral localisation. These studies provided valuable regional geophysical information for subsequent exploration programmes.

CHAPTER - IX

9.0.0. AERIAL OR GROUND GEOPHYSICAL OR GEOCHEMICAL SURVEY

9.1.0. Aerial Or Ground Geophysical Survey

9.1.1 Areal or ground geophysical survey was not been carried out during the present exploration.

9.2.0 Geochemical Survey

9.2.1 The ground geochemical survey in terms of Soil Sampling and Stream sediment sampling was carried out in the G-4 stage exploration work in Langmipi-Laching Thing Block.

9.2.2 **Stream sediment sampling**

During the course of exploration, 58 stream sediment samples were collected from first- and second-order streams within the Langmipi–Laching Thing Block to evaluate the geochemical dispersion of rare earth elements (REE). Analytical results indicate that only one sample recorded a total REE concentration exceeding 1,000 ppm, while the remaining samples exhibited comparatively lower concentrations. The average ΣREE+Sc+Y of the 58 stream sediment samples is 355.51 ppm (ΣREE average 320.66 ppm), indicating a moderate regional geochemical enrichment with a localized high-value anomaly.

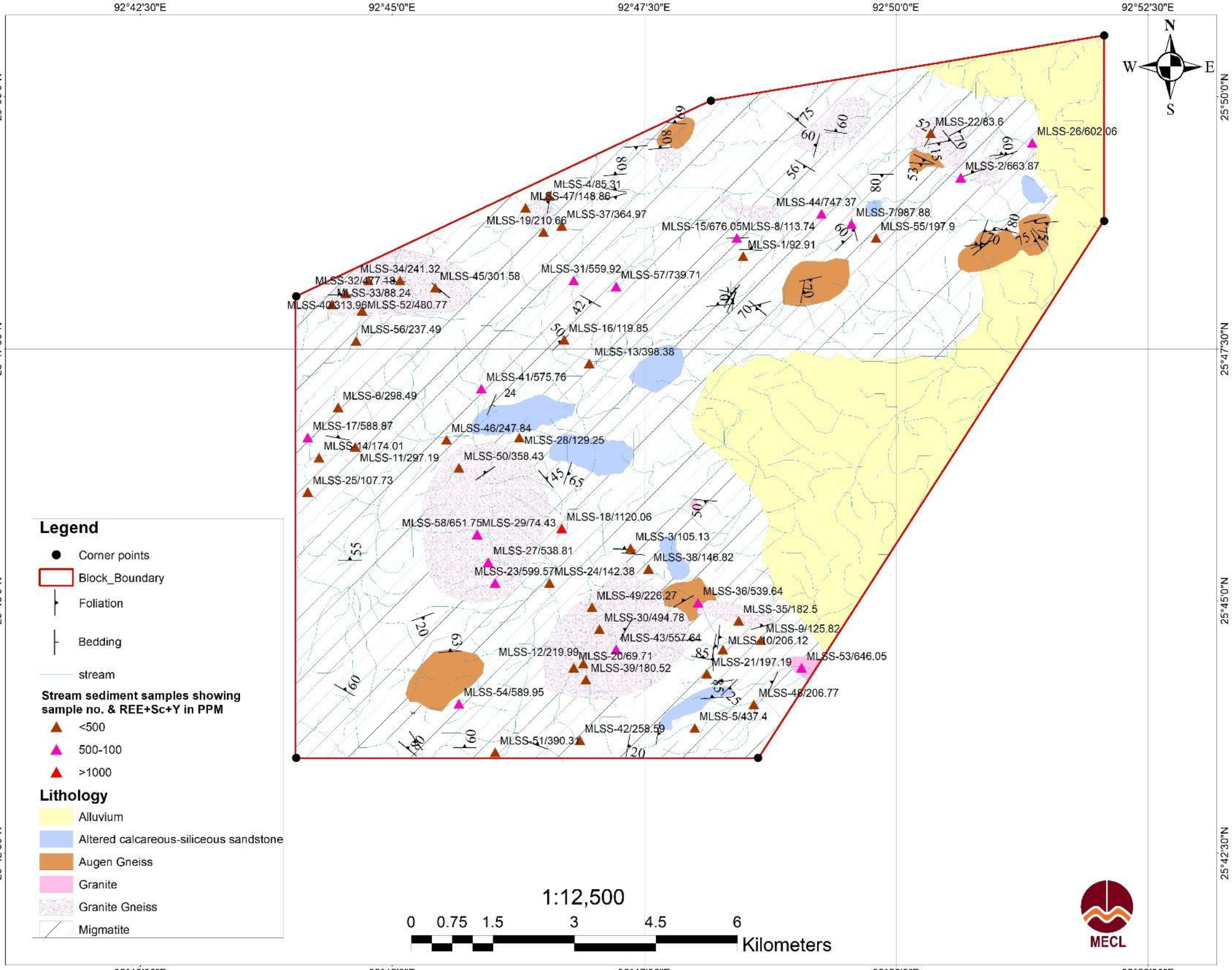

Text Fig 9.1
Location of Stream sediment samples

Photograph 9.1: Stream sediment sampling.

Geochemistry of stream sediment samples

A total of 58 stream sediment was analysed for 34 elements through ICP-MS analysis to evaluate the distribution of REE and associated trace elements. Table no 9.1. Summarized table of ICP-MS analysis of Stream sediment samples (N=58) for 34 elements.

Elements	Max(ppm)	Min(ppm)	Mean(ppm)
Li	41.54	3.65	10.34
Be	3.77	0.43	1.28
Sc	18.06	1.23	4.09
V	133.04	8.16	27.88
Cu	37.86	9.78	14.94
Zn	712.47	16.52	47.77
Ga	27.88	4.14	9.73
Rb	276.90	44.17	146.70
Sr	165.87	36.10	85.77
Y	78.82	8.49	30.76
Zr	974.91	43.87	266.59
Nb	14.12	1.12	4.97

Sn	3.84	0.57	1.10
Ba	1300.00	319.53	642.06
La	254.60	11.62	74.47
Ce	440.20	21.25	141.99
Pr	53.57	2.34	16.03
Nd	186.89	7.65	53.61
Sm	31.46	1.42	9.57
Eu	2.43	0.42	1.04
Gd	29.19	1.50	8.46
Tb	4.56	0.26	1.39
Dy	19.65	1.90	7.18
Ho	3.08	0.27	1.14
Er	7.08	0.89	2.86
Tm	0.94	0.11	0.34
Yb	5.52	0.68	2.26
Lu	0.79	0.13	0.31
Hf	33.09	1.51	8.01
Ta	4.97	0.14	0.70
W	539.69	1.60	146.34
Pb	62.62	13.52	38.32
Th	166.17	5.57	45.52
U	12.64	0.96	5.02
∑REE	1037.26	51.88	320.66
∑REEc+Sc+Y	1120.06	69.71	355.51

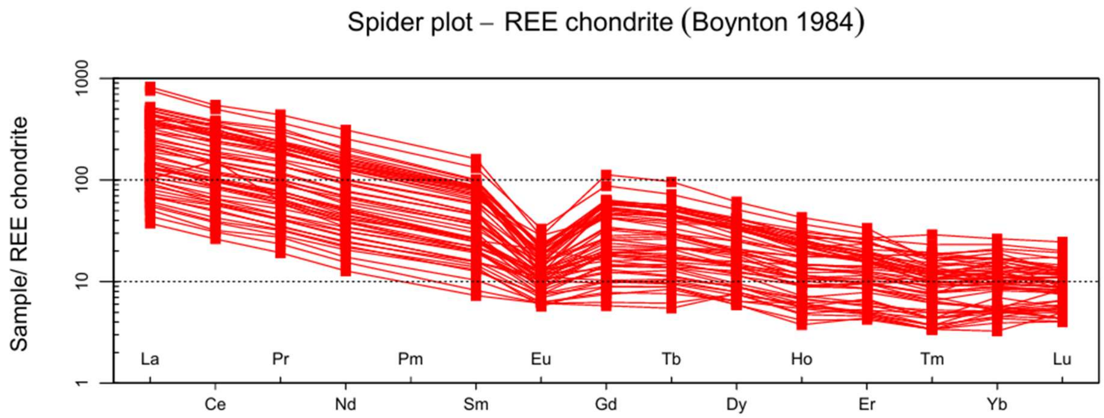

Fig 9.2: The chondrite-normalised REE spider diagram of Stream sediment samples (N=58).

The chondrite-normalized REE patterns (Boynton, 1984) of the stream sediment samples from the Langmipi–Lachingthin Block exhibit a consistent enrichment of Light Rare Earth Elements (LREE) relative to Heavy Rare Earth Elements (HREE), indicating that the sediments are predominantly derived from felsic crustal rocks. The REE patterns are characterized by steeply fractionated trends from La to Sm followed by comparatively flat to gently declining HREE segments from Gd to Lu. A conspicuous feature of the REE patterns is the pronounced negative Eu anomaly, with Eu plotting well below the trend defined by Sm and Gd in almost all samples. This negative Eu anomaly reflects significant plagioclase fractionation in the source rocks, where Eu^{2+} was preferentially incorporated into plagioclase during crystallization, leaving the residual melts and their weathering products depleted in Eu.

The stream sediments show a wide variation in total REE concentrations, with ΣREE ranging from 51.88 to 1037.26 ppm and an average of 320.66 ppm, indicating heterogeneous REE distribution within the drainage system. The average concentrations of La (74.47 ppm), Ce (141.99 ppm), Nd (53.61 ppm), and Sm (9.57 ppm) are considerably higher than those of the HREE, confirming the predominance of LREE in the sediments. Only one stream sediment sample records ΣREE exceeding 1000 ppm, whereas most samples exhibit moderate

REE concentrations, suggesting that REE mineralization is localized rather than uniformly distributed across the drainage basin. The elevated average Y content (30.76 ppm) and Sc (4.09 ppm) result in an average ΣREE + Sc + Y value of 355.51 ppm, highlighting the overall enrichment of incompatible trace elements within the study area.

The stream sediments are also enriched in several incompatible and high-field-strength elements, including Zr (average 266.59 ppm; maximum 974.91 ppm), Hf (8.01 ppm), Th (45.52 ppm), Rb (146.70 ppm), Ba (642.06 ppm), W (146.34 ppm; maximum 539.69 ppm), and Pb (38.32 ppm). The high Zr and Hf concentrations indicate a significant contribution from resistant heavy minerals such as zircon, while the elevated Th values suggest the presence of accessory REE-bearing minerals such as monazite and allanite. The enrichment of tungsten together with REE further supports the existence of evolved granitic magmatic-hydrothermal systems within the Langmipi–Laching Thing Block.

Overall, the REE geochemical characteristics of the stream sediments indicate that they are largely derived from weathering of fractionated granitic gneisses, migmatites, pegmatites, and quartzo-feldspathic veins exposed within the Langmipi–Laching Thing Block. The strong LREE enrichment, persistent negative Eu anomaly, enrichment of incompatible elements, and localized high ΣREE values demonstrate that the drainage system effectively reflects the underlying bedrock geochemistry and confirms the presence of REE-bearing source rocks within the catchment.

9.2.3 Soil sampling

A total of 65 soil (pit) samples were collected from the Langmipi-Laching Thing Block to investigate the geochemical characteristics of the subsurface soil profile and evaluate the distribution of rare earth elements (REE) and associated mineralization. The samples were obtained from different soil horizons, with the majority collected from the B-horizon and B + C horizon

The average thickness of the A-horizon is approximately 30 cm, while the B-horizon averages around 40 cm. Fresh to moderately weathered bedrock was encountered at relatively shallow depths in several pits; however, the average depth to bedrock across the study area was approximately 1.5

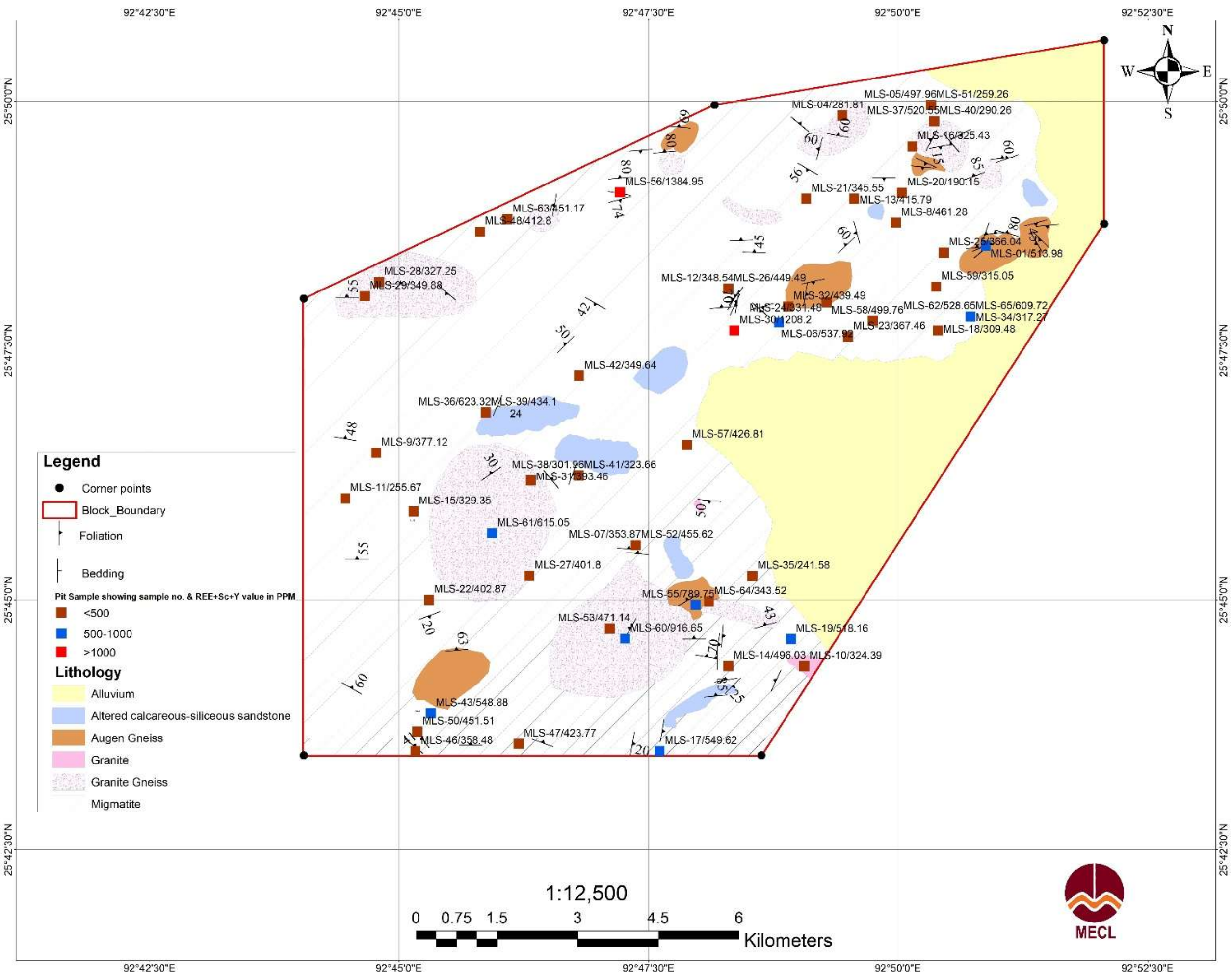

Text Fig 9.3 Location of Pit sediment samples

Geochemistry soil samples

A total of 65 soil samples were analysed for 34 elements using ICP-MS to evaluate the distribution of rare earth elements (REE) and associated trace elements within the Langmipi-Laching Thing Block.

Table no 9.2. Summarized table of ICP-MS analysis of Soil samples (N=65) for 34 elements.

Elements	**Max(ppm)**	**Min(ppm)**	**Mean(ppm)**
Li	64.62	4.69	39.33
Be	4.955	0.6	2.25
Sc	41.58	2.55	16.27
V	171.53	12.43	106.99
Cu	67.19	11.95	36.93
Zn	320.55	18.90	83.14
Ga	38.07	7.34	24.91
Rb	309.68	56.59	188.83
Sr	142.42	5.74	51.46
Y	130.58	14.29	45.94
Zr	398.05	100.79	224.70
Nb	19.51	3.47	9.64
Sn	9.14	0.14	3.37
Ba	2000	224.06	520.27
La	303.56	27.95	79.20
Ce	577.22	62.40	169.19

Pr	62.49	5.45	17.43
Nd	231.51	19.21	61.37
Sm	35.10	3.33	10.79
Eu	5.14	0.66	1.70
Gd	24.48	3.27	9.30
Tb	3.91	0.52	1.57
Dy	22.01	2.98	9.06
Ho	4.14	0.60	1.71
Er	12.25	1.43	4.67
Tm	1.87	0.16	0.63
Yb	10.08	1.29	3.86
Lu	1.53	0.2	0.54
Hf	11.99	3.40	6.97
Ta	4.54	0.35	1.89
W	392.28	2.27	31.39
Pb	81.29	17.39	42.45
Th	80.72	16.01	39.386
U	16.56	2.07	6.6976
∑REE	1235.91	139.05	371.04
∑REEc+Sc+Y	1384.95	160.92	433.26

The analytical results reveal considerable geochemical variation among the soil samples, reflecting the heterogeneous nature of the weathered profile and the underlying lithology. Among the trace elements, Ba exhibits the highest concentration with a maximum value of 2,000 ppm and an average of 520.27 ppm, indicating strong barium enrichment in certain locations. Other lithophile elements such as Rb (mean 188.83 ppm), Zr (mean 224.70 ppm), Y (mean 45.94 ppm), and Th (mean 39.39 ppm) are also relatively enriched, suggesting the presence of evolved felsic source rocks and REE-bearing accessory minerals. Tungsten (W) records a maximum concentration of 392.28 ppm with an average of 31.31 ppm, indicating localized tungsten enrichment within the study area. Transition metals including V (mean 107.00 ppm), Zn (mean 83.14 ppm), Cu (mean 36.94 ppm), and Pb (mean 42.45 ppm) display moderate abundances, while Sr shows comparatively lower concentrations with an average of 51.47 ppm.

The rare earth element concentrations indicate a well-developed enrichment pattern throughout the soil profile. Among the light rare earth elements (LREE), Ce is the most abundant, with concentrations ranging from 62.40 ppm to 577.23 ppm and an average of 169.19 ppm, followed by La (mean 79.20 ppm) and Nd (mean 61.37 ppm). The heavy rare earth elements (HREE) occur at comparatively lower concentrations, with Gd, Dy, Er, and Yb averaging 9.31 ppm, 9.06 ppm, 4.67 ppm, and 3.86 ppm, respectively. The total rare earth element content (ΣREE) ranges from 139.05 ppm to 1,235.91 ppm, with an average concentration of 371.05 ppm, indicating moderate to high REE enrichment within the soil profile. When scandium and yttrium are included, the ΣREE + Sc + Y values range from 160.91 ppm to 1,384.95 ppm, with an average of 433.26 ppm. Overall, the geochemical data indicate a pronounced enrichment of light rare earth elements relative to heavy rare earth elements, consistent with the weathering of felsic rocks and the concentration of REE-bearing accessory minerals such as monazite, allanite, and xenotime. The elevated concentrations of REE, together with the enrichment of Th, Y, Zr, and W, suggest favourable geochemical conditions for rare earth mineralization within the weathered profile of the Langmipi-Laching Thing Block.

The chondrite-normalized REE patterns exhibit a strong enrichment of light rare earth elements (LREEs; La–Sm) relative to the heavy rare earth elements (HREEs; Gd–Lu). The REE curves show high normalized values for La and Ce, followed by a gradual decrease towards the heavier REEs, producing a distinctly right-sloping pattern. This indicates pronounced LREE enrichment and significant REE fractionation within the soil profile.

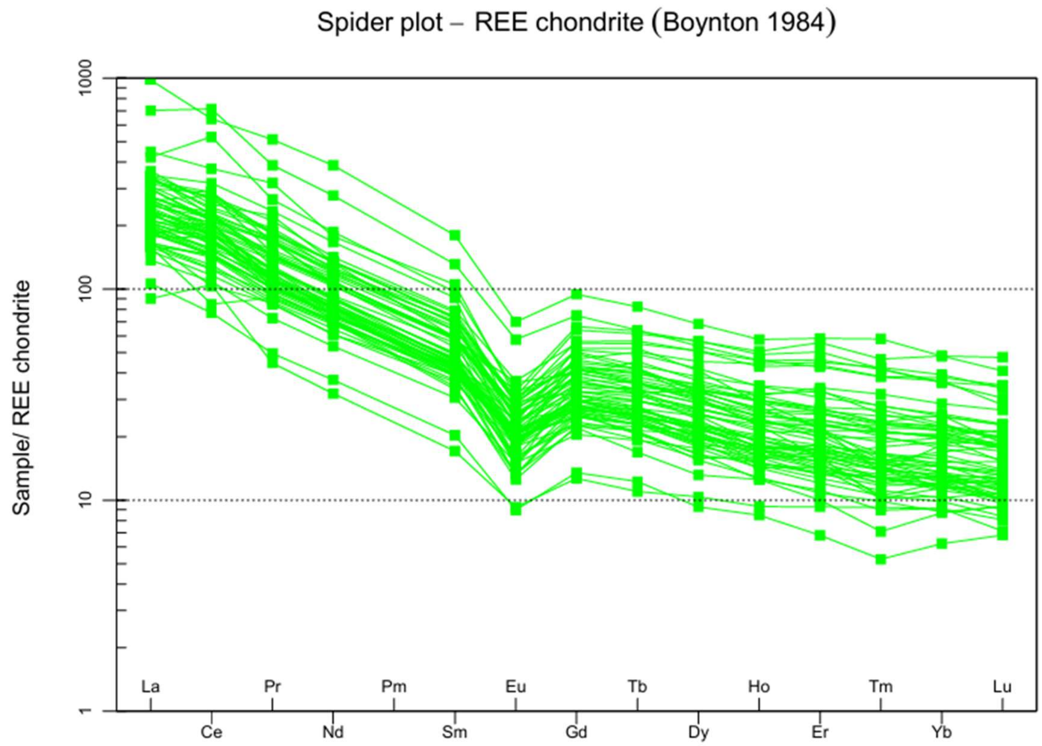

Fig 9.4: The chondrite-normalised REE spider diagram of Soil samples (N=65).

A well-developed negative Eu anomaly is evident in almost all samples, as shown by the marked depletion of Eu relative to the adjacent Sm and Gd. This negative Eu anomaly suggests that plagioclase feldspar fractionation occurred during the evolution of the parent rocks, or that Eu-bearing feldspar was preferentially removed during weathering. The HREE segment (Gd–Lu) is comparatively flatter and less variable than the LREE segment, indicating relatively uniform heavy rare earth element concentrations among the samples. The limited HREE fractionation suggests that minerals capable of concentrating HREEs (e.g., zircon, xenotime, or garnet) are either present in lower abundance or have undergone limited redistribution during weathering. Although the overall REE patterns are broadly similar, the variation in normalized concentrations among individual samples indicates differences in the degree of REE enrichment across the study area. This variability likely reflects changes in the abundance of REE-bearing accessory minerals, differences in the composition of the parent rocks, and varying intensities of chemical weathering and secondary enrichment.

CHAPTER - X

10.0.0 EXPLORATION UNDERTAKEN DURING CURRENT INVESTIGATION

10.1.0 Background

10.1.1 Langmipi-Laching Thing Block was proposed for G-4 level of exploration of REE and associated mineralisation. The Exploration has been carried out as per Minerals (Evidence of Mineral Contents) Amendment Rules, 2021 to achieve the following objective

i. To carry out large scale geological mapping on 1:12,500 scale.

ii. To collect surface samples (Bedrock and Stream sediment) and Pit (Soil sample) for analyses of REE and other associated minerals.

iii. To estimate reconnaissance resources of REE bearing minerals as per UNFC norms and Minerals (Evidence of Mineral Contents) Amendment Rules, 2021 at G-4 level mineral exploration.

10.2.0 Exploration Methodology

The components of G-4 level of exploration for REE and associated minerals in Langmipi-Laching Thing Block to full fill the above-mentioned objective in accordance with MEMC rule 2015(amended till 2021) as approved by NMEDT is furnished in the table no 10.1 and the field component wise description has been given in subsequent paragraphs.

Table No 10.1

Summarized Table showing Component wise Proposed quantum Vs. Quantum Achieved in Langmipi-Laching Thing Block, District Karbi Anglong, Assam

Sl. No.	Item of Work	Unit	Target	Achievement
1	**Geological Mapping** (on 1:12,500 Scale)	sq.km	124.68	124.68
2	**Geochemical Sampling**			
	Surface Samples (60 Stream Sediment, 50 BRS)	Nos	110	108
3	**Pitting**			
	a) Excavation (60 Nos)	Cu.m	90	90
	b) Collection of different horizon soil sample	Nos	65	65
4	**Drilling* (Phase II After Review)**			
	a) Drilling (core) Scout drilling	m	500 m	Not Recommended
	b) Geological Logging	m	500	-
	c) Borehole core samples	Nos	100	-
5	**Laboratory Studies**			
	a)REE associated Trace Elements (34 Element)by ICPMS Surface samples-110 (60 Stream Sediment, 50 BRS) Pit sample- 55 (For Soil Profile Sampling) Orientation Sample-10 (5 Pit X 2 samples from B and C Horizon), Core Sample: 100	Nos	275	173
	b) External Check Samples	Nos	28	17
	d) Major Oxide study	Nos	20	15
6	**Physical Study**			
	a) Petrological Study	Nos	15	10
	b) Mineragraphic Study	Nos	15	5
	c) XRD Study	Nos	15	10
	d) EPMA Study	Hours	15	-
7	**Report Preparation (5 Hard copies with a soft copy)**	Nos.	1	1

10.2.1 Geological Mapping

10.2.1.1 Large Scale Geological mapping (LSGM) completed in the total area of 124.68 sq. km on 1:12500 scale in the part of Survey of India Toposheet No 83C/09, 83C/10, 83C/13 & 83C/14.

10.2.1.3 During geological mapping, it was observed that the Langmipi-Laching Thing Block comprises lithologies dominated by migmatite, granite gneiss, augen gneiss, granite, pegmatite and quartzo-feldspathic veins. In addition, extensive soil and alluvial cover derived from weathering of the bedrock mantles the low-lying and valley portions of the block. The description of lithology has been described in detail in Chapter No VII.

10.2.3 Surface Sampling

10.2.3.1 In accordance with the approved NQT, the present G-4 stage exploration has been carried out with the surface sampling only which includes collection of 50 nos. of surface bedrock samples (BRS), 58 nos. of stream sediment samples and 65 nos. of soil samples collected by pitting for analysis of 34 Trace elements through ICPMS.

10.2.3.2 The sampling technique has been described in detail in the Chapter-XII.

10.2.4 Chemical Analysis

10.2.4.1 All the 173 Nos. of primary samples were analysed for 34 elements, i.e., La, Ce, Pr, Nd, Sm, Eu, Gd, Tb, Dy, Ho, Er, Tm, Yb, Lu, Y, Sc, Li, Be, Ba, Cu, Pb, Zn, Sn, W, Ga, Nb, Rb, Sr, Th, U, V, Zr, Hf, Ta by ICP-MS instrument. The results have already been described under Chapter-VII along with the lithology wise geochemistry of different lithology. However, the analysis of trace elements has been furnished in Annexure No II.

10.2.4.3 Moreover, the external check samples of 17 Nos have been analysed for same 34 elements from JNARDDC Laboratory, Nagpur.

10.2.4.4 15 bedrock samples (BRS) were analysed for major oxide geochemistry by X-ray Fluorescence (XRF), and 10 representative samples were analysed by X-ray Diffraction (XRD) for mineralogical characterization as per the approved quantum of work. The results have already been described under Chapter-VII along with the lithology-wise geochemistry of the mapped rock units. The major oxide (XRF) and XRD results are furnished in Annexure No. III and IV, respectively.

10.2.5 Physical Analysis

10.2.5.1 A total of 10 samples were examined under the microscope for detailed petrographic studies. The results of the petrographic investigation have been incorporated in the description of various lithologies under Chapter VII and are also presented as Annexure V.

10.2.5.2 5 Nos of samples has been subjected for Mineragraphy study and furnished as Annexure No VI.

10.2.6 Preparation of Geological Report:

10.2.6.1 Geological Report has been prepared in Corporate Office, MECL, Nagpur by integration of geological and geochemical data. ArcGIS and Autocad 2026 software has been used for preparation of various maps and GCD kit module of R programming language has been used for generating geochemical plots. The report has been written using Microsoft word and excel 2021 version.

10.3.0 Data spacing for reporting of exploration results

10.3.1 The geological data generated through large scale geological mapping and surface sampling were adequate for preparation of Geological Map of the block at 1:12500 scale. The investigations revealed that REE occurrence is very sporadic in nature at only few places. As a result, drilling was not undertaken. Hence, the data generated during the course of investigation are considered sufficient for concluding the exploration work and preparation of the Geological Report of the Langmipi-Laching Thing Block.

CHAPTER - XI

11.0.0 Location of Data Point

11.1.0 Accuracy and Quality of Survey

11.1.1 The current exploration for REE and associated minerals was conducted at the G-4 stage. To accurately record sample locations, stream sediments, pits and perform geological surveys, a handheld GPS device from M/S BAAP was utilized. The coordinates were recorded using the UTM coordinate system with the WGS 1984 datum.

11.2.0 Quality and adequacy of topographic control

11.2.1 The topographic survey was not carried out as it is not in the scope of present G-4 stage exploration.

CHAPTER - XII

12.0.0 SAMPLING TECHNIQUE

12.1.0 Sampling

12.1.1 Sampling is a systematic process for collection of material from any media which can provide the best representation. In the present study, sampling includes bed rock sampling (BRS), Stream Sediment Sampling and Soil sampling by pitting of different soil horizons. A total of 50 nos. of BRS, 58 nos stream sediment samples, 65 nos. of soil samples by pitting of different soil horizons collected. Moreover 10 nos. of BRS sample have been collected for petrographic and 5 nos. of mineragraphic studies from different lithologies exposed in the block.

12.2.0 Nature, quality and appropriateness of sample preparation technique

12.2.1 The detail description of sampling methods for Bed rock samples, stream sediment samples and soil samples has been discussed in subsequent paragraphs.

12.2.2 **Sampling techniques:**

A. Bedrock Sampling: A total of 50 Nos. of bed rock samples were collected systematically from different litho units exposed in the study area, mainly from the migmatite, granite gneiss, augen gneiss, quartzo feldspathic veins and pegmatite veins. Each sample were collected by cutting channels on exposed rock units in 1 – 2 m length by sledge hammer (5kg) and chisel. The sample locations are plotted on geological map (Text figure No 7.3 as well as Plate No-IV). First, each Bed rock sample of 2-3 kgs collected from the field was crushed. After crushing, the crushed samples were mixed thoroughly and reduced the sample size to 500 gm by coning and quartering. This representative samples were powdered and completely passed through (-) 200 mesh size sieves from which 100 g sample packed in polythene sample pouch and send for chemical analysis for 34 elements by ICP-MS 10 selected samples of granitic rock were also analysed for major oxides by XRF. The remaining 400 g sample has been preserved for future reference.

B. Stream sediment sampling:

i. Preparation of drainage map: The most essential requirement for collection of stream sediment is preparation of the drainage map of the area, which forms the base map for planning and executing sampling work. The drainage map has been prepared by digitizing the survey of India toposheet no 83C/09, 83C/10, 83C/13 & 83C/14 by using ArcGIS Pro. Then the probable location for collection of stream sediment samples were carefully marked on 1st or 2nd order streams within the block.

ii. Choice of Sample Collection site: First, the probable locations of 1st and 2nd order streams, marked on the prepared drainage map were visited and identified suitable trap sites around that point for collection of samples.

iii. Methodology for Collection of stream sediment samples: Each stream sediment sample comprises of material collected from five points around the suitable trap sites. Due care was taken during collection of samples from narrow channels and avoided material that has fallen from the banks. About 5 Kg samples was collected with the help of scoop and shovel and the sample was dried in natural sunlight. Thus, a total 58 nos of Stream sediment samples were collected from the Langmipi-Laching Thing block and the samples were marked systematically with suffix "SS". These samples were preserved in plastic bags and samples were transported to MECL Laboratory, Nagpur for further processing.

iv. Processing of Collected Samples: The 5 kg samples were passed through available (-)72 mesh sieve to get uniform natural fraction of the samples. Then these portions were pounded and passed through (-) 200 mesh sized sieve from which 500 gm sample has been collected by coning and quartering. From the 500gm sample, 100 gm sample packed in polythene sample pouch and submitted for chemical analysis for 34 elements by ICPMS from MECL Laboratory, Nagpur. The remaining 400 gm sample has been preserved in another polythene pouch for future reference.

C. Soil Sampling: Soil samples were collected from the suitable sites. Efforts were made to cover entire block by soil samples maintaining equal spacing. It had been observed at many places that residual soil is developed directly above the bedrock. While sampling, due care was taken to avoid the collection of transported material such as alluvium or colluvium and emphasis has been given on collecting from residual soil profile.

i. Collection of Soil Sample by pitting: Soil pits were excavated manually with the assistance of local labourers. Each pit measured approximately 1 m in length, 0.8–1.0 m in width, and 1.5–1.8 m in depth, depending on the depth to bedrock and the nature of the soil profile. Approximately 4–5 kg of representative soil material was collected from the B-horizon or the transitional B + C horizon of each pit for geochemical analysis. In total, 65 soil (pit) samples were collected from the Langmipi-Laching Thing Block to evaluate the distribution of rare earth elements (REE) and associated trace elements within the weathered profile.

Fig No 10.1: Image showing a pit of 1.8 m depth for collection of soil sample.

iii. Processing of soil samples: All the samples (65 Nos) were passed through available (-)72 mesh sieve seperately to get uniform natural fraction of the sample. Then these portions of collected samples were pounded and passed through (-) 120 mesh sized sieve from which 500 gm sample was collected by coning and quartering. From the 500-gm sample, 100 gm sample packed in polythene sample pouch and submitted for chemical analysis of 34 elements by ICPMS. The remaining 400 gm sample has been preserved in another polythene pouch for future reference.

12.3.0 Quality control procedures adopted during sampling

12.3.1 The samples have been prepared under the supervision of geologist and qualified sampling technician. All the samples collected from the field were packed properly in the polythene sample bag with proper tag. Then the entire samples were transported to central sample processing unit located in Nagpur. It has been thoroughly checked that none of the sample bags were damaged during the transportation.

12.3.2 Further measures have been taken during sieving and pounding/grinding of samples. The sieve and containers have been cleaned after processing of each sample to avoid contamination and measures have also been taken to avoid loss of powder in air.

12.4.0 Measures taken to ensure that the sampling is representative

11.4.1 It is very important to submit the representative sample of collected material for geochemical analyses. As discussed in the previously, initial sieving have been carried out on the soil and stream sediment samples to collect the natural fraction. Further after pounding and passing samples of soil and stream sediment through (-)200 mesh sieve and crushing, grinding and passing through (-) 200 mesh sieves for Bed rock samples, quantity of the samples has been reduced to 500 gm by coning and quartering method after thoroughly mixing to maintain the homogeneity of the samples. Hence it can be assumed that the samples remain representative in nature of in situ material collected.

12.5.0 Appropriateness of grain size

12.5.1 In accordance with the standard sampling procedures, it has also been observed that smaller the particle size, higher the homogeneity of the sample as well as higher the dissolvability during the chemical analysis. As per the standard practice, samples are generally pounded to (-)200 mesh size for analysis through ICP-MS.

CHAPTER - XIII

13.0.0 DRILLING TECHNIQUE AND DRILL SAMPLING EMPLOYED

13.1.0 The integrated outcome of geological mapping and chemical analyses was placed before the 31st Meeting of TCC-II, NMEDT. After detailed technical deliberation, the Committee recommended for the conclusion of the exploration work at the present stage, as the available geological and analytical data do not warrant advancement to the next stage of exploration, i.e, subsurface Core Drilling. Hence the drilling work has not been taken up during the investigation.

<u>**CHAPTER - XIV**</u>

14.0.0 SUB-SAMPLING TECHNIQUES AND SAMPLE PREPARATION

14.1.0 As drilling was not taken up at present exploration work, hence drill core samples has not been generated in the present project. The sampling technique of bed rock and trench samples has been discussed in Chapter XII.

CHAPTER - XV

15.0.0 QUALITY OF ASSAY DATA AND LABORATORY TEST

15.1.0 The nature, quality and appropriateness of Chemical analysis

15.1.1 All the 173 Nos of primary samples which includes 50 Nos of Bedrock samples, 58 Nos of Stream sediment samples and 65 Nos of Soil samples have been analysed for 34 elements, i.e., La, Ce, Pr, Nd, Sm, Eu, Gd, Tb, Dy, Ho, Er, Tm, Yb, Lu, Y, Sc, Li, Be, Ba, Cu, Pb, Zn, Sn, W, Ga, Nb, Rb, Sr, Th, U, V, Zr, Hf, Ta by ICP-MS instrument and 15 nos of samples were analysed for major oxides, i.e., SiO_2, Al_2O_3, Fe_2O_3, MnO, MgO, CaO, Na_2O, K_2O, TiO_2, P_2O_5, LOI by XRF instrument.

15.1.2 Methodology of Chemical Analyses by ICP-MS

Chemical Laboratory, MECL, Nagpur is having Agilent make ICPMS 7800 model for elemental analyses. ICP-MS (inductively coupled plasma-mass-spectrometry) is a technique to determine low-concentrations (ppb = parts per billion = µg/l) and ultra-low-concentrations of elements (ppt = parts per trillion = ng/l). ICP-MS can also measure elements at concentrations up to 100s or even 1000s of parts per million (ppm). Accuracy and precision (standard deviation) for 34 of these elements is either excellent (<5%) or good (5–10%).

Methodology for analysing 34 elements: A simple HCL-HF-HNO3 dissolution in screw top Teflon bombs is used in microwave Digester for sample preparation. ICP-MS instrumental sensitivity is measured by external solutions (Tuning solution provided by Agilent), with surrogate calibration for 4 elements (Li, Co, Y). Matrix correction is made by use of standard CRM (Certified reference material).

The following Precautions are followed in the laboratory while doing chemical analysis.

- Safety goggles (department approved) and apron dress must be worn in the lab at all times.
- Use of fume hoods for dangerous or irritating chemicals.
- Label all containers to identify their contents.
- Never put anything back into a reagent bottle. Once a reagent has passed the mouth of its container, it has passed the point of no return. Always take as

little of a chemical as possible. Use only clean, dry spatulas for removing chemicals from bottles. Properly dispose of excess chemicals.

- Avoid touching hot objects. Burns are a common accident in the chemistry lab. Be careful when using hot plates and objects which have been heated on them. Use beaker tongs to remove hot containers from the hot plate.
- Rinse off any chemicals spilled on the skin immediately with large amounts of water.
- Clean up broken glassware immediately. Place it in the labelled crock at the front of the lab.
- Properly dispose of waste chemicals. Certain liquids can be poured into the sink and flushed with water while others are poured into designated waste containers. Most solid wastes are placed in designated crocks.

15.1.3 Methodology of Chemical Analyses by XRF

Chemical Laboratory, MECL, Nagpur have RIGAKU make ZSX PRIMUS IV XRF instrument for analyses of major oxides.

First pellets of the powdered samples are made using hydraulic press. Then the XRF instrument is calibrated using suitable matrix matching CRMs. After calibration of the instrument the samples are analyzed and the values of the SiO2, Al2O3, Fe2O3, MnO, MgO, CaO, Na2O, K2O, TiO2, P2O5 are obtained from the software. The Loss on Ignition has been determined by calculating the loss in weight of the sample after igniting the sample taken in a Pt crucible at 1000oC in a muffle furnace.

15.2.0 Quality control procedure

15.2.1 The standard procedure of quality control has been adopted during the chemical analysis in Chemical laboratory, MECL, Nagpur which includes

(i) Analysis of Certified reference materials/measurement standards

(ii) Analysis of blind samples

(iii) Use of QC samples and control charts

(iv) Analysis of blank samples

(v) Analysis of spiked samples

(vi) Analysis in duplicate samples.

15.3.0 External Check Analyses

15.3.1 In accordance to the standard practice of quality assurance and quality control, 17 numbers of primary samples (10% of Primary samples) were analysed at JNARDDC, Nagpur, as external check samples.

15.3.2 The analytical results of the external check samples have been represented as Annexure No XII.

15.3.3 A statistical comparison has been carried out between the primary analytical results of the MECL Chemical Laboratory, Nagpur and the corresponding external check results of JNARDDC, Nagpur, for the 17 paired samples. The evaluation follows the methods normally adopted for geochemical quality assurance and quality control and comprises element-wise correlation, coefficient of determination (R^2), reduced major axis regression, examination of the primary-to-external ratio, and assessment of the reproducibility of the derived geochemical parameters on which the interpretation of the block depends.

15.3.4 The results for the rare earth suite, together with yttrium and scandium, are summarised in Table No 15.1. For the total rare earth content (ΣREE+Y) the coefficient of determination is $R^2 = 0.796$ and the Spearman rank correlation is 0.936, which becomes 0.959 on exclusion of a single reversed pair (MLEC-17). The summed light rare earth content (ΣLREE) returns $R^2 = 0.807$ with a Spearman rank correlation of 0.968. Among the individual elements, the coefficient of determination is 0.848 for lanthanum, 0.825 for europium, 0.794 for gadolinium, 0.785 for cerium, 0.774 for samarium, 0.768 for praseodymium, 0.765 for neodymium, 0.702 for terbium and 0.690 for scandium.

15.3.5 The geochemical parameters upon which the interpretation of the block depends are reproduced by both laboratories. The chondrite-normalised pattern slope, expressed as $(La/Lu)_N$, returns median values of 19.07 for the primary and 15.37 for the external check data; the LREE/(HREE+Y) ratio returns $R^2 = 0.791$ with median values of 5.48 and 4.73 respectively; and the rank order of ΣREE+Y is reproduced with a Spearman coefficient of 0.959. The lithological discrimination, the relative enrichment of the individual lithological units and the light-to-heavy rare earth fractionation described in Chapter-VII are accordingly supported by the external check analyses.

15.3.6 The external check analyses indicate analytical reproducibility between the primary and external laboratories for the light rare earth elements and for the total rare earth content of the block, the summed light rare earth (ΣLREE) and total rare earth (ΣREE+Y) contents returning coefficients of determination of 0.807 and 0.796 and Spearman rank correlations of 0.968 and 0.959 respectively. The relative distribution of the rare earths between samples and between lithological units, the shape of the chondrite-normalised patterns and the light-to-heavy rare earth fractionation are reproduced. The analytical data generated during the present investigation are considered reliable and suitable for the geological interpretation presented in this report.

Table No 15.1: Statistical comparison of primary and external check analyses for the rare earth suite, yttrium and scandium, Langmipi–Laching Thing Block (17 paired samples)

Element	N	r	R^2	RMA slope	External/Primary (median)
La	17	0.921	0.848	0.668	0.49
Ce	17	0.886	0.785	0.763	0.47
Pr	17	0.876	0.768	0.763	0.52
Nd	17	0.875	0.765	0.576	0.49
Sm	17	0.880	0.774	0.593	0.43
Eu	17	0.908	0.825	0.764	0.56
Gd	17	0.891	0.794	0.589	0.51
Tb	17	0.838	0.702	0.482	0.37
Dy	17	0.790	0.624	0.501	0.40
Ho	17	0.595	0.354	0.499	0.46
Er	17	0.491	0.241	0.521	0.56
Tm	17	0.247	0.061	0.425	0.55
Yb	17	0.258	0.067	0.569	0.56

Lu	17	0.130	0.017	0.473	0.47
Y	17	0.463	0.214	0.501	0.46
Sc	17	0.830	0.690	0.838	0.66
ΣLREE	**17**	**0.898**	**0.807**	**0.704**	**0.48**
ΣHREE+Y	**17**	**0.602**	**0.362**	**0.520**	**0.51**
ΣREE+Y	**17**	**0.892**	**0.796**	**0.674**	**0.48**

Note: r = Pearson correlation coefficient; R^2 = coefficient of determination; RMA slope = reduced major axis regression slope (external on primary); $(La/Lu)_N$ normalised to chondrite values of Boynton (1984). ΣLREE = La+Ce+Pr+Nd+Sm+Eu; ΣHREE+Y = Gd+Tb+Dy+Ho+Er+Tm+Yb+Lu+Y; ΣREE+Y = ΣLREE+ΣHREE+Y. Primary: MECL Chemical Laboratory, Nagpur; external check: JNARDDC, Nagpur.

15.4.0 Security and chain of control of samples

15.4.1 The samples have been prepared at centralized mechanized sampling unit with proper lebeling and tag and sent to chemical laboratory in supervision of qualified sampling technician.

15.4.2 The samples has been transported from field to sample processing unit with proper sealing of sampling bags and the same has been verified in the sampling unit before opening the bags.

15.4.3 At the sampling unit, standard procedure has been followed and all the precautionary measures have been taken to avoid the contamination. Further the remaining samples are propoerly preserved with sample tags for any future reference under the custody of the company.

MECL

CHAPTER - XVI

16.0.0 MOISTURE

16.1.0 Method of determination of the moisture content.

16.1.1 All the analysis has been carried out with natural moisture. Moisture content has not been determined.

CHAPTER - XVII

17.0.0 BULK DENSITY

17.1.0 Method of determination and result

17.1.1 Drilling of scout boreholes was not recommended owing to the non-encouraging REE results in the area. So, resource estimation was not carried out. As a result, bulk density or specific gravity has not been determined.

CHAPTER - XVIII

18.0.0 BENEFICIATION STUDIES AS MAY BE REQUIRED

18.1.0 Details of beneficiation studies

18.1.1 Beneficiation studies have not been carried out in the present exploration as it was out of the scope of the approved quantum of work.

CHAPTER - XIX

19.0.0. RESOURCE ESTIMATION TECHNIQUES

The REE mineral is mainly confined in few sporadic places. Hence drilling has not been taken up in the present stage of exploration in Langmipi-Laching Thing Block, as a result resource has not been estimated in the block.

<u>**CHAPTER - XX**</u>

20.0.0. REPORTING OF RESOURCE

As mentioned in the Chapter – XIX, resource has not been estimated in the present stage of exploration.

CHAPTER - XXI

SUMMARY AND RECOMMENDATIONS

21.0.0 SUMMARY AND RECOMMENDATIONS

21.1.0 Summary of the exploration outcome

The Reconnaissance Survey (G-4 stage) carried out over the 124.68 sq. km Langmipi–Laching Thing Block delineated a terrain dominated by migmatite, granite gneiss and augen gneiss of the Assam–Meghalaya Gneissic Complex, intruded by pegmatite, quartz and quartzo-feldspathic veins and locally overlain by altered calcareous siliceous sandstone and Quaternary cover. The rocks record polyphase ductile deformation with a dominant NE–SW to E–W foliation, folding and shearing. REE mineralisation, carried by accessory monazite, allanite, zircon, sphene and apatite, is developed within the felsic gneisses and veins and is characterised throughout by strong LREE enrichment and a negative Eu anomaly. The granite gneiss is the most REE-enriched lithounit (mean ΣREE 816.73 ppm; range 87.17–1458.80 ppm), followed by the pegmatite and quartzo-feldspathic veins; however, the enrichment is erratic and confined to isolated, spatially discontinuous occurrences. Mineralisation was recorded only from surface evidence (mapping, bedrock, stream sediment and soil sampling) and its extension in depth could not be established, as subsurface exploration was not undertaken.

REE mineralisation in the block is hosted principally by magmatic accessory minerals (chiefly monazite, with subordinate zircon and titanite) within evolved, high-K, metaluminous, ferroan felsic gneisses and their anatectic pegmatitic and quartzo-feldspathic veins, and is strongly light-REE-enriched with limited heavy-REE potential. Integrated geochemical and spatial analysis demonstrates that the high-value samples are erratic and spatially discontinuous and do not define a continuous or mappable REE zone.

21.2.0 Resources estimated under various classes with grade

No mineral resource has been estimated for the Langmipi–Laching Thing Block. As detailed in Chapters XIX and XX, the REE occurrences are sporadic and lack the geological and grade continuity required for resource estimation, and drilling was not recommended. Consequently, no Measured, Indicated or Inferred resource under the UNFC framework is reported.

21.3.0 Possibility of economic extraction

As no resource has been established, the question of economic extraction under the present technological, environmental, social and market conditions do not arise at this stage of exploration.

21.4.0 Recommendations and future strategy

Exploration in the Langmipi–Laching Thing Block is recommended to be concluded at the present stage of investigation. The REE occurrences identified within the block are anomalous but sporadic and spatially discontinuous. No sustained, mappable zone of significant REE enrichment has been delineated, and the observed mineralisation does not demonstrate the geological continuity or grade persistence required to establish a viable target for subsurface exploration. In view of the above, the block is not recommended for advancement to G-3 (Preliminary) Stage of Exploration or drilling. However, the isolated high-value REE occurrences associated with granite gneiss and vein systems may be revisited in future investigations.

CHAPTER - XXII

PLATES AND MAPS

22.0.0 PLATES AND MAPS

The following plates and maps form part of this Geological Report:

Plate No.	Title	Scale
Plate I	Location Map of the Langmipi–Laching Thing Block	1:50,000
Plate II	Regional Geological Map of the study region	1:50,000
Plate III	Large-Scale Geological Map of the Langmipi–Laching Thing Block	1:12,500
Plate IV	Geological Map with Bedrock Sample locations (with ΣREE+Sc+Y values)	1:12,500
Plate V	Geological Map with Pit (Soil) Sample locations (with ΣREE+Sc+Y values)	1:12,500
Plate VI	Geological Map with Stream Sediment Sample locations (with ΣREE+Sc+Y values)	1:12,500
Plate VII	Geochemical Anomaly Map (ΣREE+Sc+Y)	1:12,500

CHAPTER - XXIII

ANNEXURES OR ENCLOSURES TO THE REPORT

23.0.0 ANNEXURES OR ENCLOSURES TO THE REPORT

The following annexures are enclosed in support of the estimates, observations and interpretations presented in this report:

Annexure No.	**Description**
Annexure I	Co-ordinates of Corner Points of Block Boundary, Langmipi-Laching Thing Area, District: West Karbi Anglong, Assam
Annexure II	Details of the 50 Nos. of Bed rock Samples analysed for REE and associated Trace Elements (34 Element) by ICP-MS
Annexure III	Details of the BRS samples analysed for Whole Rock Analysis for Major Oxides
Annexure IV	Details of the BRS samples analysed for XRD mineral phases
Annexure V	Details of the 58 Nos. of Stream sediment Samples analysed for REE and associated Trace Elements (34 Element) by ICP-MS
Annexure VI	Details of the 65 Nos. of Pit Samples analysed for REE and associated Trace Elements (34 Element) by ICP-MS
Annexure VII	Petrographic study results
Annexure VIII	Mineragraphic study results
Annexure IX	Photomicrographs / mineragraphic plates
Annexure X	Approval / sanction order (MoM letter No. F/No./23/532/2024-NMET/591 dated 13th December 2024)
Annexure XI	Minutes of the 31st meeting of TCC-II (16th–17th June 2026) advising conclusion of the exploration
Annexure XII	Details of 17 Nos. of external check samples analysed for REE and associated Trace Elements (34 Element) by ICP-MS.
Annexure XIII	Action Taken Report on peer review comments.

CHAPTER - XXIV

ANY OTHER INFORMATION

24.0.0 ANY OTHER INFORMATION

All geological, geochemical and analytical data generated during the investigation shall be duly compiled and subjected to peer review, and after successful peer review it will be uploaded to the National Geoscience Data Repository (NGDR) in accordance with the prescribed MERT template and guidelines.

24.1.1 References

Angami, J., Shyamkumar Singh, M., Pai, P.R., & Mishra, A.K. (2012). *Regional Geochemical Mapping in parts of Toposheet No. 78 J/3 & 7 and 78 N/15 & 16 in Kamrup, Darrang, Nagaon, Goalpara and Kokrajhar districts of Assam*. Unpublished GSI Report, FS 2010–12.

Bandhopadyay, D.N. (1983). *Systematic Geological Mapping around Burnihat and surrounding areas, Khasi Hills district, Meghalaya and part of Kamrup district, Assam*. Unpublished GSI Progress Report, FS 1975–76.

Baranov, V., & Naudy, H. (1964). Numerical calculation of the formula of reduction to the magnetic pole. *Geophysics*, 29, 67–79.

Bhattacharya, D.D., Pal, T., & Acharya, A. (2000). *Report on Systematic Geological Mapping around Umden-Umlaper and Kyrdemkulai Bhalta areas, Ri-Bhoi and West Khasi Hills districts, Meghalaya*. Unpublished GSI Progress Report, FS 1995–96.

Boynton, W.V. (1984). Geochemistry of Rare Earth Elements: Meteorite Studies. In P. Henderson (Ed.), *Rare Earth Element Geochemistry* (pp. 63–114). Elsevier, New York.

Bucher, K., & Frey, M. (1994). *Petrogenesis of Metamorphic Rocks*. Springer-Verlag, Berlin, Heidelberg and New York, xiv + 318 pp.

Chakraborty, P.K., & Ravi Kumar, Ch. (2016). *Report on Gravity-Magnetic Mapping in parts of Darrang-Kamrup-Nagaon districts of Assam and Ri-Bhoi district of Meghalaya*. Unpublished GSI Progress Report, FS 2015–16.

Chatterjee, N., Bhattacharya, A., Duarah, B.P. & Mazumdar, A.C. (2011). Late Cambrian reworking of Paleo-Mesoproterozoic granulites in the Shillong-Meghalaya Gneissic Complex (Northeast India): evidence from P–T pseudosection analysis and monazite chronology and implications for East Gondwana assembly. *Journal of Geology*, 119, 311–330.

Choudhary et al. / Yin et al. (2017). Contribution of Columbia and Gondwana supercontinent assembly- and growth-related magmatism in the evolution of the Meghalaya Plateau and the Mikir Hills, Northeast India: constraints from U–Pb SHRIMP zircon geochronology and geochemistry. *Lithos*, 277, 356–375.

Cox, K.G., Bell, J.D., & Pankhurst, R.J. (1979). *The Interpretation of Igneous Rocks*. George Allen & Unwin, London.

Geology and Mineral Resources of Meghalaya. (2009). *Geological Survey of India Miscellaneous Publication No. 30, Part IV, Vol. 2(ii), Meghalaya*.

Grant, F.S. (1985). Magnetic and gravity methods continue to be a viable approach to unraveling the geological setting for mineralization.

Harley, S.L. (1989). The origins of granulites: A metamorphic perspective. pp. 215–247.

Holom, D.I., & Oldow, J.S. (2007). Gravity reduction spreadsheet to calculate the Bouguer anomaly using standardized methods and constants.

Hurn, M.T. (1950). Structure and petrology of the Lovewell Mountain quadrangle, New Hampshire. *Geological Society of America Bulletin*, 61, 43–89.

Irvine, T.N., & Baragar, W.R.A. (1971). A guide to the chemical classification of the common volcanic rocks. *Canadian Journal of Earth Sciences*, 8, 523–548.

Khonglah, M.A., Sougrakpam, S., Dutta, A., & Deepty, R. (2017). *Report on Study on Genesis of Ion-Adsorption Type REE Mineralisation in parts of Nongpoh Granitoid, Ri-Bhoi district, Meghalaya*. Unpublished GSI Report, FS 2015–17.

Lafehr, T.R. (1991). An exact solution for the gravity correction.

Mahji, S., & Alam Siddiqui, M. (2016). *Investigation for W, Sn & REE in the Kumarkuchi and Chagaligaon areas, Kamrup (Metro) district, Assam*. Unpublished GSI Progress Report, FS 2015–16.

Mazumder, S.K. (1976). A summary of the Precambrian geology of the Khasi Hills, Meghalaya. *Geological Survey of India Miscellaneous Publication No. 23, Part II*, 311–339.

Medlicott, H.B. (1869). Geological sketch of the Shillong Plateau. *Memoirs of the Geological Survey of India*, 7, Plate 1.

Middlemost, E.A.K. (1994). Naming materials in the magma/igneous rock system. *Earth-Science Reviews*, 37, 215–244.

Murthy, M.V.N., Chakravorty, C., & Talukdar, S.C. (1976). Stratigraphic revision of the Cretaceous–Tertiary sediments on the Shillong Plateau. *Records of the Geological Survey of India*, 107(2), 83–90.

Pathak, B., & Dharmwal, G.S. (2012). *Report on Gravity-Magnetic Evidences across Meghalaya Massif from Guwahati to Cherrapunjee*. Unpublished GSI Report, FS 2010–12.

Pearce, J.A. (2008). Geochemical fingerprinting of oceanic basalts with applications to ophiolite classification and the search for Archean oceanic crust. *Lithos*, 100(1–4), 14–48.

Pearce, J.A., Harris, N.B.W., & Tindle, A.G. (1984). Trace element discrimination diagrams for the tectonic interpretation of granitic rocks. *Journal of Petrology*, 25(4), 956–983.

Pierre, K., & Pascal, S. (2004). Use of the analytic signal to identify magnetic anomalies due to kimberlite pipes. *Geophysics*, 69(1), 180–190.

Reid, A.B., Allsop, J.M., Granser, H., Millet, A.J., & Somerton, I.W. (1990). Magnetic interpretation in three dimensions using Euler deconvolution. *Geophysics*, 55, 80–91.

Shand, S.J. (1943). *Eruptive Rocks: Their Genesis, Composition, Classification, and Their Relation to Ore Deposits, with a Chapter on Meteorites*. John Wiley & Sons, New York.

Shima, R.K., Mahmood, A., & Mohsen, P. (2016). Review and analysis of geological structural model by using geomagnetic study. *Journal of Geology*, 5(2), 39.

Shil, R., Ranjan, R., Babu, M. M., Mahendar, S., & Reddy, P. R. (2020). *Final report on reconnaissance survey for REE and associated mineralization in and around Byrnihat area, Ri-Bhoi District, Meghalaya and Kamrup (Metro) District, Assam (Stage: G-4)* (Field Season 2019–20). Geological Survey of India, North Eastern Region, Shillong.

Syiem, S.M., Sunder Raj, B., Divakar Reddy, P., & Dharmwal, G.S. (2012). *Report on Gravity-Magnetic Mapping in parts of East Khasi Hills and Ri-Bhoi districts, Meghalaya*. Unpublished GSI Progress Report, FS 2010–12.

Varma, O.P., & Pandian, M.S. (1984). Conceptual models for exploration of tungsten deposits in India—their integrated exploitation and economics. *Proceedings of the Indian National Science Academy*, 50A(5), 523–540.

CHAPTER - XXV

25.0.0 CERTIFICATE FROM THE QUALIFIED PERSON

This is to certify that the Geological Report on the Reconnaissance Survey (G-4 stage) for REE and associated minerals in the Langmipi–Laching Thing Block, West Karbi Anglong District, Assam, has been prepared on the basis of the exploration data generated by Mineral Exploration and Consultancy Limited (MECL) in accordance with the Minerals (Evidence of Mineral Contents) Amendment Rules, 2021 and Part-IVA – Reporting of Mineral Resources thereof. The data, observations, interpretations and conclusions presented herein are, to the best of my knowledge and belief, true, complete and correct.

Name: Shrikant Sharma

Designation: HoD (Exoploration)

Affiliation: Mineral Exploration and Consultancy Limited (MECL), Nagpur

Place: Nagpur

Date:

Signature: ____________